https://doi.org/10.5194/egusphere-2026-3649
Preprint. Discussion started: 9 July 2026

Global atmospheric aerosol distributions and composition from the Earth's surface to the stratosphere

Matthias Kohl[1], Christoph Brühl[1], Holger Tost[2], Christos Xenofontos[3], Theodoros Christoudias[3], Sergey Gromov[1], Oliver Appel[2,4], Stephan Borrmann[2,4], Adam Bourassa[5], Pedro Campunzano-Jost[6], Yafang Cheng[4], Oliver Eppers[2,4], Karl D. Froyd[6,7], Bruna A. Holanda[8,a], Jose L. Jimenez[5], Patrick Jöckel[9], Philipp Joppe[2,4], Katharina Kaiser[4], Joseph M. Katich[6,7,b], Klaus Klingmüller[1], Franziska Köllner[2,4], Agnieszka Kupc[10], Anna Martin[1], Christopher Pöhlker[8,c], Mira L. Pöhlker[11], Ulrich Pöschl[8], Landon Rieger[12], Samuel Ruhl[1], Gregory P. Schill[7], Johannes Schneider[4], Christiane Schulz[4,d], Joshua P. Schwarz[7], Alexandra P. Tsimpidi[13], Ryan Vella[1,2,e], Christina J. Williamson[14,15], Yifan Yang[11], Daniel Zawada[5], Jos Lelieveld[1,3], and Andrea Pozzer[1,3]

[1]Atmospheric Chemistry Department, Max Planck Institute for Chemistry, Mainz, Germany
[2]Institute for Physics of the Atmosphere, Johannes Gutenberg University, Mainz, Germany
[3]Climate and Atmosphere Research Center, The Cyprus Institute, Nicosia, Cyprus
[4]Aerosol Chemistry Department, Max Planck Institute for Chemistry, Mainz, Germany
[5]Institute of Space and Atmospheric Studies, University of Saskatchewan, Saskatchewan, Canada
[6]University of Colorado Boulder, Boulder, Colorado, USA
[7]NOAA Chemical Sciences Laboratory, Boulder, Colorado, USA
[8]Multiphase Chemistry Department, Max Planck Institute for Chemistry, Mainz, Germany
[9]Deutsches Zentrum für Luft- und Raumfahrt (DLR), Institut für Physik der Atmosphäre, Oberpfaffenhofen, Germany
[10]Aerosol Physics and Environmental Physics, Faculty of Physics, University of Vienna, Vienna, Austria
[11]Leibniz Institute for Tropospheric Research (TROPOS), Leipzig, Germany
[12]Climate Modelling Division, Environment and Climate Change Canada, Victoria BC, Canada
[13]Institute of Climate and Energy Systems: Troposphere (ICE-3), Forschungszentrum Jülich GmbH, Jülich, Germany
[14]Finnish Meteorological Institute, Helsinki, Finland
[15]Institute for Atmospheric and Earth System Research/Physics, Faculty of Science, University of Helsinki, Helsinki, Finland
[a]now at Hessian Agency for Nature Conservation, Environment and Geology, Wiesbaden, Germany
[b]now at BAE Systems, Inc., Boulder, CO, USA, 80301
[c]now at Physikalisch-Technische Bundesanstalt (PTB), Braunschweig, Germany
[d]now at Leibniz-Zentrum für Agrarlandschaftsforschung (ZALF) e. V., Müncheberg, Germany
[e]now at Institute for Atmospheric and Climate Science, ETH Zurich, Zurich, Switzerland

Correspondence: Matthias Kohl (m.kohl@mpic.de) and Andrea Pozzer (andrea.pozzer@mpic.de)

Abstract. Atmospheric aerosols play a crucial role in Earth's climate system, yet their spatio-temporal distribution, particularly in the free troposphere (FT) and upper troposphere–lower stratosphere (UTLS), remains poorly constrained, a major source of uncertainty in estimates of aerosol radiative forcing. To address this, we perform ECHAM/MESSy Atmospheric Chemistry (EMAC) model simulations with a newly developed setup, bridging the tropospheric and stratospheric regimes. Model output is evaluated against a comprehensive suite of observations of aerosol mass, number concentrations, and optical properties, showing good agreement across vertical layers and most geographical regions. The resulting simulations provide a unified description of global distributions of key aerosol species, their composition, and number concentrations from the Earth's

https://doi.org/10.5194/egusphere-2026-3649
Preprint. Discussion started: 9 July 2026

surface to the stratosphere. Simulated aerosol mass exhibits a global minimum between 400 and 200 hPa, marking the transition between FT and UTLS, with particle numbers peaking at similar altitudes or slightly higher in the tropics. Primary particles contribute less than 3.5% to aerosol mass in the stratospheric overworld up to 10 hPa, substantially less than suggested by previous modelling studies and in closer agreement with recent observations. Stratospheric aerosol mass is dominated by sulfate, with a notable contribution ($\sim 15\%$) from secondary organic aerosol throughout the global lower stratosphere. This work provides new constraints on aerosol distributions in the FT and UTLS, which remain underrepresented in global modelling studies, and enables future research on aerosol-climate interactions in this critical atmospheric regime.

1 Introduction

Atmospheric aerosol particles, composed of a mixture of condensed phase compounds of varying size, origin, and composition, play a key role in Earth's climate system (Szopa et al., 2021). They originate from both natural (e.g., dust, sea salt, volcanic ash) and anthropogenic (e.g., black and organic carbon) sources, either through direct emission or via gas-to-particle conversion of oxidized precursors such as sulfur, nitrogen, and organic compounds (e.g., Pöschl, 2005; Boucher, 2015). Once airborne, aerosols undergo a range of complex processes, including mixing, growth, long-range transport, and removal, which collectively influence Earth's radiative balance, the hydrological cycle, atmospheric chemistry, and human health (e.g., Lohmann and Feichter, 2005; Lelieveld et al., 2015; Klobas et al., 2017; Murray et al., 2020; Szopa et al., 2021).

Uncertainties in aerosol direct and indirect (through aerosol-cloud interactions) radiative forcing remain the largest contributor to total anthropogenic forcing uncertainty in the latest IPCC report, largely due to limited knowledge of vertical aerosol profiles, and a scarcity of comprehensive model–observation comparisons (Heald et al., 2011; Reddington et al., 2017; Watson-Parris et al., 2019; Szopa et al., 2021). While most CMIP6 (Coupled Model Intercomparison Project phase 6) models rely on prescribed aerosol climatologies or implement simplified chemistry schemes, they typically do not simulate a comprehensive set of aerosol species that adequately reflect the chemical diversity of the atmosphere (Szopa et al., 2021).

Aerosols in the boundary layer (BL) have been extensively studied through a combination of ground-based measurements, satellite observations, and numerical simulations (e.g., Zhang et al., 2007; Pozzer et al., 2012; van Donkelaar et al., 2016; Gordon et al., 2017; Kohl et al., 2023), with aerosol composition and abundance strongly influenced by local sources due to the short lifetime of aerosols near the surface.

Stratospheric aerosols are dominated by sulfur species, primarily formed from precursor gases emitted by natural sources (most notably carbonyl sulfide; e.g., Crutzen, 1976; Brühl et al., 2012) and occasional volcanic injections (e.g., Schmidt et al., 2018; Schallock et al., 2023), giving rise to the Junge layer (Junge et al., 1961), which spans altitudes between 12 and 28 km. Observations of stratospheric aerosols are limited, with most data originating from sparse aircraft missions (mostly in the lower stratosphere; e.g., Yu et al., 2016; Murphy et al., 2021; Appel et al., 2022; Lyu et al., 2026), balloon-borne in situ measurements (e.g., Deshler et al., 2003; Hertzog and Plougonven, 2021) and satellite remote sensing (e.g., Vernier et al., 2009; Bourassa et al., 2012; Kovilakam et al., 2023), providing information about aerosol optical properties but offer limited insight into particle composition and size. The contribution of non-sulfur species to the stratospheric aerosol burden remains particularly

https://doi.org/10.5194/egusphere-2026-3649
Preprint. Discussion started: 9 July 2026

uncertain (e.g., Kremser et al., 2016). For instance, while model studies have suggested a significant presence of dust in the upper troposphere (UT) and lower stratosphere (UTLS; e.g., Brühl et al., 2018; Ma et al., 2019; Bossolasco et al., 2021), recent observations report a very low abundance of primary particles, particularly with mineral dust composition (Appel et al., 2022; Ebert et al., 2024).

Similarly, aerosol particles and their properties in the free troposphere (FT) and UTLS can only be studied through spatially and temporally limited aircraft- and balloon-based measurements, or via satellite observations that provide only aerosol optical properties (e.g., Winker et al., 2013; Maheshwarkar et al., 2024). As a result, no global long-term observations of aerosol composition and size distributions exist for these regions. An increasing number of aircraft campaigns have investigated atmospheric aerosol populations in the FT and UTLS, focusing on either background conditions, e. g. during the NASA ATom mission (Thompson et al., 2022) and IAGOS (e.g., Ditas et al., 2018; Martinsson et al., 2019; Schneider et al., 2025), or on specific atmospheric processes. These studies have exemplarily revealed high concentrations of freshly formed particles in the tropical and subtropical UT (Borrmann et al., 2010; Williamson et al., 2019; Zhao et al., 2020; Weigel et al., 2021; Curtius et al., 2024), the formation of the Asian Tropopause Aerosol Layer (ATAL; Vernier et al., 2011; Höpfner et al., 2019; Mahnke et al., 2021; Appel et al., 2022), and the long-range transport and sustained persistence of biomass burning and dust particles throughout the troposphere (Schill et al., 2020; Froyd et al., 2022b), including strong wildfire emissions that reach the stratosphere (Ditas et al., 2018; Katich et al., 2023; Ma et al., 2024; Shen et al., 2025).

Given the spatial and temporal limitations of observational data, numerical models are essential for constructing a global picture of aerosol distributions and composition, extrapolating localized findings to global and seasonal scales, and assessing their broader implications. The vertical distribution of aerosols is particularly important, as their indirect radiative effect strongly depends on their altitude relative to cloud-forming levels (Choi and Chung, 2014; Mishra et al., 2015; Watson-Parris et al., 2019; Zhu et al., 2024). However, no study has yet provided a fully consistent, observation-constrained global aerosol climatology from the Earth's surface to the stratosphere.

We present the results of a first unified, comprehensively evaluated global simulation of atmospheric aerosol distributions, number concentrations, and composition of key aerosol species from the Earth's surface to the stratosphere using the ECHAM/MESSy Atmospheric Chemistry (EMAC) model. The simulations are based on a newly developed model setup that integrates and extends previously used tropospheric (e.g., Pringle et al., 2010; Lelieveld et al., 2015; Kohl et al., 2023; Tsimpidi et al., 2025) and stratospheric setups (e.g., Schallock et al., 2023; Brühl et al., 2025; Kohl et al., 2025), enabling a consistent representation of aerosols across the entire troposphere and stratosphere. Simulated aerosol properties are evaluated against a comprehensive dataset, combining ground-based observations, satellite remote sensing data, and in situ measurements from multiple aircraft campaigns, with particular focus on the FT and UTLS.

Section 2 outlines the methodology and experimental setup, including the observational datasets, the EMAC model configuration, and the newly developed model setup. Model evaluation is presented in Sect. 3, followed by a description of the resulting global aerosol distributions and composition in Sect. 4. Section 5 discusses the key findings, their implications and the limitations of the simulations.

https://doi.org/10.5194/egusphere-2026-3649
Preprint. Discussion started: 9 July 2026

2 Methods & Model Setup

2.1 Observations

2.1.1 Surface in situ observations

The Globally Harmonised Observations in Space and Time (GHOST; Bowdalo et al., 2024) dataset compiles extensive surface in situ observations of atmospheric composition from multiple monitoring networks, harmonized into a standardized format. The following networks are used for this study: EPA Air Quality (USA), EEA Air Quality and EMEP (Europe), Canada NAPS (Canada), UK Air (UK), Chile SINCA (Chile), MEXICO CDMX (Mexico), MITECO (Spain) and EANET (East Asia). All included measurement stations are indicated by pink dots in Fig. 1.

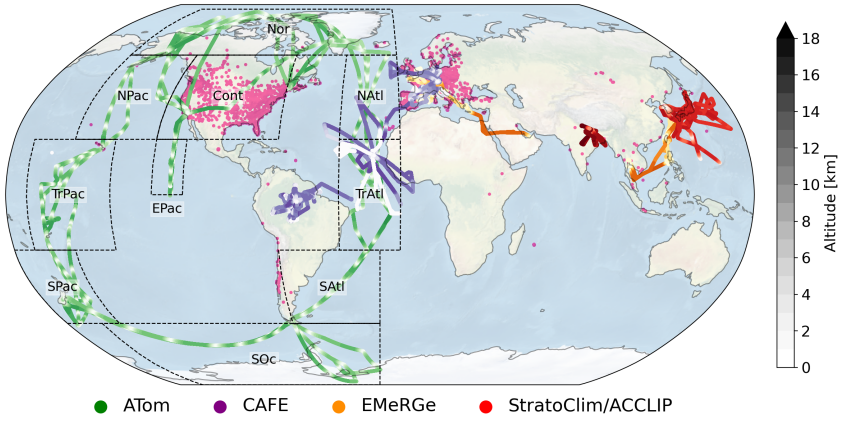

Figure 1. Overview of in situ observations used for the evaluation of EMAC simulations. Surface stationary measurements are indicated by pink dots, while flight paths are color-coded according to the legend. Altitude profiles of aircraft missions are provided by the shading in the corresponding colors. Observations from the Atom mission are categorized into 10 characteristic regions for evaluation: Tropical Pacific (TrPac), Tropical Atlantic (TrAtl), North Pacific (NPac), North Atlantic (NAtl), South Pacific (SPac), South Atlantic (SAtl), East Pacific (EPac), Continental US/Canada (Cont), Northern Polar (Nor), and Southern Ocean (SOc).

2.1.2 Aircraft in situ observations

We combine observational datasets from aircraft missions that target both background conditions and specific regions or atmospheric processes. Figure 1 provides a global overview of the flight paths from the campaigns included in this study.

- **NASA ATom mission:** The NASA ATom mission (Thompson et al., 2022) sampled background atmospheric conditions over continental North America, the Pacific, Atlantic, and Southern Ocean during four sub-campaigns (11–13 flights each): ATom-1 (July/August 2016), ATom-2 (January/February 2017), ATom-3 (September/October 2017), ATom-4 (April/May 2018). Numerous vertical profiles spanning from 200 m to 12 km altitude were recorded, providing a ro-

https://doi.org/10.5194/egusphere-2026-3649
Preprint. Discussion started: 9 July 2026

bust basis for evaluating the model's ability to represent background aerosol distributions in the FT and UTLS. Aerosol mass concentrations were measured using the University of Colorado (CU) High-Resolution Aerosol Mass Spectrometer (HR-AMS; PM_1; DeCarlo et al., 2006; Canagaratna et al., 2007; Jimenez et al., 2019) and the Single Particle Soot Photometer (NOAA SP2; 90–550 nm; Gao et al., 2007; Schwarz et al., 2010; Katich et al., 2018; Schwarz and Katich, 2019). Aerosol Microphysical Properties (AMP), specifically particle number concentrations and size distributions, were derived from a suite of instruments (Kupc et al., 2018; Williamson et al., 2019; Brock et al., 2019a, b): the Nucleation-Mode Aerosol Size Spectrometer (NMASS; 2–60 nm), the Ultra-High-Sensitivity Aerosol Spectrometer (UHSAS; 60–600 nm), and a Laser Aerosol Spectrometer (LAS; 0.6–4.8 µm). Biomass burning, sea salt and dust mass concentrations in the 0.1–4.8 µm physical diameter range were calculated by combining measurements of the NOAA PALMS airborne single-particle mass spectrometer instrument (Thomson et al., 2000; Murphy et al., 2006; Froyd et al., 2019; Schill et al., 2020) with size distribution measurements (see above; Froyd et al., 2019). Gas phase mixing ratios were measured using the NOAA Nitrogen Oxides and Ozone (NO_yO_3) 4-channel chemiluminescence (CL) instrument (NO; Ryerson et al., 2019), the Picarro G2401 spectrometer (CO; McKain and Sweeney, 2021), the Airborne Tropospheric Hydrogen Oxides Sensor (ATHOS; OH; Brune et al., 2021), the California Institute of Technology Chemical Ionization Mass Spectrometer (CIT-CIMS; SO_2 & HNO_3; Allen et al., 2021), and the Unmanned Aircraft Systems (UAS) Chromatograph for Atmospheric Trace Species (UCATS; O_3; Elkins et al., 2020).

– **HALO campaigns (CAFE and EMeRGe)** The **H**igh **A**ltitude and **LO**ng range research aircraft (HALO) is regularly equipped for atmospheric research. We use aerosol mass concentration measurements from the Compact Time-of-Flight Aerosol Mass Spectrometer (C-ToF-AMS; 40–800 nm; Drewnick et al., 2005; Schulz et al., 2018), and the Single Particle Soot Photometer (SP2; 70–500 nm; Holanda et al., 2020; Krüger et al., 2022), collected during three CAFE (**C**hemistry of the **A**tmosphere: **F**ield **E**xperiments; altitudes 0–15 km) and two EMeRGe (**E**ffect of **Me**gacities on the transport and transformation of pollutants on the **R**egional to **G**lobal scal**e**s; altitudes 0–14 km) missions. CAFE-Africa (August/September 2018, from Cape Verde) investigated the influence of biomass burning on the tropical and subtropical Atlantic Ocean. CAFE-Brazil (December 2022/January 2023, from Manaus) focussed on chemical processes in the remote atmosphere over the Amazon rainforest. CAFE-EU (May/June 2020, from Oberpfaffenhofen; Voigt et al., 2022) studied the atmospheric impacts of emission reductions during the COVID-19 lockdown in Europe. The EMeRGe missions (Andrés Hernández et al., 2022) targeted polluted regions above major population centres in Europe (EMeRGe-EU; May–August 2017) and Asia (EMeRGe-Asia; February–April 2018).

– **StratoClim/ACCLIP:** The Asian Monsoon Anticyclone (AMA) has been identified as a key driver of UTLS aerosol loading, by uplifting aerosol precursor gases via deep convective systems, which contributes to the formation of the ATAL (e.g., Vernier et al., 2011; Höpfner et al., 2019; Appel et al., 2022). In this study, we incorporate data from two recent aircraft missions that directly investigated this phenomenon. The StratoClim mission (July/August 2017, from Kathmandu, Nepal) aimed to probe the ATAL and convective outflow, using the high-altitude research aircraft M-55 Geophysica, reaching altitudes up to 20 km. The ACCLIP mission (Sept. 2022, from South Korea) combined

https://doi.org/10.5194/egusphere-2026-3649
Preprint. Discussion started: 9 July 2026

measurements from two research aircraft (NASA WB-57 and the NCAR G-V) to study transport pathways of ATAL-origin aerosols over the Western Pacific (Eppers et al., 2025b). Aerosol mass concentration were measured with the ERC Instrument for the Chemical composition of Aerosols (ERICA-AMS; Dragoneas et al., 2022; Hünig et al., 2022) during both campaigns. Additionally, black carbon (BC) measurements during ACCLIP were obtained from the NOAA SP2 instrument (see above).

2.1.3 Remote sensing

Stratospheric aerosol optical properties are evaluated using the Global Space-based Stratospheric Aerosol Climatology (GloSSAC V2.21; Thomason et al., 2018; Kovilakam et al., 2020, 2023). GloSSAC merges remote sensing data from multiple satellite instruments and provides monthly mean aerosol extinction in the stratosphere, interpolated to four wavelengths (386, 452, 525, and 1020 nm). For this study, GloSSAC observations from 2016 to 2018 are used, relying on the following instruments:

- **The Optical Spectrograph and InfraRed Imaging System (OSIRIS)**, onboard the ODIN satellite, uses limb-scattered sunlight for the retrieval of aerosol extinction at 750 nm (Bourassa et al., 2012). The OSIRIS-derived extinction (v7.0; Rieger et al., 2019) is converted to 525 nm using the Angstrom exponent and bias-corrected (Kovilakam et al., 2020).
- **The Cloud-Aerosol Lidar with Orthogonal Polarization (CALIOP)** instrument, onboard the CALIPSO satellite, observes backscattered laser signals in near-nadir geometry, providing aerosol extinction at 532 and 1064 nm (Winker et al., 2009). For GloSSAC, these values are extrapolated to 525 nm and 1020 nm for GloSSAC, respectively.
- **The Stratospheric Aerosol and Gas Experiment III (SAGE-III)**, externally mounted on the International Space Station, is a solar occultation instrument that retrieves aerosol extinction at nine wavelengths. These observations are interpolated to the four wavelengths used in GloSSAC (Kovilakam et al., 2023).

Aerosol extinction profiles at 746 nm are further obtained from the OMPS Limb Profiler (OMPS-LP) aboard the Suomi National Polar-orbiting Partnership (Suomi NPP) satellite. The retrieval is based on measurements of limb-scattered solar radiances and employs a two-dimensional tomographic inversion to derive aerosol extinction profiles (Rieger et al., 2021; Bourassa et al., 2023). Version 2.1.0 Level-2 data, gridded to 5-day averages, are used in this analysis.

Simulated column aerosol optical depth (AOD) at 550 nm is evaluated against ground- and space-based remote sensing observations. The AErosol RObotic NETwork (**AERONET**; Holben et al., 1998) combines a global network of standardized ground-based sunphotometers, providing high-quality measurements of AOD. In this study, we use cloud-screened quality assured Level 2 AOD from the AERONET version 3 database (Giles et al., 2019; AERONET, 2026). The MODerate Resolution Imaging Spectroradiometer (**MODIS**) measures AOD onboard the Terra satellite. We use the $1^\circ \times 1^\circ$ gridded MODIS Level 3 product (Platnick et al., 2015), applying the Deep Blue retrieval algorithm (Hsu et al., 2004).

2.2 Model setup

Model simulations are performed using the ECHAM/MESSy Atmospheric Chemistry (EMAC) model (Jöckel et al., 2006), which combines the general circulation model ECHAM (version 5.3.02, Roeckner et al., 2003) with submodels from the Mod-

https://doi.org/10.5194/egusphere-2026-3649
Preprint. Discussion started: 9 July 2026

ular Earth Submodel System (MESSy version v2.55.1, Jöckel et al., 2010). The model is operated at a spectral resolution of T63 ($1.875° \times 1.875°$) with 90 vertical levels extending up to 0.01 hPa ($\sim$80 km), including additional layers in the middle atmosphere, and a time step of 7.5 minutes. Temperature, surface pressure (logarithmic), divergence, and vorticity are nudged towards meteorological reanalysis data (ERA5, Hersbach et al., 2020) from the European Centre for Medium-Range weather forecasts (ECMWF) below 100 hPa using Newtonian relaxation (see also Jeuken et al., 1996; Jöckel et al., 2006), with prescribed transient sea surface temperatures and sea ice coverage. In addition, zonal winds are nudged to observational data (Giorgetta and Bengtsson, 1999, compiled up to present day by the Free University of Berlin and Karlsruhe Institute of Technology; see https://www.atmohub.kit.edu/english/807.php, last access: 27 May 2026) between 10 and 90 hPa to prevent phase drift of the quasi-biennial oscillation (QBO).

The main simulations cover the years 2016 to 2018, following a half-year spin-up period. Additional shorter simulations were conducted for the periods January 2019 to June 2020 (for comparison with the CAFE-EU campaign) and January 2022 to January 2023 (for comparison with the ACCLIP and CAFE-Brazil campaigns). Tracer initialization is based on ten-year simulations to ensure the establishment of stratospheric background aerosol equilibrium.

Aerosol microphysics are simulated with the MESSy submodel GMXe (Pringle et al., 2010), which uses hydrophilic and hydrophobic lognormal modes to describe the particle size distribution (PSD). Detailed information about the modal setup in this study is provided in Sect. 2.2.1. In GMXe, inorganic aerosol thermodynamics are computed using ISORROPIA-II (Fountoukis and Nenes, 2007), whereas the phase partitioning of organic aerosols (OA) is processed by the ORACLE submodel (Tsimpidi et al., 2014, 2017), based on source and volatility. While organic and inorganic species are treated separately thermodynamically, they are internally mixed within each aerosol size mode. Aerosols can transfer between modes due to changes in size or solubility after each timestep. Sulfate evaporation in the UTLS at low humidity and in the absence of ammonia is computed based on molality following Tabazadeh et al. (1997), relying on the tabulation of Giauque et al. (1960).

Key speciated aerosols included in the simulations are sulfur aerosol (SO_4^{2-} or HSO_4^-; hereafter referred to as sulfate), ammonium (NH_4^+), nitrate (NO_3^-), sodium (Na^+), chloride (Cl^-), potassium (K^+), calcium (Ca^{2+}), and magnesium (Mg^{2+}). OA is categorized based on source, volatility, and primary (POA) or secondary (SOA) origin, amounting to 36 different organic species (more details by Tsimpidi et al., 2014, 2017). In addition, the model includes bulk aerosol species: black carbon (BC), desert dust (DU), and sea salt (SS). Desert dust emissions are primarily represented by the DU bulk species, which accounts for approximately 90% of total dust mass, with minor contributions from speciated cationic components (Klingmüller et al., 2018). Sea salt aerosol is predominantly emitted as sodium chloride (86%), with additional contributions from sulfate (8%), bulk SS (0.8%), and other mineral salt constituents.

Stratospheric heterogeneous reactions and the formation of Polar Stratospheric Clouds (PSCs) are simulated by the MESSy submodel MSBM (Jöckel et al., 2010). Neutral and ion-induced particle formation is simulated with the NAN submodel with ion concentrations provided by the IONS submodel (Ehrhart et al., 2018). We use new particle formation (NPF) parameterisations from the CLOUD experiment, including binary (H_2SO_4-H_2O) and ternary (H_2SO_4-NH_3-H_2O) nucleation (Dunne et al., 2016), enhanced with HNO_3 (H_2SO_4-NH_3-HNO_3; Wang et al., 2022), and pure organic nucleation (Kirkby et al., 2016) of highly oxygenated organic molecules (HOMs).

https://doi.org/10.5194/egusphere-2026-3649
Preprint. Discussion started: 9 July 2026

Global anthropogenic emissions of reactive gases and aerosols at the surface are sourced from the Community Emission Data System (CEDS v2021-04-21[1]; McDuffie et al., 2020), aircraft emissions are taken from CAMS Global Aviation Emissions (CAMS-GLOB-AIR; Granier et al., 2019) up to 2023. Biomass burning and agricultural waste burning emissions are calculated based on observed dry matter burned and fire type, following Andreae (2019), using the BIOBURN submodel. Natural emissions of biogenic VOCs are computed online using the MEGAN model (Guenther et al., 2012) within MESSy. Sea salt (Guelle et al., 2001) and dust emissions (Klingmüller et al., 2018) are computed online with the ONEMIS submodel (Kerkweg et al., 2006), and are emitted as a combination of bulk aerosol, along with specific compounds (see above). Size distributions for anthropogenic primary particle emissions are applied as described by Kohl et al. (2023). Sea salt and dust emission size distributions were adjusted to the new modal size distributions (see Sect. 2.2.1).

Emissions from volcanic eruptions that reach the stratosphere are simulated with the EVER submodel (Kohl et al., 2025), including volcanic eruptions from 1990 to 2023 based on the emission inventory from Schallock et al. (2023). Degassing tropospheric volcanoes are applied based on a volcanic climatology from AEROCOM (Dentener et al., 2006).

Gas-phase chemistry is simulated using the MECCA submodel (Sander et al., 2019), utilizing the Mainz Isoprene Mechanism (MIM1; Pöschl et al., 2000; Jöckel et al., 2006), which includes over 100 gas-phase species and more than 250 chemical reactions. Removal of gas and aerosol species via sedimentation, dry deposition, and wet deposition is computed by the SEDI, DDEP (both Kerkweg et al., 2006), and SCAV submodels (Tost et al., 2006), respectively. The re-evaporation of cloud droplets and the respective release of cloud-processed aerosols was adjusted to the new modal structure (Sect. 2.2.1), and evaporation of particles into smaller than the original modes was prohibited to better represent the transport of coarse dust and sea salt particles.

Aerosol optical properties are diagnosed using the newly developed MESSy submodel AOP (Tost et al., manuscript in preparation), which is comparable in concepts to the AEROPT scheme, described by Dietmüller et al. (2016). AOP computes mode-averaged refractive indices based on the chemical composition, and derives optical properties like extinction, single scattering albedo and asymmetry factor, using pre-calculated Mie parameters. The total optical effects per model grid cell are then obtained by weighting the contributions of the individual modes according to their number distributions and interpolating or calculating their optical properties at the target wavelengths. Radiative transfer calculations are performed with the MESSy submodel RAD (Dietmüller et al., 2016; Nützel et al., 2024), using the original ECHAM5 radiation scheme (E5rad; Roeckner et al., 2003).

All simulations are performed in quasi chemistry-transport model (QCTM; more details by Deckert et al., 2011) mode, in which feedbacks of aerosol and gas phase chemistry on atmospheric dynamics are disabled. This configuration enables a more direct comparison between the different model setups, as differences in results can be attributed solely to variations in chemical and microphysical processes, rather than dynamic feedbacks.

[1]The newest version (v2025-04-18) was tested, however strongly deviating locally from the previous version. The sensitivity of the results to the respective emissions are discussed in Appendix C.

https://doi.org/10.5194/egusphere-2026-3649
Preprint. Discussion started: 9 July 2026

Table 1. Modal size distribution in the new setup for the entire lower and middle atmosphere (TS; used in this study) in comparison to size distributions used in earlier studies, which focussed either on the troposphere (TROPO) or the stratosphere (STRATO). The *small coarse mode* was added between the accumulation and the coarse mode in the TS setup. The median diameter can adjust within the given diameter boundaries. Additionally, the globally constant sigma of the log-normal distribution is given for each mode.

Setup		Nucleation	Aitken	Accumulation	Small Coarse	Coarse
TROPO	Diameter [nm]	1–12	12–120	120–1400	–	> 1400
	Sigma	1.59	1.59	1.59	–	2.0
STRATO	Diameter [nm]	1–12	12–140	140–3200	–	> 3200
	Sigma	1.59	1.59	1.49	–	1.7
TS	Diameter [nm]	1–12	12–120	120–800	800–3200	> 3200
	Sigma	1.59	1.59	1.4	1.25	1.7

2.2.1 Aerosol size distribution

An important aspect for consistent numerical simulations across the entire atmosphere is the representation of aerosol size distributions. Due to differences in aerosol lifetime, ambient pressure, and pollution levels across the BL, FT, UTLS, and the stratospheric overworld, size distributions vary significantly. GMXe provides an adjustable modal size distribution, allowing the aerosol median diameter to evolve freely within user-defined mode boundaries, with particles transferred to neighbouring modes when they grow too large or too small. Within each mode, particles are internally mixed, while the modes themselves remain externally mixed with respect to each other. The boundaries and standard deviation of the logarithmic modes are globally constant, resulting in varying microphysical behaviour across different regions of the lower atmosphere.

Past studies on tropospheric aerosol (e.g., Lelieveld et al., 2015; Pozzer et al., 2022; Kohl et al., 2023; Tsimpidi et al., 2025) typically considered 4 soluble log-normal modes (see Table 1; here referred to as **TROPO**): a nucleation mode for freshly formed particles up to 12 nm, the Aitken mode for fine anthropogenic primary emissions and grown nucleation mode particles (12–120 nm), the accumulation mode for further grown particles and larger primary particles (120–1400 nm), and a coarse mode for particles larger than 1400 nm, primarily consisting of dust and sea salt particles. Additionally, three insoluble log-normal modes are used (Aitken, accumulation and coarse) with the same mode boundaries as the respective soluble modes. Insoluble particles can transfer to the soluble mode through coagulation with soluble particles or coating with soluble species (more details in Pringle et al., 2010).

Stratospheric studies (e.g., Schallock et al., 2023; Brühl et al., 2025; Kohl et al., 2025) used the same number of modes, but with modified mode boundaries and widths (Table 1; here referred to as **STRATO**). While the nucleation mode remains identically defined, the Aitken mode is extended to slightly larger diameters (140 nm). The accumulation mode is expanded to include particles up to 3200 nm, with a narrower modal width (sigma = 1.49). This adjustment suppresses the rapid transfer of particles to the coarse mode, thus reducing sedimentation and prolonging aerosol lifetimes in the stratosphere. However, for the same reason this setup fails to reproduce BL aerosol distributions, where the inhibited transfer to the coarse mode leads

https://doi.org/10.5194/egusphere-2026-3649
Preprint. Discussion started: 9 July 2026

to overestimated particle lifetimes. More details on the performance of the setups are provided in the evaluation (Sect. 3) and discussed in more detail in Sect. 5.

In this study, we present a new modal configuration for GMXe, combining elements of the TROPO and STRATO setups (here referred to as **T**rop**S**trat or **TS**) to represent the entire lower and middle atmosphere (Table 1). This setup introduces an additional mode (soluble and insoluble), termed the *small coarse mode*, positioned between the accumulation and the coarse mode, and spanning the size range from 800 to 3200 nm. This mode serves three main purposes. First, it prevents particles in the stratosphere from growing too large and sedimenting in the coarse mode, and thus reproducing stratospheric aerosol distributions similar to the STRATO setup. Second, in the BL, accumulation mode particles grow into the small coarse mode, reducing BL aerosol lifetimes compared to the STRATO setup. Third, it better represents sea salt and dust emissions, which typically peak between 800 and 1000 nm, with a substantial amount emitted directly into the small coarse mode in the new TS setup. In the STRATO and TROPO setups, these particles were instead emitted into the accumulation mode, internally mixing with particles freshly grown from the Aitken mode with median diameters around 200 nm, thus effectively downscaling the actual emission size.

2.3 Data sampling

Observational data are inherently tied to the characteristics of the measurement instrument and are strictly limited in time and space for in situ observations. This limitation can lead to significant biases in model evaluations (e.g., Schutgens et al., 2016, 2017; Guo et al., 2021). Such biases can be mitigated, though not fully eliminated, through appropriate sampling of model output to match the spatio-temporal resolution and observational constraints of the corresponding measurements.

2.3.1 Particle size range

Measurements of aerosol mass and number are typically confined to a specific size range (see also Sect. 2.1). To ensure a direct and meaningful comparison between model results and observations, we integrate the particle number size distribution, respectively particle volume size distribution, over the same lower and upper size limits used in the measurements (see also Kohl et al., 2023). For aerosol mass spectrometers (HR-AMS, C-ToF-AMS, and ERICA, used in this study), the size limits are defined in terms of vacuum aerodynamic diameter d_{va}. To compare with model output, d_{va} has to be converted to volume equivalent diameter d_{ve}, which is then used to define the integration range (DeCarlo et al., 2004; Guo et al., 2021). The conversion from d_{va} to d_{ve} is based on the vacuum dynamic shape factor χ_v (assumed to be 1, corresponding to spherical particles), the particle density ρ_p and the standard reference density ρ_0 (1 $\mathrm{g\,cm^{-3}}$):

$$d_{v_e} = \frac{\rho_0 \chi_v}{\rho_p} d_{v_a} \tag{1}$$

In addition, for the HR-AMS (operational during the ATom mission), a transmission curve was characterized with respect to vacuum aerodynamic diameter: it increases logarithmically from 0 to 1 between 35 and 71 nm, remains constant at 1 between 71 and 482 nm (ATom-1 and -2) or 520 nm (ATom-3 and -4), and then decreases logarithmically back to 0 up to 1175 nm

https://doi.org/10.5194/egusphere-2026-3649
Preprint. Discussion started: 9 July 2026

(ATom-1 to -3) or 1750 nm (ATom-4). This instrument-specific transmission function was applied to the model output to ensure consistency with observations.

2.3.2 Instrument wavelength

The MODIS instrument provides AOD at 550 nm, whereas AERONET stations primarily report AOD at 500 nm. To enable consistent comparison, AERONET AOD is interpolated to 550 nm using the provided Ångström exponent. Model AOD is calculated at 550 nm with the AOP submodel (see above).

2.3.3 Spatial and temporal sampling

Finally, all datasets are homogenized through consistent spatial and temporal sampling. Stationary observations (AERONET AOD and GHOST surface concentrations) are included only if more than 50% daily measurement coverage is reached. Temporal collocation is performed, using only model output from days with corresponding available observations. Subsequently derived observed annual averages are directly compared to model annual averages from the lowest model grid box containing each measurement site. Annual averages are used for comparison, as the model's spatial resolution and inherent temporal sampling limitations may not fully capture observed short-term variability (e.g., Pozzer et al., 2022).

For AOD derived from MODIS, observations are regridded to match the horizontal resolution of the model. In the case of GloSSAC and OMPS-LP, the modelled aerosol extinction is regridded to align with both the horizontal and vertical resolution of the observational dataset.

Aircraft measurements, typically available at sub-minute temporal resolution and spanning a significant vertical range within a single model timestep, are handled by sampling the full vertical column of model output along the flight tracks at each timestep using the MESSy S4D submodel (Jöckel et al., 2010). The resulting model output is then binned by altitude for each time step and geographical location, and subsequently spatio-temporally collocated with the corresponding observations.

3 Evaluation

The evaluation primarily focuses on the new TS setup, comparing its performance to other simulation results using the modal size distributions from the TROPO and STRATO setups. A more detailed assessment of the TROPO and STRATO setups is provided in the Supplementary Material. For statistical comparison with observations, the following statistical metrics are applied:

- $\overline{\mathrm{M/O}}$: Geometric mean of the ratio between model simulated (M) and observed (O) values
- PF2: Percentage of simulated values within a factor of two of the observed values
- $\mathrm{R}^2_{\log}$: Coefficient of determination R^2 (with R the Pearson correlation coefficient) using the logarithm of observed and simulated values

https://doi.org/10.5194/egusphere-2026-3649
Preprint. Discussion started: 9 July 2026

– RMSLE: Root Mean Squared Error (RMSE) using the logarithm of observed and simulated values

For R^2 and the RMSE logarithmic values are used, as the value range typically spans several orders of magnitudes.

3.1 Surface in situ observations

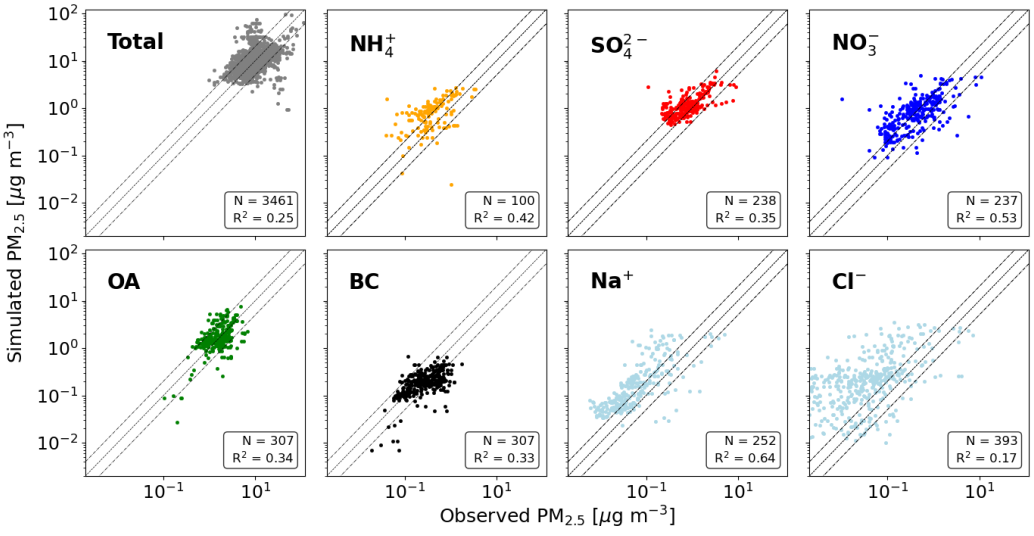

Figure 2. Comparison of annually averaged (2017) $PM_{2.5}$ mass concentrations at the Earth's surface from EMAC simulations (TS setup) with stationary observations from the GHOST (Bowdalo et al., 2024) database, showing total $PM_{2.5}$ and contributions from key aerosol species. The central dotted line indicates 1:1 agreement between observations and simulations, the surrounding dashed lines represent overestimation and underestimation by a factor of two.

Figure 2 compares total observed (GHOST database; Bowdalo et al., 2024) and simulated (TS setup; see Sect. 2.2.1) $PM_{2.5}$ surface mass concentrations, along with the most dominant observed components. Table 2 provides a statistical summary of the comparison, including results from simulations with the STRATO and TROPO setups. Total $PM_{2.5}$ mass concentrations are slightly underestimated in the TS simulation ($\overline{M/O} = 0.9$), yet, 90% of simulated values fall within a factor of two of the observations. The TROPO simulation performs similarly, whereas STRATO simulates higher $PM_{2.5}$ values, and overestimates observations ($\overline{M/O} = 1.38$), with slightly lower PF2 and higher RMSLE.

The TS and TROPO simulations exhibit similar performance in predicting surface mass concentrations of key aerosol species (see Table 2), confirming the suitability of the TS setup for surface-level studies. The overestimation in NO_3^- concentrations in the TROPO and STRATO simulations, also present in earlier evaluations using the TROPO modal setup (e.g., Pozzer et al., 2022), is significantly reduced in the TS setup, showing improved agreement with observations, although a residual overestimation remains. In general, the STRATO setup predicts high mass concentrations in comparison to observations, primarily due to suppressed transfer of accumulation-mode particles to the coarse mode, which prolongs particle lifetimes and limits the

https://doi.org/10.5194/egusphere-2026-3649
Preprint. Discussion started: 9 July 2026

Table 2. Summary of annually averaged (2017) observed (Bowdalo et al., 2024, Obs; GHOST database;) surface $PM_{2.5}$ concentrations and composition, compared to EMAC simulations using the TS, TROPO and STRATO setups, evaluated with the statistical metrics defined earlier. The number of available observational stations is indicated by N_{obs}.

	Observations		**TS**				**TROPO**				**STRATO**			
	N_{obs}	Obs ($\mu g\,m^{-3}$)	$\overline{M/O}$	PF2	R^2_{log}	RMSLE	$\overline{M/O}$	PF2	R^2_{log}	RMSLE	$\overline{M/O}$	PF2	R^2_{log}	RMSLE
NH_4^+	100	0.44	2.16	37	0.42	1.01	2.14	34	0.37	1.05	2.54	30	0.39	1.16
SO_4^{2-}	238	0.8	1.48	73	0.35	0.61	1.18	88	0.54	0.44	1.91	59	0.4	0.79
NO_3^-	237	0.57	1.96	45	0.53	0.95	3.05	28	0.44	1.33	4.77	9	0.46	1.71
OA	307	1.79	1.04	79	0.34	0.58	1.42	65	0.29	0.68	1.7	57	0.26	0.77
BC	307	0.34	0.69	66	0.33	0.75	0.65	65	0.35	0.78	0.74	70	0.35	0.7
Na^+	252	0.08	3.0	25	0.64	1.27	6.08	8	0.3	1.99	17.59	0	0.21	3.0
Cl^-	393	0.07	7.55	16	0.17	2.55	10.09	14	0.08	2.83	30.16	3	0.07	3.76
$PM_{2.5}$	3461	11.63	0.9	90	0.25	0.47	0.93	90	0.24	0.45	1.38	84	0.22	0.55

model's suitability for BL applications. The agreement for BC is very similar across all three simulations, with R^2_{log} values between 0.33 and 0.35, and RMSLE between 0.7 and 0.78.

Pollutants, such as ammonium, sulfate, nitrate, and BC exhibit a consistent pattern: low observed concentrations are systematically overestimated, while higher observed concentrations are better captured or slightly underestimated (Fig. 2). This bias is likely attributable to the model's limited spatial resolution, which artificially enhance $PM_{2.5}$ concentrations in rural or remote grid cells that co-locate with strong point sources, while simultaneously diluting high concentrations near emission sources due to averaging with surrounding low-concentration regions. A similar pattern has been identified by Kohl et al. (2023) for ultrafine particles, and they demonstrated that this bias can be reduced through observation-guided downscaling.

The representation of sea salt sodium and chloride is significantly improved in the TS setup, primarily due to the updated sea salt emission size distribution that aligns with the new modal structure, and the explicit prevention of sea salt particles evaporating into smaller modes after cloud processing (see Sect. 2.2). However, sea salt concentrations remain overestimated relative to observations. A detailed comparison between modelled sea salt and reanalysis data from CAMS (Inness et al., 2019) and MERRA-II (Gelaro et al., 2017; Randles et al., 2017) indicates that the applied changes (particularly the adjusted re-evaporation) reduce the long-range transport of sea salt particles to continental regions. This leads to a more realistic representation of sea salt gradients between oceanic and continental areas compared to simulations with previously used setups, and results in substantially improved agreement with observations and reanalysis data across all size ranges (Appendix A and Fig. A1).

It is noteworthy that the model agreement with sea salt particles with MERRA-2 assimilation data (Appendix A) is much better than with direct measurement data of the GHOST instrument. It cannot be ruled out that the GHOST PM2.5 measurements of sodium and chloride are overestimated because the PM2.5 inlet does not provide a perfectly sharp size cut, which

https://doi.org/10.5194/egusphere-2026-3649
Preprint. Discussion started: 9 July 2026

can allow some larger coarse-mode sea-salt particles to penetrate into the sampled fraction. In addition, the highly hygroscopic nature of sea salt particles can alter their size and inlet transmission efficiency under humid conditions, leading to a high-bias in $PM_{2.5}$ sodium and chloride concentrations.

3.2 Aerosol Optical Depth (AOD)

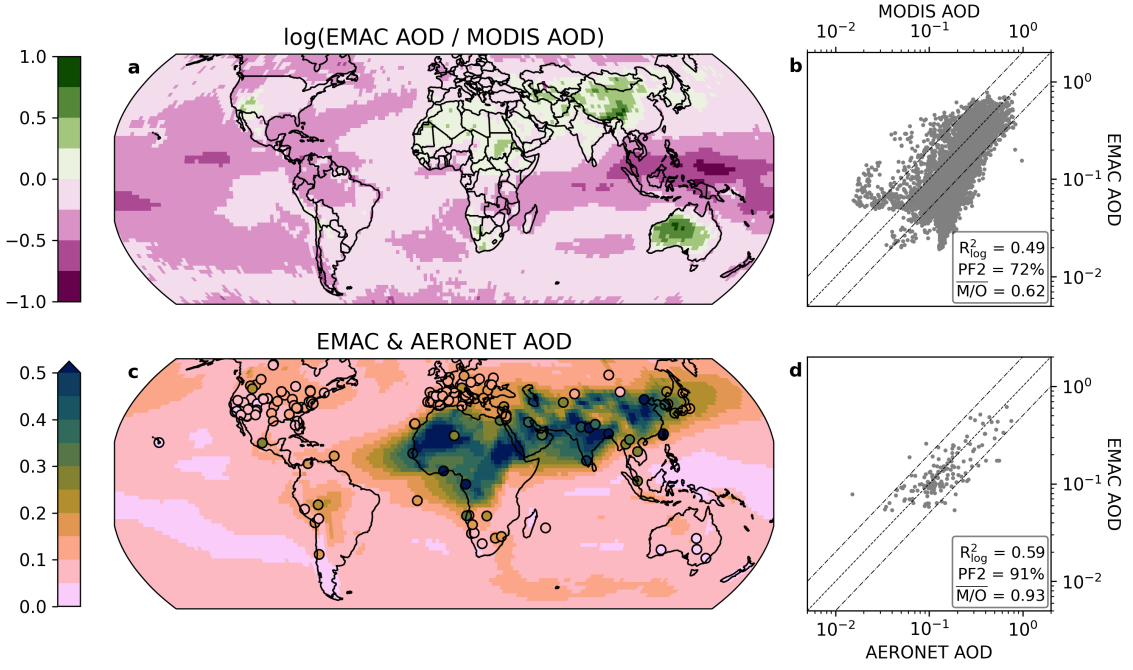

Figure 3. Comparison of annually averaged (2017) simulated column Aerosol Optical Depth (AOD) from EMAC (TS setup) with MODIS and AERONET observations at 550 nm. (a) Global map of the logarithmic ratio of simulated to MODIS AOD; green indicates overestimation by the model, pink underestimation. (b) Corresponding scatter plot, with each dot representing one model grid box. The central dotted line indicates 1:1 agreement, the surrounding dashed lines represent over- and underestimation by a factor of two. (c) Model AOD at 550 nm, overlayed with AERONET observations extrapolated to 550 nm. (d) Corresponding scatter plot, comparing model and AERONET AOD at each AERONET station.

For evaluation of global AOD, we combine space-based (MODIS) and stationary (AERONET) observations. Figure 3a and b compares annually averaged simulated column AOD (TS setup) with MODIS observations at 550 nm for the year 2017. MODIS AOD over continental regions is generally well captured by the model (Fig. 3a), with a slight overestimation over Australia, where organic aerosol dominates the AOD signal, and remote areas of China, potentially due to overestimated desert dust emissions from the Gobi and Taklamakan deserts. Comparison with AERONET AOD (Fig. 3c and d) confirms the model's good representation of continental AOD, with 91% of simulated AOD values falling within a factor of two of observations.

https://doi.org/10.5194/egusphere-2026-3649
Preprint. Discussion started: 9 July 2026

The largest discrepancy between MODIS and simulated AOD originates in Southeast Asia, and propagates across the Indian and Pacific Oceans. Rosanka et al. (2021) demonstrated that biomass burning emissions from peatlands in this region are likely underestimated in EMAC, which may contribute to the observed biases. The model underestimation relative to MODIS observations is particularly pronounced at low observed AOD values. A previous study reported a potential high bias in satellite-derived AOD compared to in situ observations over the remote ocean at low AOD in similar regions (Wang et al., 2024). Therefore, it cannot be ruled out that satellite instruments may underestimate low AOD due to detection limits.

The simulated column AOD varies markedly across the three model setups (see also Supplementary Material Fig. S13 and S14). The TROPO setup exhibits the lowest bias compared to MODIS ($\overline{\mathrm{M/O}} = 0.93$, $\mathrm{PF2} = 88\%$), whereas the TS setup achieves the highest $R^2_{\log}$ (0.49). The opposite pattern is observed for AERONET comparisons (lowest bias in TS simulations: $\overline{\mathrm{M/O}} = 0.93$, $\mathrm{PF2} = 91\%$; highest $R^2_{\log}$ in TROPO: 0.63). Given that column AOD is predominantly influenced by surface-level aerosols, the STRATO setup strongly overestimates AOD ($\overline{\mathrm{M/O}} = 1.6$ against MODIS observations, and $\overline{\mathrm{M/O}} = 2.19$ against AERONET), likely due to an increased aerosol lifetime resulting from less efficient growth from the accumulation to the coarse mode (as discussed above).

3.3 Vertical profiles

3.3.1 Atmospheric background conditions – ATom campaign

Figure 4 compares simulated mass concentrations of sulfate, ammonium, nitrate, total OA (all $\mathrm{PM_1}$), BC (90–550 nm) and desert dust (0.1–4.8 $\mu\mathrm{m}$) as well as particle number concentrations (PNC; 2.7 nm—4.8 $\mu\mathrm{m}$) to corresponding ATom observations. Observations were divided into 10 geographic regions, detailed in Fig. 1, five of which are shown here. The remaining regions are presented in Supplementary Material Fig. S1. Table 3 shows a statistical comparison of the three model setups[2] to observations, using observed and simulated median values at each region, season and altitude. An additional evaluation of sea salt, dust and size-segregated PNC is provided in Supplementary Material Fig. S4 to S7, along with evaluations of key gas-phase species (Fig. S9 and S10). Supplementary Material Fig. S8 presents PSDs across the observed layers in the different regions.

Gas-phase species generally agree well with observations, especially CO, OH, $\mathrm{O_3}$, and NO, with minor discrepancies in $\mathrm{O_3}$ at higher altitudes. $\mathrm{SO_2}$ mixing ratios are slightly underestimated in the East Pacific but overestimated in the North and South Pacific and the North American Arctic. This may be attributed to tropospheric volcanic degassing events, which are included in the model based on climatological data, which, however, do not represent irregular and unpredictable emissions.

Overall, the model captures the magnitude and temporal and spatial variability of aerosol observations, though the level of agreement varies by region and season. Low $\overline{\mathrm{M/O}}$ for mass concentrations values are partly attributable to the detection limits of the observational datasets.

A systematic discrepancy is evident in sulfate concentrations in the FT and UTLS outside the tropics, where observed sulfate concentrations are often underestimated by the simulations. This bias exhibits strong regional and seasonal dependence.

[2] Analogous evaluation of the TROPO and STRATO setup is presented in Supplementary Material Fig. S2 and S3

https://doi.org/10.5194/egusphere-2026-3649
Preprint. Discussion started: 9 July 2026

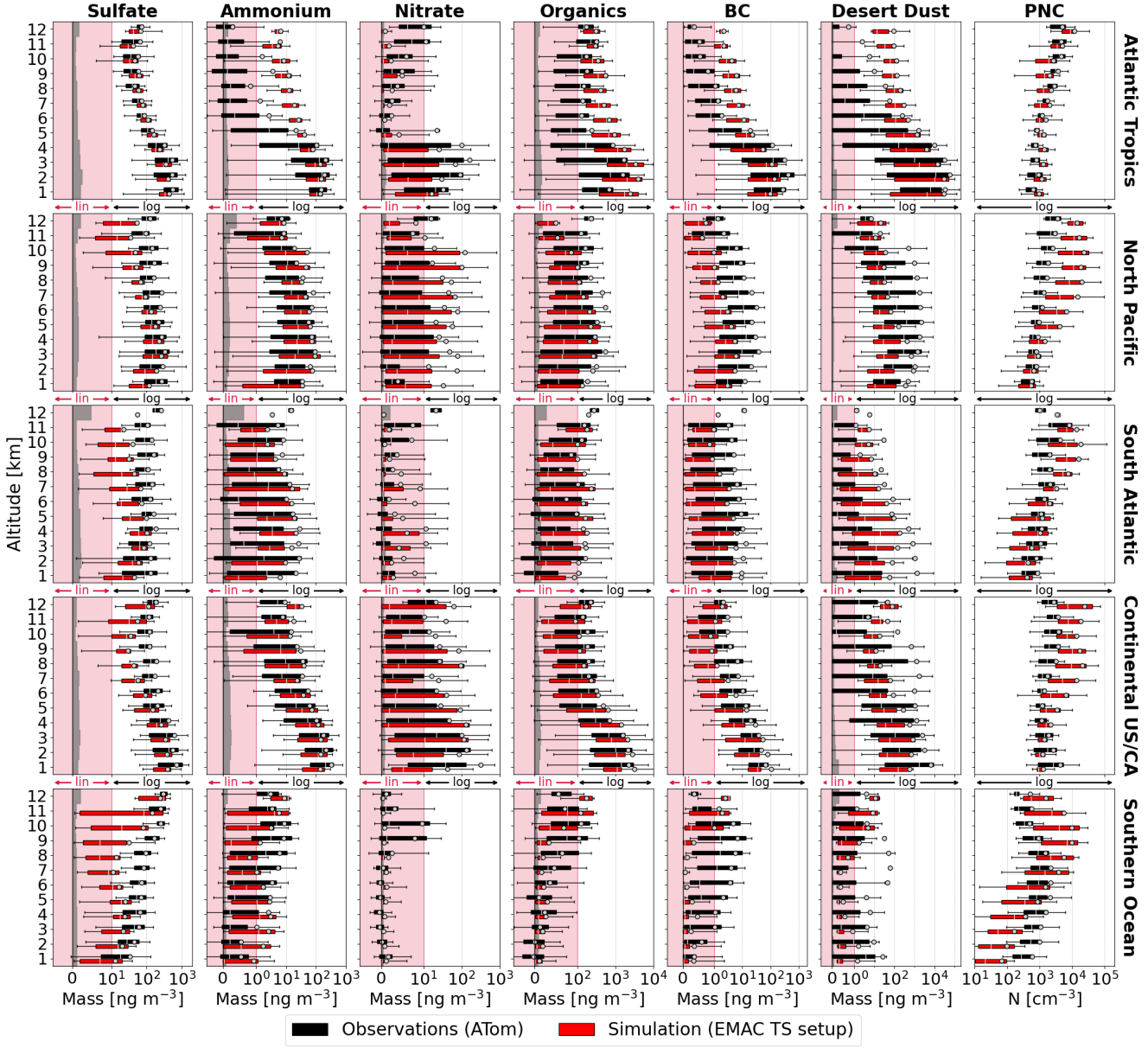

Figure 4. Comparison of simulated (red; TS setup) and observed (black; ATom) mass concentrations of sulfate, ammonium, nitrate, organic aerosol (all PM_1), black carbon (BC; 90—550 nm) and desert dust (0.1–4.8 µm), and particle number concentrations (PNC; 2.7 nm–4.8 µm) across selected regions, as defined in Fig. 1. Grey points indicate mean values, white vertical lines represent medians, boxes show the interquartile range and whiskers the 5th and 95th percentiles. Grey shaded area indicates the altitude-averaged detection limit of the instrument. The pink area marks the linear range of the symlog plots, while the x-scale is logarithmic for higher values. All concentrations are provided at standard temperature and pressure (STP; $T = 273.15\,K$ & $p = 1013.25\,hPa$).

https://doi.org/10.5194/egusphere-2026-3649
Preprint. Discussion started: 9 July 2026

Table 3. Summary of observed mass concentrations of key aerosol species and number concentrations during the ATom mission. Observations are compared to EMAC simulations with the TS, TROPO and STRATO setups, evaluated with statistical metrics defined earlier. For statistical comparison, the medians of observed and simulated values at each region, season and altitude (1 km-binned; see Fig. 4) are used.

	TS				TROPO				STRATO			
	$\overline{M/O}$	PF2	R^2_{log}	RMSLE	$\overline{M/O}$	PF2	R^2_{log}	RMSLE	$\overline{M/O}$	PF2	R^2_{log}	RMSLE
SO_4^{2-}	0.44	49.5	0.31	1.26	0.39	43.1	0.29	1.42	0.58	50.3	0.29	1.2
NH_4^+	1.42	32.7	0.38	1.79	0.69	30.8	0.37	1.98	0.71	28.7	0.36	2.01
NO_3^-	0.24	9.6	0.32	2.55	0.98	10.6	0.12	2.75	2.29	9.1	0.05	2.72
OA	0.7	36.5	0.37	1.5	0.78	33.1	0.38	1.57	1.11	31.2	0.37	1.49
BC	0.63	28.7	0.27	1.89	0.49	30.6	0.34	1.85	0.76	33.3	0.34	1.73
PNC	1.52	49.5	0.25	1.38	2.11	46.3	0.25	1.44	1.5	51.6	0.21	1.3

In certain regions (e.g., Southern Ocean and the Arctic) and during specific seasons, the sulfate underestimation coincides with underestimations of other aerosol species, including ammonium, nitrate, OA, and BC. Schill et al. (2020) demonstrated that biomass burning pollution aerosols are widespread in the FT, with enhanced concentrations in regions and seasons that coincide with the model's most pronounced biases. In Appendix B, we confirm that this underestimation is strongly correlated with biomass burning mass in areas where the model bias is most pronounced. This suggests that either biomass burning emissions or injection altitude is underestimated in the EMAC model. In fact, SO_2 emissions from biomass burning are highly uncertain, and strongly differ between emissions databases (Akagi et al., 2011; Andreae, 2019). In other regions (e.g., South Pacific), the sulfate underestimation occurs independently of other aerosol components. We hypothesize that this may be due to missing emissions from degassing volcanoes or smaller eruptions that contribute to background sulfate in remote regions.

Simulated sulfate aerosol concentrations in the lower 1 to 3 km nicely align with ATom observations in both continental and marine regions using the TS and TROPO setup, while the STRATO setup overestimates BL values. Ammonium concentrations correlate reasonably well ($R^2_{log} = 0.38$) with observations throughout the troposphere, though PF2 values remain low due to high observed variability. Surface nitrate is represented well in the TS setup, with local underestimation at higher altitude. The TROPO and STRATO setups strongly overestimate nitrate at lower altitudes (resulting in higher RMSLE and lower R^2_{log}), especially in dust-dominated regions.

OA and BC are well represented in most regions of the background atmosphere (especially in mid-latitudes), with the exception of the Southern Ocean and the Arctic (as discussed above). Simulated BC, OA and desert dust concentrations slightly increase toward the stratosphere in high latitudes, inconsistent with observations, suggesting overly efficient transport or insufficient scavenging of hydrophobic primary particles in the tropics (see also overestimated desert dust and BC in the Atlantic Tropics FT and UT). The stratospheric overestimation of these species over the Southern Ocean coincides with elevated simulated O_3 above 10 km (Supplementary Material Fig. S9), possibly reflecting different vertical sampling between model and observations. Near the surface, the model reproduces the observed contrast between high BC/OA over the Atlantic

https://doi.org/10.5194/egusphere-2026-3649
Preprint. Discussion started: 9 July 2026

(BC $\sim 100\,\mathrm{ng\,cm^{-3}}$; influenced by Central African biomass burning) and low values over the Pacific (1–2 $\mathrm{ng\,cm^{-3}}$), consistent with Katich et al. (2018). However, concentrations are underestimated at higher altitudes over the Pacific. Dust concentrations generally match observations near the surface, and horizontal dust transport appears to be well represented.

Near the Earth's surface, simulated PNC mostly captures observations, with values ranging from 100 to 1000 particles per $\mathrm{cm^3}$ over the ocean, and slightly higher PNC over background continental regions. However, surface PNC are underestimated by almost an order of magnitude over the Southern Ocean. The current model setup does not yet include recently proposed NPF from MSA and iodic acid (Baccarini et al., 2021; He et al., 2021; Zhang et al., 2025), which may contribute to this underestimation. In most regions, UT PNC is overestimated, likely due to underestimated condensational and coagulation sink (i.e., sulfate concentrations in the same regions; see above). In fact, we show in Appendix B, that in seasons with strongest overestimations in PNC over the Southern Ocean, observed PNC is substantially anti-correlated with observed biomass burning mass concentrations. Conversely, over the Atlantic Tropics and the East Pacific, PNC are slightly underestimated. These regions are closest to the Amazon rainforest and may be influenced by NPF from isoprene oxidation products, as recently discovered by Curtius et al. (2024) and Shen et al. (2024a), which is not yet incorporated into the EMAC model.

The AMP instrument also measured PSDs ranging from 2.7 nm to 4.8 $\mu\mathrm{m}$. Supplementary Material Fig. S8 compares observed PSDs with those simulated using the three different model setups. Due to their modal structure, the simulated PSDs exhibit local minima between modes, which introduces spurious deviations from the observed distributions. In most regions, the TS setup reproduces the observed PSDs well. Over the Southern Ocean, the Aitken and accumulation modes are underestimated (see above). Coarse mode particles appear underestimated in most FT regions; however, observational data in this size range are close to the detection limit (see also Supplementary Material Fig. S4 and S5).

3.3.2 HALO campaigns

While the ATom mission focused on atmospheric background conditions, HALO campaigns primarily aimed at investigating specific processes or regions. Figure 5 summarizes the comparison of the TS simulation with CAFE and EMeRGe observations[3], while Table 4 provides a statistical evaluation of the three model setups against the observations. The TS simulation achieves the best or comparable statistical agreement with observations across most species, except for nitrate. This highlights the capacity of the TS setup to satisfactorily simulate vertical aerosol profiles spanning the BL, FT, and UTLS. The persistent underestimation of nitrate is likely due to a mismatch in the treatment of organic nitrates: in EMAC, organic nitrates are classified as part of OA, whereas the AMS quantifies them as nitrate[4]. A detailed separation of organic and inorganic nitrate (as available for ATom) is essential for a reliable evaluation of nitrate concentrations. However, this separation could not be performed for the HALO campaigns here.

[3] Analogous evaluation of the TROPO and STRATO setup is presented in Supplementary Material Fig. S11.

[4] The same applies to the separation of organic and inorganic sulfate. However, both HR-AMS and PALMS data indicate that the organic sulfate fraction remains consistently below 1% during the ATom missions (Schueneman et al., 2021). This may not necessarily hold for the HALO missions, which are conducted closer to emission source regions, where organic sulfate contributions could be higher.

https://doi.org/10.5194/egusphere-2026-3649
Preprint. Discussion started: 9 July 2026

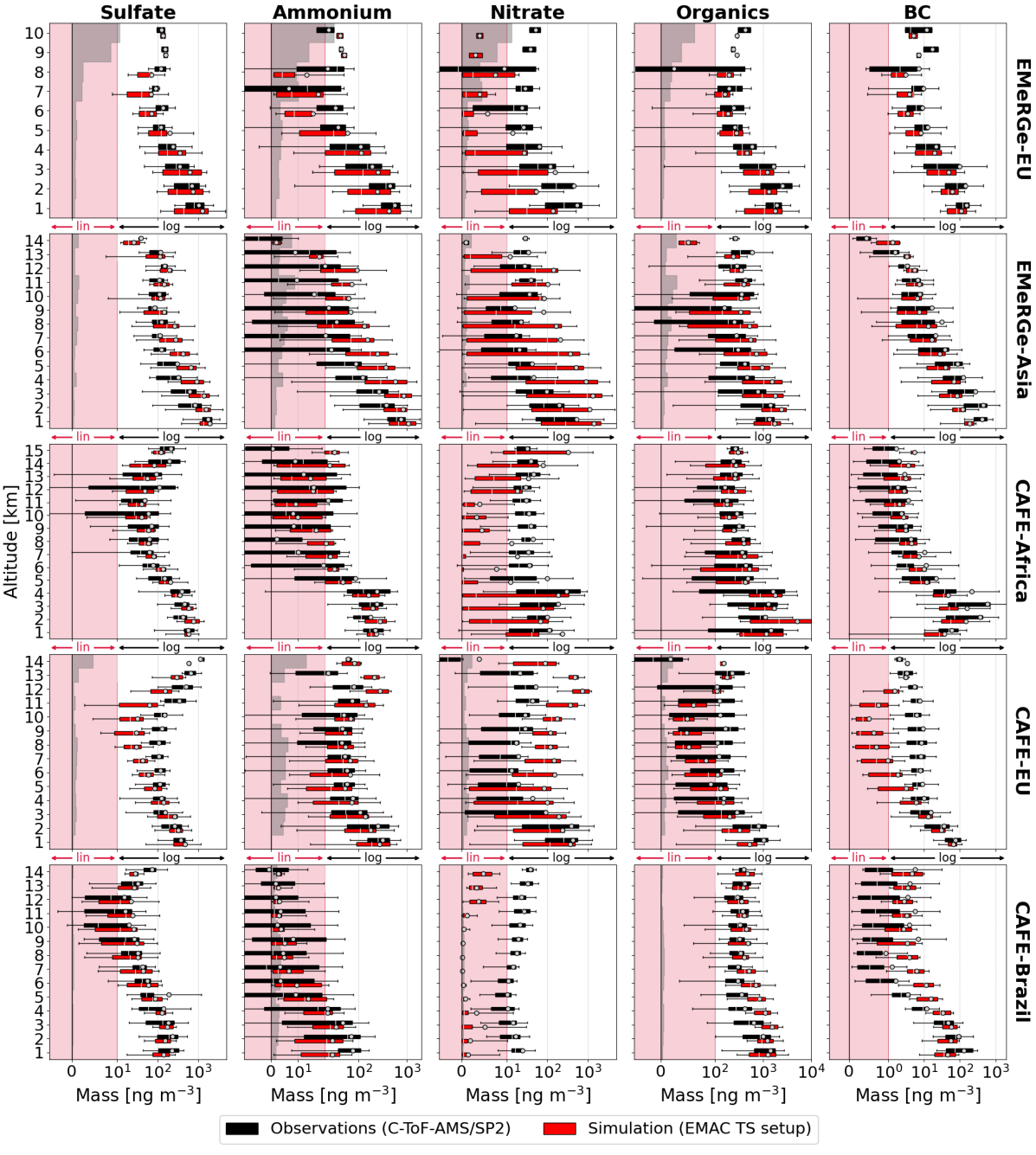

Figure 5. Comparison of simulated (red; TS setup) and observed (black; HALO campaigns) mass concentrations of sulfate, ammonium, nitrate, organic aerosol (all PM_1; C-ToF-AMS), and BC (90—550 nm; SP2). Box-whisker plots follow the format of Fig. 4, as well as the symlog scale. All concentrations are provided at standard temperature and pressure (STP; $T = 273.15\,K$ & $p = 1013.25\,hPa$).

https://doi.org/10.5194/egusphere-2026-3649
Preprint. Discussion started: 9 July 2026

Table 4. Summary of observed mass concentrations of key aerosol species from various HALO campaigns. Observations are compared to EMAC simulations with the TS, TROPO and STRATO setups, evaluated with statistical metrics defined earlier. For statistical comparison, the medians of observed and simulated values of each campaign and altitude (1 km-binned; see Fig. 4) are used.

	TS				TROPO				STRATO			
Spec.	$\overline{M/O}$	PF2	R^2_{log}	RMSLE	$\overline{M/O}$	PF2	R^2_{log}	RMSLE	$\overline{M/O}$	PF2	R^2_{log}	RMSLE
SO_4^{2-}	0.94	70.1	0.7	0.68	1.13	53.7	0.59	0.9	1.79	43.3	0.68	1.01
NH_4^+	1.46	55.2	0.57	1.3	1.35	64.2	0.59	1.32	1.53	46.3	0.58	1.42
NO_3^-	0.25	14.9	0.08	2.92	1.03	16.4	0.06	2.35	2.13	19.4	0.04	2.23
OA	1.0	77.6	0.56	0.63	1.35	65.7	0.53	0.82	1.78	49.3	0.53	0.98
BC	1.04	55.2	0.59	1.13	0.92	52.2	0.59	1.15	1.33	50.7	0.61	1.14

EMeRGe-EU and EMeRGe-Asia focused particularly on polluted megacities and their outflow at lower altitudes, resulting in large BL and FT aerosol concentrations. Observed sulfate concentrations are well reproduced by the model in the lower 5 km, indicating adequate vertical transport at these altitudes. Ammonium, nitrate, and OA are slightly underestimated compared to EMeRGe-EU, but overestimated compared to EMeRGe-Asia. These discrepancies may be due to biases in the emission inventories or the limited horizontal resolution.

The CAFE-Africa and CAFE-Brazil missions aimed to investigate biogenic and biomass burning emissions and their transport in the tropics. Simulated mass concentrations of sulfate, ammonium, OA, and BC agree well with observations for both campaigns, except for a slight overestimation of BC above 4 km during CAFE-Brazil. Simulated nitrate concentrations, however, show strong discrepancies with observations. Schulz et al. (2018) demonstrated that, above the Amazon rainforest, nearly all nitrate is present as organic nitrates. This is further supported by the ATom mission, which sampled a similar region to CAFE-Africa: attributing the observed organic nitrate fraction to OA results in negligible observed inorganic nitrate over the Atlantic Tropics. Therefore, we conclude that the observed nitrate during CAFE-Africa and CAFE-Brazil is virtually entirely organic in nature, and the model's low simulated inorganic nitrate concentrations are consistent with observations, and the model does not represent organic nitrates in the current configuration.

The CAFE-EU mission (2020) investigated the atmospheric impacts of the COVID-19 lockdown, and we applied lockdown-induced anthropogenic emission reductions based on Doumbia et al. (2021). Observations in the BL and lower FT are well reproduced by the model. However, above 4 km, simulated sulfate concentrations underestimate observations, though substantially improved compared to previous EMAC studies (Reifenberg et al., 2022). Joppe et al. (2024) identified that CAFE-EU observations in this altitude range were likely influenced by SO_2 emissions from the Shiveluch volcanic eruption, which were transported zonally in the tropopause region. These emissions were not routinely included in our simulations. The observed overestimation of ammonium in the UT may stem from overestimated detrainment associated with the South Asian monsoon system (see next section), while the concurrent nitrate overestimation is likely driven by the combination of excess ammonium

https://doi.org/10.5194/egusphere-2026-3649
Preprint. Discussion started: 9 July 2026

and low sulfate, favoring ammonium nitrate formation. Ammonium nitrate enhancements in these altitude regions are also observed, albeit at lower magnitude.

3.3.3 Asian monsoon related aircraft campaigns

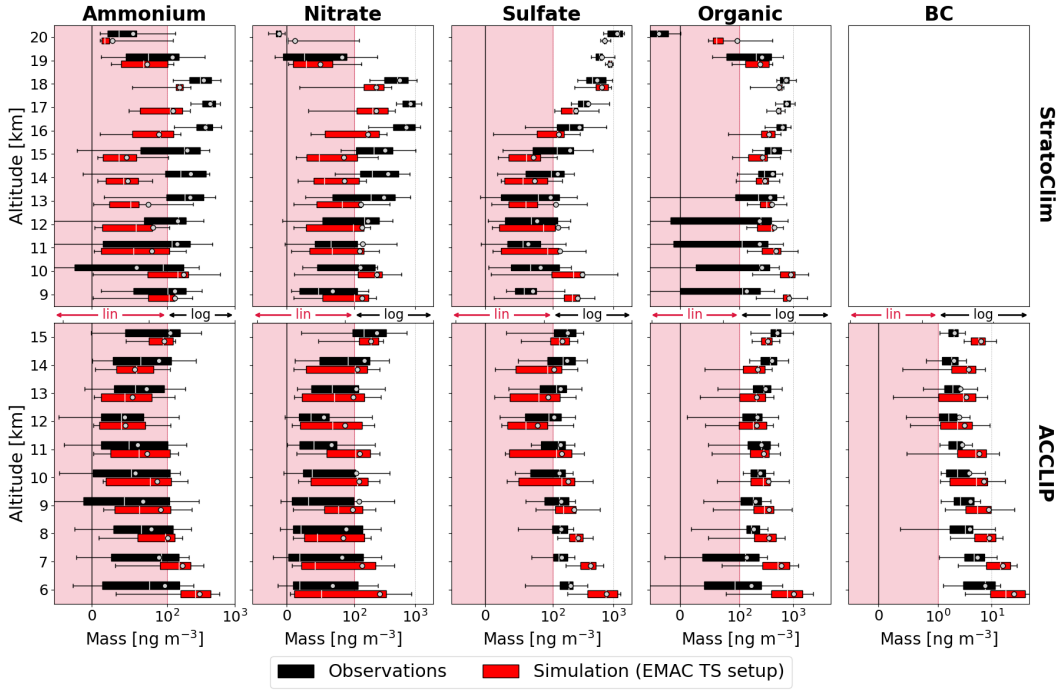

Figure 6. Comparison of simulated (red) and observed (black) mass concentrations of ammonium, nitrate, sulfate, and organic aerosol (all PM1) from ERICA-AMS measurements, during the StratoClim and ACCLIP missions, and black carbon (BC) measurements from the SP2 instrument (only for ACCLIP as BC was not measured during StratoClim). Box-whisker plots follow the format of Fig. 4, as well as the symlog scale. All concentrations are provided at standard temperature and pressure (STP; $T = 273.15\,K$ & $p = 1013.25\,hPa$).

Figure 6 compares simulated (TS setup) aerosol mass concentrations with ERICA-AMS and SP2 (only for ACCLIP) measurements from the StratoClim and ACCLIP campaigns, targeting the ATAL[5]. The evaluation focuses on the UTLS region (12–19 km), where the ATAL forms. While OA and sulfate are overestimated in the BL and lower FT, the ATAL itself is well captured. During StratoClim, enhancements in ammonium, nitrate, and OA were observed but are underestimated in the simulation, likely due to flight planning targeting convective outflow, which the model's coarse horizontal resolution cannot fully resolve. Notably, the upper limit of the ATAL is also well reproduced in the simulations. At 20 km, simulated ammonium, nitrate, and OA mass concentrations tend towards zero, in close agreement with the observations.

[5]Analogous evaluation of the TROPO and STRATO setup is presented in Supplementary Material Fig. S12

https://doi.org/10.5194/egusphere-2026-3649
Preprint. Discussion started: 9 July 2026

The ATAL enhancement observed during the ACCLIP mission is captured by the model. Unlike StratoClim, ACCLIP sampled the ATAL at various stages of its development, making it more representative of the average ATAL, and better reproducable by model simulations. Both campaigns observed low concentrations of primary particles, especially dust and BC, in the ATAL (e.g., Berberich et al., 2025; Ebert et al., 2024; Appel et al., 2022). The model successfully reproduces these low UTLS BC concentrations, with values below 10 $\mathrm{ng\,m^{-3}}$.

Xenofontos et al. (2024, 2025) demonstrated the critical role of ammonia in the formation of the ATAL and UTLS aerosol in general. In Appendix C, we show that recent updates to the CEDS emission inventory, particularly changes in the spatial distribution of ammonia emissions, substantially affect ATAL formation, highlighting the sensitivity of UTLS aerosol to ammonia emissions and the importance of accurate emission representation.

3.4 Stratosphere

Figure 7 presents a timeline of stratospheric AOD (sAOD) from January 2016 to December 2018, comparing GloSSAC observations and model simulation results at 386 nm, 525 nm, and 1020 nm. Additionally, direct OSIRIS and SAGE-III observations are compared to model AOD at 750 nm, along with OMPS-LP observations at 746 nm. The sAOD at 386 nm depends on observations from SAGE-III/ISS, which became operational in mid-2017 (Kovilakam et al., 2023). Additionally, we provide a comparison of zonally averaged aerosol extinction for the considered time period in Supplementary Material Fig. S15. The displayed period was relatively volcanically quiescent (e.g., Schallock et al., 2023), mostly representing background stratospheric conditions. A detailed evaluation of the model's skill to reproduce stratospheric SO_2 injections from explosive volcanic eruptions using the EVER submodel is provided by Kohl et al. (2025).

In general, the simulation with the STRATO setup produces the highest sAOD, while the TROPO setup produces the lowest. This is explained by the underlying size distribution, shown in Supplementary Fig. S17. In the TROPO setup, aerosols rapidly grow into the coarse mode and subsequently sediment from the stratosphere. In contrast, the accumulation mode in the STRATO setup has wider mode boundaries and narrower sigma of the log-normal distribution, which limits growth into the coarse mode, resulting in a more realistic stratospheric size distribution. The introduction of the intermediate mode in the TS setup moderates this effect. While particles still grow into the small coarse mode, sedimentation is reduced compared to the tropospheric setup, although the stratospheric lifetime of the particles slightly decreases compared to the STRATO setup. Especially at higher wavelength (1020 nm), the TS and STRATO setup agree very well.

In addition to the differences between the setups, simulations show systematic deviations from observations (Fig. 7). At northern midlatitudes, the simulated sAOD exhibits seasonality across all wavelengths. This seasonality results from the seasonal stratospheric input of the AMA, likely overestimated in the model. Moreover, a sudden rise in sAOD is observed at northern midlatitudes (August 2017), which is not reproduced by the simulations, likely attributed to the British Columbia wildfires in 2017 (Healy et al., 2019; Daniels et al., 2020; Brühl et al., 2025). While volcanic eruptions are included in the simulations, we did not account for strong wildfires that directly inject particles and precursor gases into the stratosphere (e.g., Ditas et al., 2018; Katich et al., 2023; Ma et al., 2024; Brühl et al., 2025). The observed increase of sAOD in the tropics in mid-2018 coincides with the eruption of the Ambae volcano (Kloss et al., 2020). This eruption is included in the simulations

https://doi.org/10.5194/egusphere-2026-3649
Preprint. Discussion started: 9 July 2026

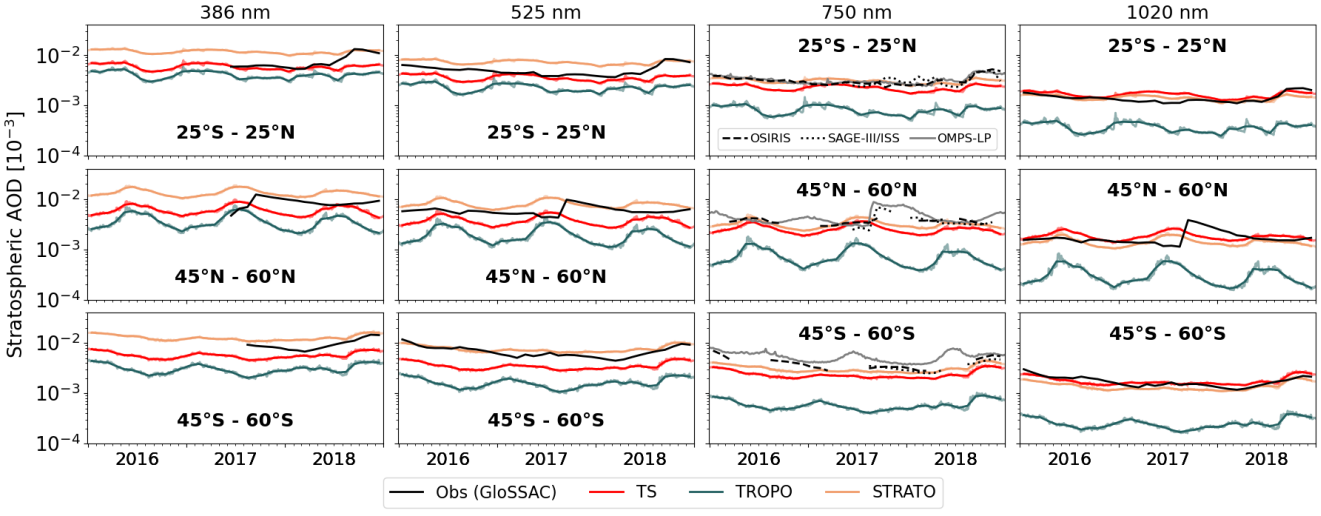

Figure 7. Timeline of simulated stratospheric Aerosol Optical Depth (sAOD) for the three model setups, compared to observations from the GloSSAC database at 386 nm, 525 nm, and 1020 nm, and to OSIRIS (750 nm), SAGE-III (756 nm) and OMPS-LP (746 nm) observations (model AOD at 750 nm). The comparison is subdivided by region: tropics (top), NH midlatitudes (middle), and SH midlatitudes (bottom). Simulated and observed AOD represents monthly averages, with daily model values shown as faint lines.

based on the emission inventory by Schallock et al. (2023), resulting in a slight sAOD enhancement, particularly at 1020 nm, however, magnitude and plume top altitude may be underestimated.

While the TS simulation reasonably reproduces the magnitude of observed sAOD in the tropics and at northern midlatitudes (except during individual events; see above), it underestimates sAOD at southern mid- to high latitudes, particularly when compared with OMPS-LP observations at 746 nm. Whether this discrepancy reflects underestimated aerosol sources or deficiencies in the representation of relevant transport and microphysical processes remains unclear.

4 Global aerosol distributions and composition

Global aerosol distributions and composition from the Earth's surface to the stratosphere are derived from EMAC simulations using the new TS setup, which is found to best reproduce the observed vertical aerosol column. For this analysis, the lower atmosphere and stratosphere is subdivided into four layers based on pressure ranges: the BL (1000–750 hPa), the FT (750–300 hPa), the UTLS (300–85 hPa), and the stratospheric Overworld (OW; 85–10 hPa).

Figure 8 presents global zonally averaged particulate matter (PM) mass concentrations (b) and total PNC (c) within the defined atmospheric layers and across six latitudinal bins, along with the corresponding averaged profiles. The composition of PM in each region and layer is shown in Fig. 9. Figure 10 displays horizontal distributions of individual aerosol components, visualising regional contrasts between polluted and background conditions, which are apparent from in zonal profiles.

https://doi.org/10.5194/egusphere-2026-3649
Preprint. Discussion started: 9 July 2026

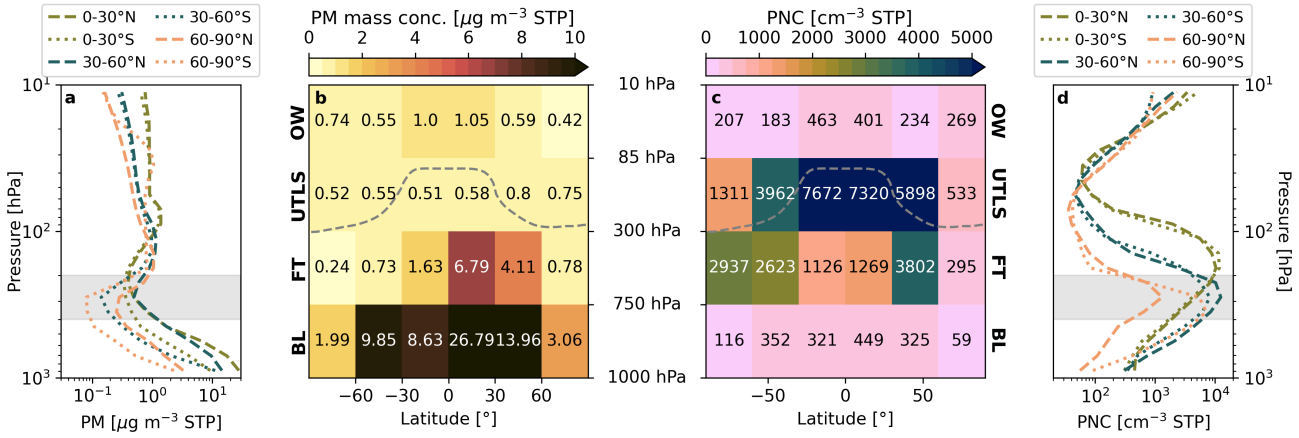

Figure 8. Zonally and annually (2017) averaged simulated global particulate matter (PM) mass (b) and total particle number concentrations (PNC; c) in the boundary layer (BL), the free troposphere (FT), the upper troposphere / lower stratosphere (UTLS), and the stratospheric overworld (OW), along with the corresponding averaged profiles (a,d). The grey dashed line in b and c indicates the zonally and temporally averaged tropopause. The grey shaded area between 400 and 200 hPa in a and d marks the transition region between the FT and the UTLS, where lowest mass concentrations are simulated.

BL aerosol mass concentrations and composition have been extensively studied before using both observations (e.g., Putaud et al., 2004; Zhang et al., 2007; Nault et al., 2021) and models (e.g., Lelieveld et al., 2015; van Donkelaar et al., 2016; Shen et al., 2024b). Dust dominates aerosol mass in tropical and subtropical northern latitudes (up to 70%), primarily due to emissions from the dust belt (see Fig. 10). In densely populated regions OA, sulfate and nitrate dominate, with smaller contributions from ammonium and BC. Over tropical rainforests, OA dominates, either directly from biomass burning as POA or formed via oxidation of biogenic volatile organic compounds (BVOCs) as SOA. Marine regions are characterized by a mixture of sea salt (defined here as bulk sea salt + sodium chloride; exceeding 70% at high southern latitudes) and (sea salt) sulfate aerosol.

The FT at low northern latitudes remains dominated by dust, exhibiting similar spatial patterns to those in the BL, yet more diffuse and reduced in absolute mass concentrations (Fig. 10). The FT is still strongly influenced by surface emissions, mostly driven by convective transport of intermediate strength and outflow altitude (congestus type or weak cumulonimbus) without substantial removal of particles by precipitation. The importance of SOA increases in the FT, as oxygenated semi-volatile organic compounds start to condense at decreasing temperatures.

In the UTLS we can distinguish the UT in the tropics and the lowermost stratosphere at higher latitudes, that are separated by transport barriers (e.g., Gettelman et al., 2011). The tropical UT is mostly influenced by deep convective updrafts, carrying anthropogenic or biogenic precursor gases that can form new particles (mostly SOA here, with additional contributions of ammonium nitrate, particularly in the ATAL). Primary particles, such as dust, BC, and POA are reduced in the tropical UT, as they sediment or are washed out in convective clouds (Lund et al., 2018; Appel et al., 2022; Ebert et al., 2024; Berberich et al., 2025). However, in the NH tropical and subtropical UTLS, significant amounts of dust are present, likely overestimated (see

https://doi.org/10.5194/egusphere-2026-3649
Preprint. Discussion started: 9 July 2026

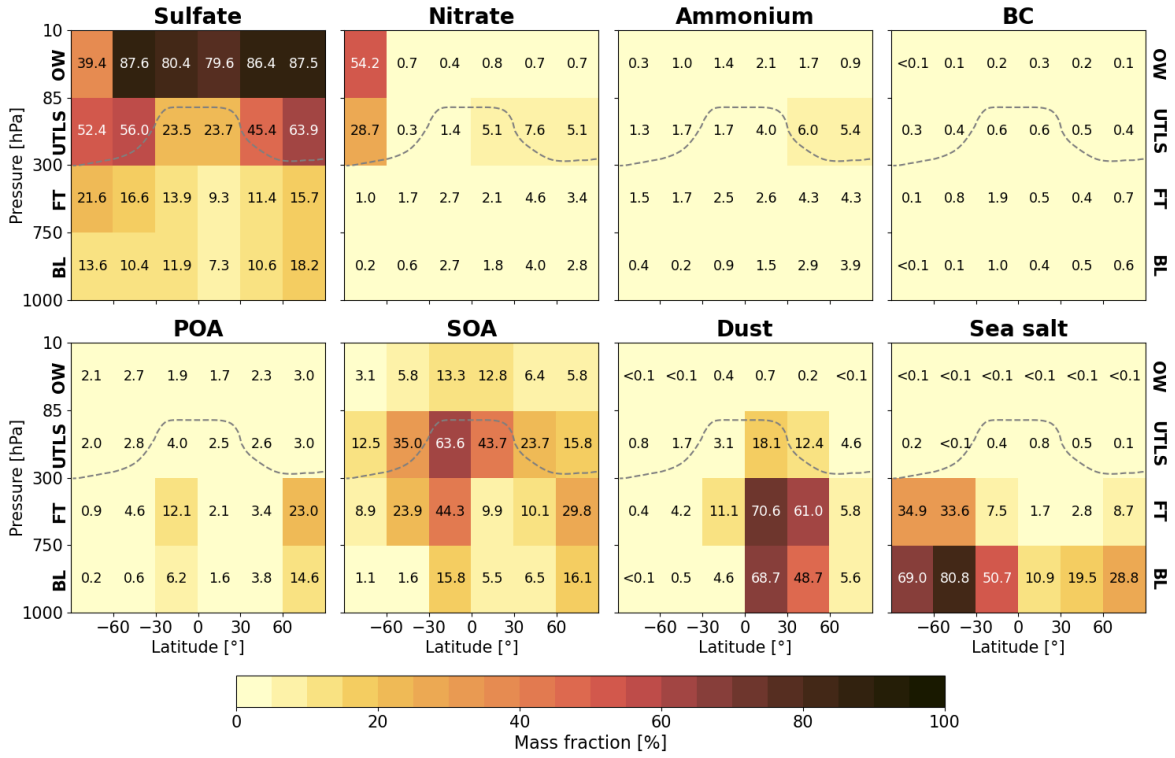

Figure 9. Zonally and annually (2017) averaged simulated aerosol composition of key aerosol species in the lower/middle atmosphere (see Fig. 8). The grey dashed line indicates the zonally and temporally averaged tropopause.

Sect. 3.3.1) due to underestimated wet removal probably related to the representation of parametrised convection as grid box mean mass fluxes.

The stratosphere is strongly dominated by deliquesced sulfate, that forms either as a consequence of OCS transport from the surface, photolytically converted to SO_2, and subsequently oxidized to H_2SO_4, or from explosive volcanic eruptions (e.g., Kremser et al., 2016). In the tropical stratosphere, sulfate accounts for about 75% of the aerosol mass, with a notable 15% contribution from SOA, which decreases rapidly with altitude (see Fig. 11). This decline in SOA with altitude is primarily driven by the evaporation of semi-volatile compounds under increasing temperature in the stratosphere. In the subtropical and polar stratospheric overworld, sulfate fractions increase to around 90%. However, in the southern polar regions, this dominance is reduced due to polar stratospheric cloud formation, leading to an annual average nitrate contribution of up to 54%.

Primary particle abundance is limited in the stratosphere, falling below 3.5% globally in the stratospheric overworld. Recent observations revealed very small amounts of dust in the UTLS and lower stratosphere, below 10 $\mathrm{ng\,m^{-3}}$ (Appel et al., 2022; Ebert et al., 2024), while previous model studies overestimated the importance of dust in the stratosphere (e.g., Brühl et al., 2018; Ma et al., 2019; Bossolasco et al., 2021).

https://doi.org/10.5194/egusphere-2026-3649
Preprint. Discussion started: 9 July 2026

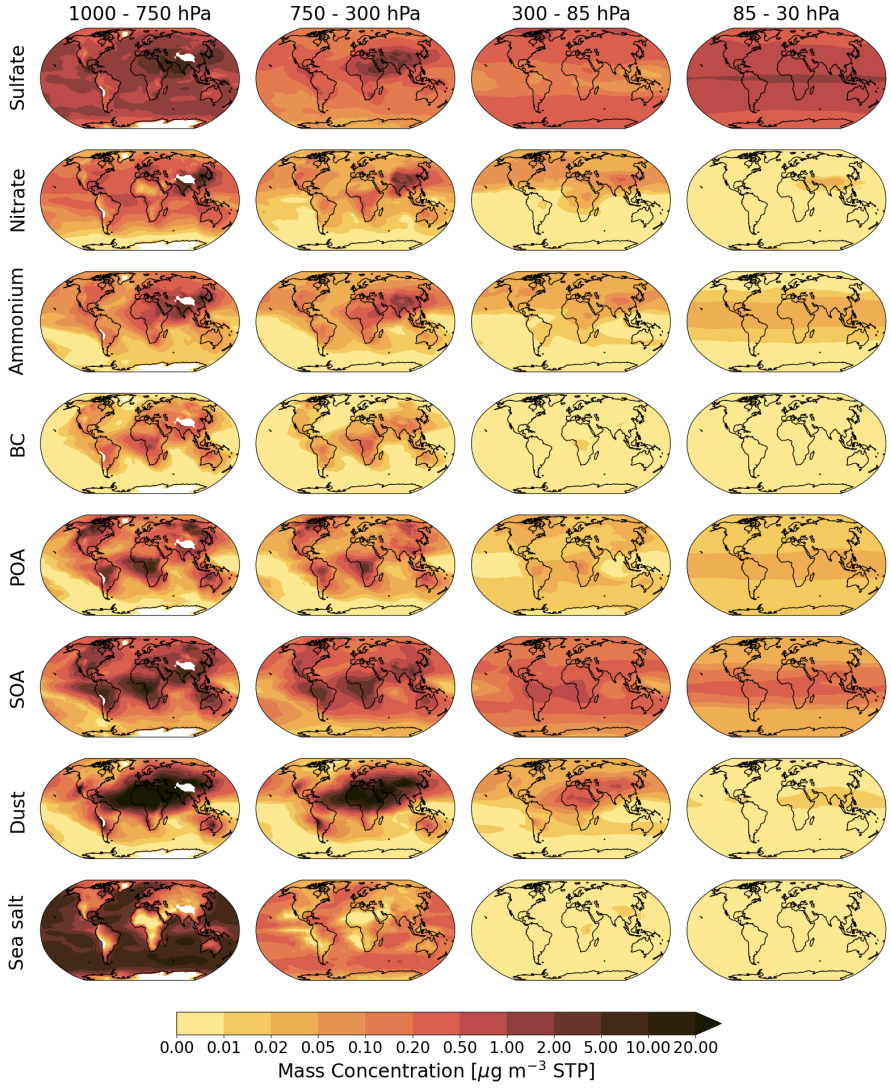

Figure 10. Annually averaged (2017) horizontal distributions of simulated mass concentrations of key aerosol species in the four vertical layers as defined in Fig. 8.

Lowest total aerosol mass concentrations are simulated in the transition between the FT and UTLS, typically between 400 and 200 hPa (grey shaded area in Fig. 8a). BL and stratosphere serve as sources of primary and secondary atmospheric aerosols. Surface emitted primary aerosols are largely removed by wet deposition during convective uplift, while stratospheric influence typically extends only down to the upper FT. This global minimum in PM mass concentrations reduces the condensational and coagulation sink, enabling high PNC (see Fig. 8d). Model evaluation shows slightly underestimated mass in this region, suggesting that contributions from biomass burning or unaccounted volcanic emissions may further suppress PNC. Maximum

https://doi.org/10.5194/egusphere-2026-3649
Preprint. Discussion started: 9 July 2026

PNC occurs at the mass minimum in higher latitudes, while in the tropics, the peak is slightly elevated, likely due to enhanced precursor availability in deep convective outflow. This tropical PNC enhancement just below the tropopause has also been observed by Borrmann et al. (2010) over Brazil, Australia, and Burkina Faso.

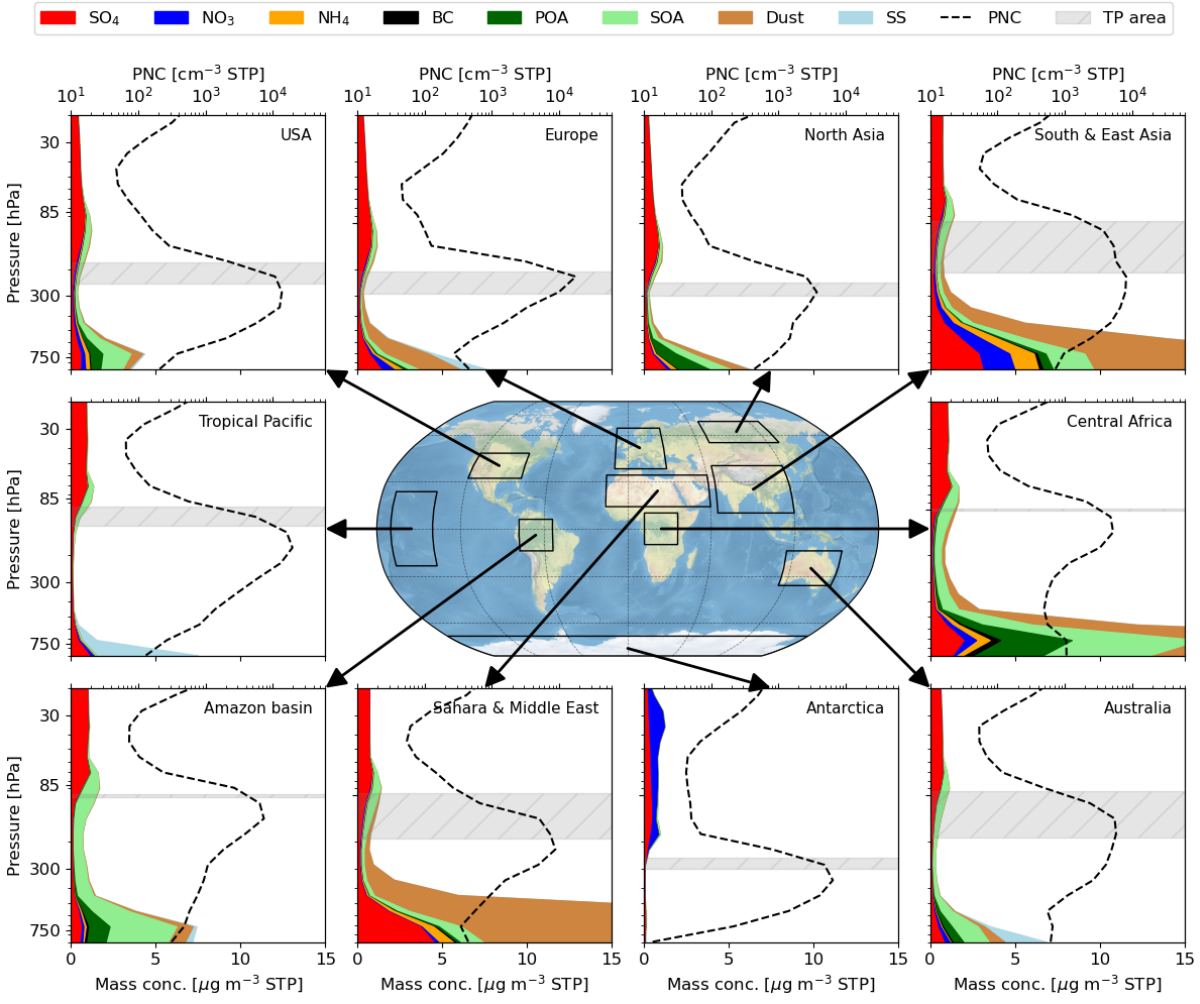

Figure 11. Profiles of simulated annually averaged (2017) aerosol mass concentrations and corresponding composition in selected regions worldwide, spanning from the BL to the stratospheric OW. PNC are shown as black dashed lines. The grey shaded area indicates the range of monthly averaged tropopause altitudes.

Figure 11 provides a more detailed view of aerosol composition profiles across global regions. While BL composition reflects regional surface sources, some consistent global patterns emerge. As previously discussed, all regions exhibit a distinct minimum in PM mass concentrations between 400 and 200 hPa, separating the surface-dominated lower atmosphere from the sulfur chemistry-dominated UT and stratosphere. Only a few intense source regions, such as the Sahara, South and East

https://doi.org/10.5194/egusphere-2026-3649
Preprint. Discussion started: 9 July 2026

Asia, South America, and Central Africa, significantly impact the UTLS and the stratosphere. Above the tropopause, the global Junge layer forms, composed primarily of deliquesced and mostly sulfate droplets.

Elevated OA concentrations are simulated in the UTLS across most regions, diminishing near 70–80 hPa, consistent with StratoClim observations showing organic contributions of $\sim 40\%$ up to 19 km (Appel et al., 2022). Additionally, Fig. 4 and 6 show that lower stratospheric OA mass concentrations are well reproduced, both at the top of the ATAL, and in the lowermost stratosphere over the Southern Ocean and at high northern latitudes. These elevated SOA concentrations in the tropical lower stratosphere (originating from key source regions such as the Amazon basin, Central Africa, and South & East Asia) form a global band (Fig. 10) driven by strong horizontal winds and are transported throughout the UTLS.

Aerosol distributions typically exhibit substantial seasonality, particularly near source regions. For example, the Amazon rainforest transitions between a relatively clean air state during the wet season and a highly polluted regime during the dry season (e.g., Andreae et al., 2015; Pöhlker et al., 2018), while aerosol profiles over South and East Asia are strongly modulated by the monsoon cycle (e.g., Appel et al., 2022; Eppers et al., 2025b). This seasonal variability is not further investigated here, and will be addressed in future studies.

5 Discussion & Limitations

Simulations with the new TS setup provide the best overall agreement with observations across the troposphere and stratosphere. The setup performs comparably to the TROPO setup at the surface and in the BL, and similarly to the STRATO setup in the stratosphere, while most accurately capturing vertical aerosol profiles across the troposphere–stratosphere transition. The key difference lies in the width and geometric standard deviation of the accumulation mode: TROPO enables rapid coarse-mode growth, shortening stratospheric lifetimes, while STRATO suppresses it, prolonging lifetimes. Using either setup outside its intended domain introduces systematic biases: overestimation in the stratosphere (TROPO) and underestimation in the troposphere (STRATO). The additional small coarse mode in the TS setup mitigates these issues: near the surface, it allows modest growth and slightly shorter lifetimes than STRATO; in the stratosphere, it delays coarse-mode formation and enhances longevity relative to TROPO. Thus, the TS setup offers a balanced, physically consistent representation across the lower and middle atmosphere, with a 5–10% increase in computational cost.

Sulfate concentrations are systematically underestimated in the remote FT outside the tropics, while closer to source regions they are well-captured. In the regions with the strongest aerosol mass underestimation, PNC are simultaneously overestimated. Further analysis suggests, that insufficient representation of biomass burning aerosol and volcanic degassing emissions may be responsible for this model bias. Accurately injecting these emissions at appropriate altitudes and magnitudes is crucial for a better global representation. However, current estimates rely primarily on satellite observations with large uncertainties.

Modelling OA formation remains challenging. Here, gas-aerosol partitioning is treated with the ORACLE submodel (Tsimpidi et al., 2014, 2017), specifically developed and evaluated for the lower troposphere. Unlike inorganic partitioning, ORACLE does not account for the Kelvin effect and the kinetic limitations in condensation on available aerosol surfaces, assuming equilibrium partitioning. However, in the FT and UTLS, where aerosol surface areas are low, equilibrium may not be rapidly

https://doi.org/10.5194/egusphere-2026-3649
Preprint. Discussion started: 9 July 2026

achieved due to kinetically limited condensation. Additionally, organic aerosol mixing times, which are critical for aerosol growth and evaporation, are typically below one hour in the BL, supporting equilibrium assumptions. In the FT and UTLS, however, mixing times can extend to several hours, exceeding typical model timesteps, and secondary organic aerosol (SOA) may exist in glassy or highly viscous semi-solid states with low diffusivity (Shiraiwa et al., 2011, 2017; Maclean et al., 2021). These factors likely contribute to an overestimation of OA in the FT, as evidenced by model evaluation near source regions such as the Asian monsoon and the Amazon.

Simulations with the new TS setup reduce desert dust concentrations in the UTLS in line with recent observations (see Sect. 4). In the previous TROPO and STRATO setups, dust was partly emitted into the accumulation mode and, upon ageing, became internally mixed with particles that grew into this mode, averaging $\sim$200 nm diameter. This configuration effectively downscaled the typical dust size (900 nm), enhancing vertical transport and leading to overestimated stratospheric dust. Emitting desert dust into the additional small coarse mode reduces this effect and, thereby, stratospheric dust concentrations. Supplementary Material Fig. S16a illustrates this shift in PSD in desert regions. The accumulation mode is less pronounced in the TS setup, with particles shifting toward larger sizes. Nevertheless, dust in the UTLS remains slightly overestimated. Good model agreement with observed gas-phase tracers such as CO (Supplementary Material Fig. S9 and S10), indicates reasonably accurate vertical transport, suggesting that insufficient wet scavenging, likely due to the grid-box averaged parametrization of convective transport, is the most probable cause of the residual overestimation

The presented simulation results do not include meteoric material or spacecraft debris. Although most significant in the mesosphere, meteoric material is also observed in the lower stratosphere (particularly within the polar vortex) and can extend down to the UTLS (Murphy et al., 1998; Curtius et al., 2005; Murphy et al., 2007; Schneider et al., 2021). Despite its low mass fraction, meteoric material can influence stratospheric aerosol microphysics and chemistry. While the current spacecraft debris loading in the stratosphere is still relatively low, it can already be detected (Murphy et al., 2023), and is predicted to strongly increase in the next decades (Schulz and Glassmeier, 2021).

The evaluation of simulated PNC during the ATom campaign revealed several noteworthy patterns. In most regions of the FT and UTLS, PNC is slightly overestimated (see above). However, the regions closest to the Amazon rainforest exhibit an UT underestimation in PNC, where recent studies suggest that NPF from isoprene oxidation products can occur in the UT (Curtius et al., 2024; Shen et al., 2024a), a process not yet implemented in the model. Additionally, PNC in the BL over the Southern Ocean is underestimated, potentially due to the absence of NPF pathways involving iodic acid and MSA (Baccarini et al., 2021; He et al., 2021; Zhang et al., 2025; He et al., 2026).

Lastly, since all simulations were performed under QCTM conditions, feedbacks between aerosol and gas-phase chemistry and atmospheric dynamics were not included. This simplification, applied to ensure comparability across model setups, may limit the model's ability to reproduce local dynamic effects, such as radiative lofting of volcanic or biomass burning plumes or changes in cloud properties driven by aerosol loading.

https://doi.org/10.5194/egusphere-2026-3649
Preprint. Discussion started: 9 July 2026

6 Conclusions

This study presents global simulations of aerosol distributions and composition from the Earth's surface to the stratosphere using a new EMAC model setup that unifies previous tropospheric and stratospheric configurations using a customized modal size distribution. An additional intermediate mode between the accumulation and coarse mode limits excessive growth into the coarse mode in the stratosphere while preserving accurate boundary layer removal processes.

Comprehensive evaluation against observations shows good agreement across all vertical layers and most geographical regions, demonstrating the setup's ability to represent aerosol distributions consistently in the entire troposphere and stratosphere. Remaining discrepancies and uncertainties are primarily attributed to uncertainties in emissions from biomass burning, degassing volcanoes, and anthropogenic precursor gases. Additional process improvements are likely needed in the removal of insoluble species during convective updrafts, and in the gas–aerosol partitioning of organic compounds in the FT.

Simulations reveal a global minimum in aerosol mass concentrations between 400 and 200 hPa, marking the transition from the FT to the UTLS, and separating boundary layer- and stratospherically-influenced atmospheric domains. This feature coincides with a peak in PNC at altitudes close to or slightly above it, not only in the tropics and subtropics as observed by Williamson et al. (2019), Weigel et al. (2021), and Curtius et al. (2024), but across all latitudes. Further analysis suggests that biomass burning aerosol and volcanic emissions may contribute to reduced aerosol number in the remote FT and UTLS. Given its importance for cloud formation, this transition layer is particularly sensitive to indirect climate effects via aerosol–cloud interactions. Therefore, further studies on these processes are recommended. Additionally, underestimations of PNC in regional UT and in the Southern Ocean boundary layer align with proposed, not yet implemented (but planned), new particle formation pathways from isoprene oxidation products, iodic acid, and MSA.

In the stratosphere, deliquesced sulfur aerosol dominates the Junge layer, consistent with previous findings. SOA contributes $\sim 15\%$ to the tropical stratospheric aerosol burden, but declines sharply with altitude, in line with recent observations, forming a tropical band throughout the UTLS. We find that primary particles contribute less than 3.5% to aerosol mass in the stratospheric overworld, significantly lower than reported by previous model studies, and more consistent with recent observations. The lower abundance of primary particles in the stratosphere is attributed to a revised emission size distribution tailored to the new modal aerosol setup. Further in situ observations of stratospheric aerosol composition are needed to validate these findings.

This study demonstrated the EMAC model's capability to simulate atmospheric aerosols from the surface to the stratosphere, providing first consistent global estimates of key aerosol species across this entire domain, comprehensively evaluated against in-situ aircraft and stationary, as well as remote sensing observations. These simulations offer new insights, especially into the FT and UTLS, regions previously underrepresented in model studies. The newly developed model setup enables future process studies on critical phenomena such as new particle formation in the UT, troposphere–stratosphere exchange, and the transport of wildfire emissions, volcanic emissions, and spacecraft debris, all of which play key roles in shaping atmospheric composition and climate.

https://doi.org/10.5194/egusphere-2026-3649
Preprint. Discussion started: 9 July 2026

Appendix A: Evaluation of surface sea salt concentrations with pseudo-observations

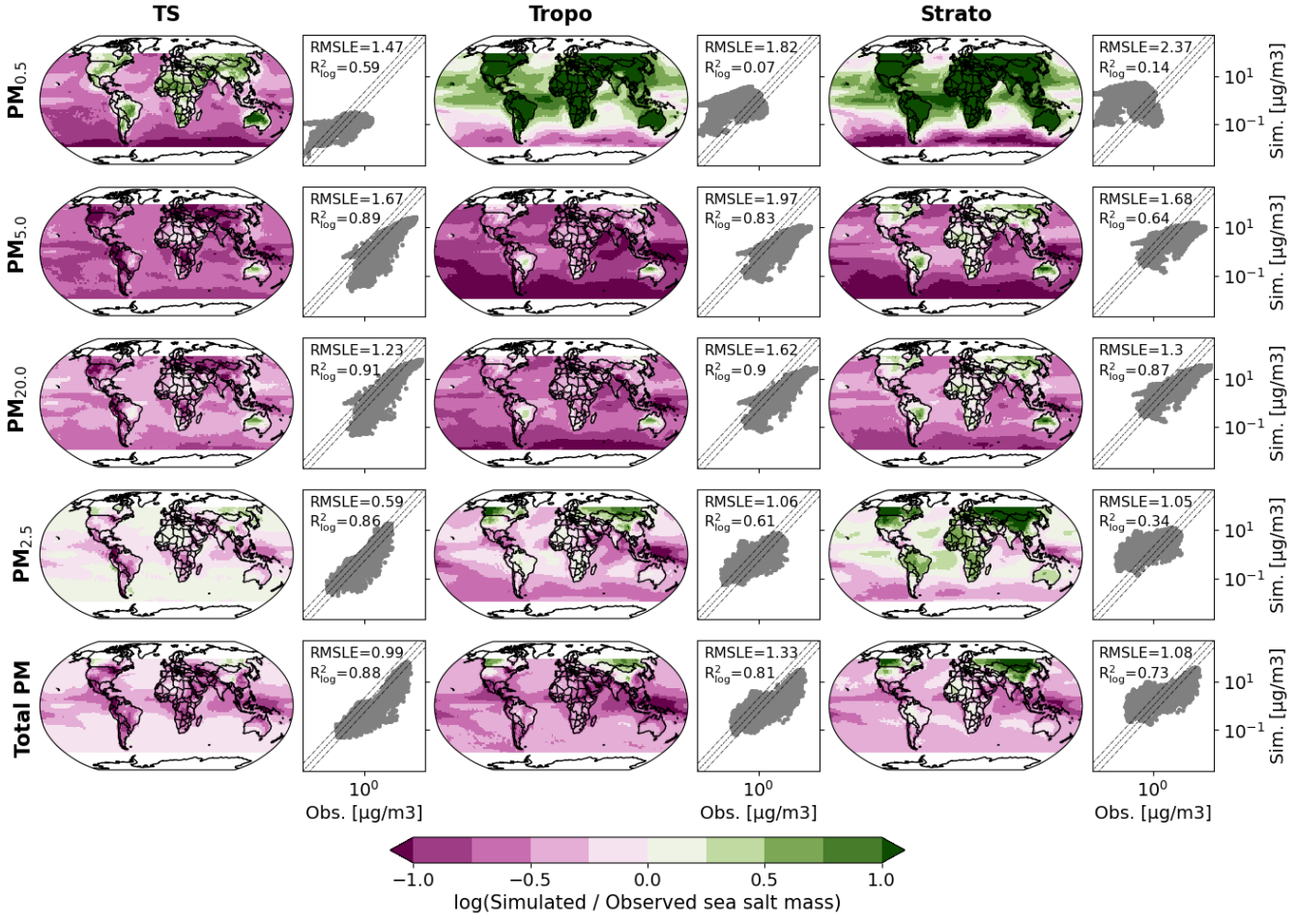

Figure A1. Comparison of simulated (TS, TROPO and STRATO setup) surface sea salt concentrations with different upper size limits to pseudo-observations from CAMS (upper three rows) and MERRA-II (lower 2 rows). Global maps show the ratio of simulated to observed sea salt mass, scatter plots perform a grid box-level comparison.

To better evaluate global sea salt distributions, we compare simulated surface sea salt concentrations from the three model setups (TS, TROPO, and STRATO) with reanalysis data from MERRA-II (Modern-Era Retrospective analysis for Research and Application) and CAMS (Copernicus Atmosphere Monitoring Service). The MERRA-II dataset (Randles et al., 2017; Gelaro et al., 2017) is produced using the GEOS-5 atmospheric model and assimilates observations from the MODIS, MISR, and AVHRR satellite instruments, as well as AERONET ground-based stations. In this study, we use version M2TMNXAER. The CAMS reanalysis product (Inness et al., 2019) is based on the ECMWF Integrated Forecasting System (IFS) and assimilates a broad range of satellite observations, including MODIS and AATSR for AOD. In this study, we use version EAC4

https://doi.org/10.5194/egusphere-2026-3649
Preprint. Discussion started: 9 July 2026

(ECMWF Atmospheric Composition Reanalysis 4). Importantly, these reanalysis datasets are not direct observations but represent pseudo-observations, as they are derived from model simulations and rely on specific assumptions and parameterizations during the assimilation process.

Figure A1 compares modelled sea salt mass concentrations with pseudo-observations across different size cuts. CAMS provides data for PM_{20}, PM_5 and $PM_{0.5}$ (top three rows), while MERRA-II offers $PM_{2.5}$ and total PM (bottom two rows). The TS setup consistently outperforms the TROPO and STRATO configurations in comparison to the pseudo-observations, achieving the lowest RMSLE and highest R^2_{log} across all size bins. The improvement is most pronounced for sub-500 nm particles, where agreement with pseudo-observations is significantly enhanced.

The improvement is mostly due to two changes. First, a large fraction of the sea salt mass that was previously emitted into the accumulation mode is now assigned to the additional mode between the accumulation and coarse mode, better reflecting the observed emission size distribution of sea salt aerosols. This shift reduces the long-range transport of fine sea salt particles and improves the representation of spatial gradients between oceanic and continental regions. Second, evaporation of sea salt particles into smaller modes after cloud-processing (previously permitted) has been explicitly prevented in the TS setup, further limiting their transport and enhancing agreement with observations (see main text) and pseudo-observations. Despite these advances, a bias persists: sea salt concentrations remain slightly underestimated over oceans and slightly overestimated over continents, particularly for small particles.

Appendix B: Impact of biomass burning on remote UTLS

Sulfate concentrations in the background FT outside the tropics are systematically underestimated in the EMAC model (see Sect. 3). Major sources of FT sulfate include SO_2 emissions from volcanic degassing and biomass burning. The largest model biases occur over the Southern Ocean, where underestimations are accompanied by low simulated mass concentrations of ammonium, nitrate, OA and BC.

Model–observation agreement varies strongly with season. Figure B1 shows comparisons over the Southern Ocean during ATom-3 (September–October 2017) and ATom-4 (April/May 2018). During ATom-3, high mass concentrations of aerosols in the FT and UTLS were observed but not captured by the model, whereas agreement is substantially better during ATom-4 and is mostly limited to sulfate. Schill et al. (2020) demonstrated that FT and UTLS over the Southern Ocean and Southern Pacific were strongly influenced by biomass burning aerosol during ATom-3.

Figure B2 shows the correlation between observed sulfate (PM_1) and biomass burning mass (PALMS instrument) during ATom-3 and ATom-4 over the Southern Ocean, with color-coded O_3/CO ratios indicating stratospheric influence. During ATom-3, sulfate and biomass burning mass are strongly correlated, particularly below 4.5 km ($R^2_{log} = 0.58$) and in the UTLS between 7.5 and 10.5 km ($R^2_{log} = 0.52$). During ATom-4, the correlation persists but is weaker, with lower biomass burning influence. This suggests that biomass burning was the dominant sulfate source during ATom-3, while other sources, such as volcanic degassing, may have played a larger role during ATom-4. Nevertheless, the consistent positive correlation across both sub-campaigns indicates that widespread biomass burning aerosol is a key driver of remote sulfate concentrations, as

https://doi.org/10.5194/egusphere-2026-3649
Preprint. Discussion started: 9 July 2026

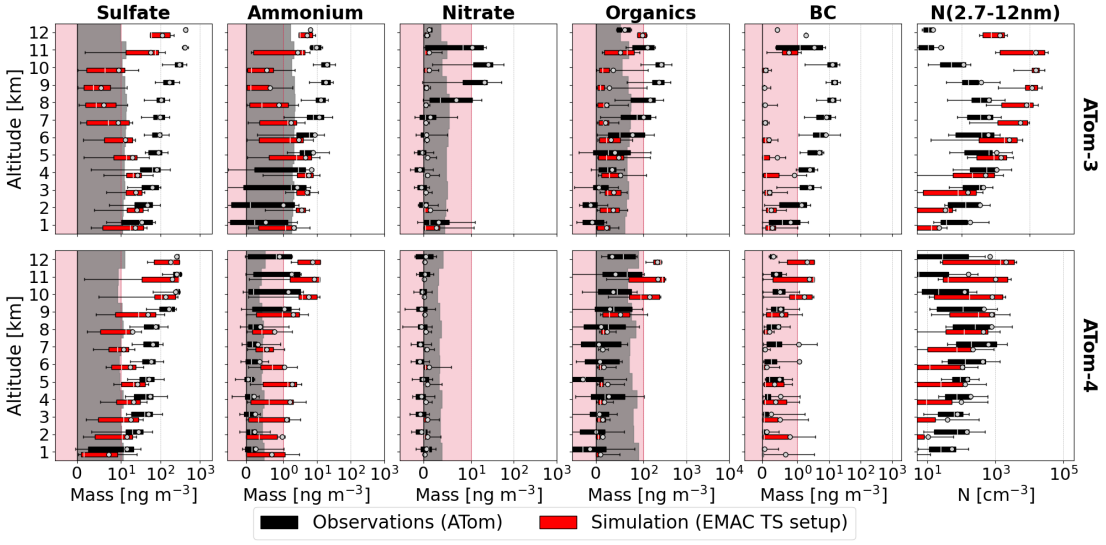

Figure B1. Comparison of simulated (red; TS setup) and observed (black; ATom mission) mass concentrations of sulfate, ammonium, nitrate, organic aerosol (all PM_1) and black carbon (BC; 90—550 nm), concentrations of nucleation mode particles (N_{nucl}; 2.7–12 nm) over the Southern Ocean during ATom-3 (top) and ATom-4 (bottom). Box-Whisker plots as in Fig. 4.

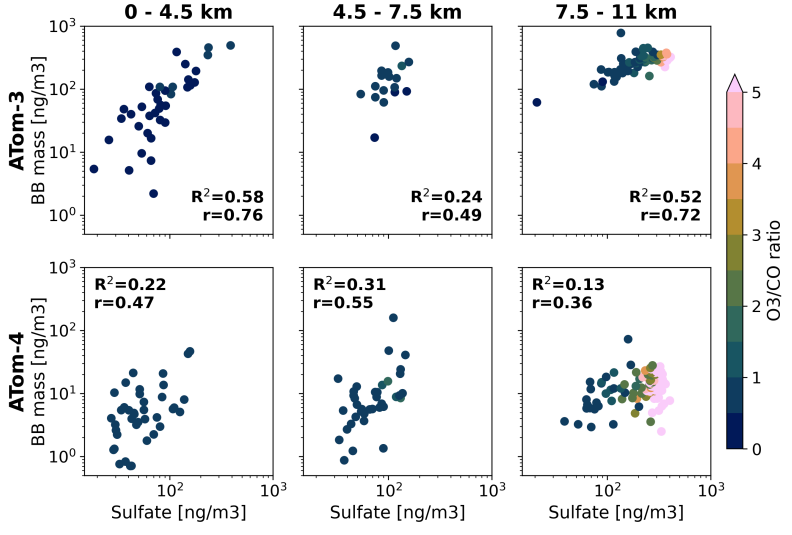

Figure B2. Correlations between observed biomass burning (BB) mass (PALMS) and sulfate (PM_1; AMS) concentrations in different altitude regions during ATom-3 (top) and ATom-4 (bottom). Color represents the O_3/CO ratio as an indicator for stratospheric air.

695 demonstrated by Schill et al. (2020). The correlation only breaks down at high O_3/CO ratio, indicating that these particles are mainly transported within the FT and the UTLS.

https://doi.org/10.5194/egusphere-2026-3649
Preprint. Discussion started: 9 July 2026

Further correlation of biomass burning mass with nucleation mode PNC (N_{nucl}; Fig. B3) during ATom-3 reveals a substantial negative relationship especially in the altitude range between 7.5 and 11 km ($R^2_{log} = 0.58$). This region coincides with pronounced model underestimation of aerosol mass and overestimation of PNC. The observed negative correlation suggests that long-range transported biomass burning aerosol particles suppress NPF and the subsequent growth and transport of newly formed particles by acting as condensation and coagulation sink.

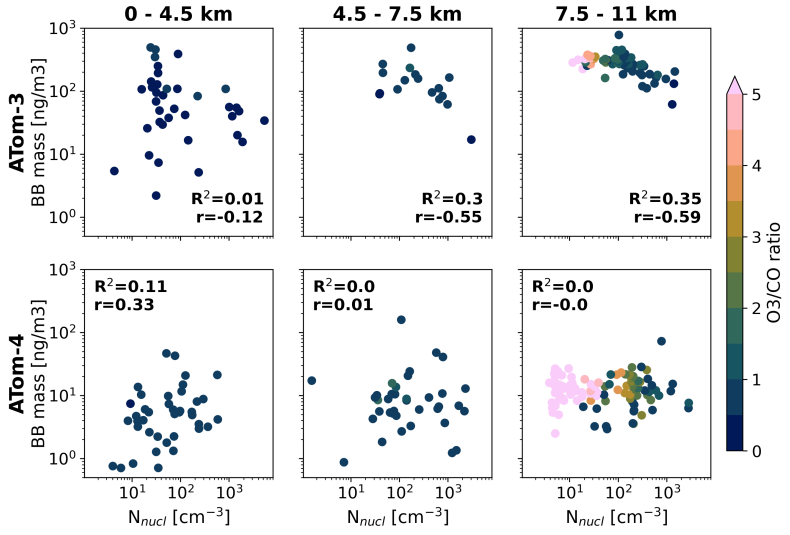

Figure B3. As Fig. B2 with observed concentration of nucleation mode particles (N_{nucl}; 2.7 nm–12 nm) instead of sulfate PM_1.

Appendix C: Sensitivity of simulation results to emission dataset

Emission datasets can be subject to significant uncertainties (e.g., Beusen et al., 2008). The Community Emissions Data System (CEDS) emission database is regularly updated. The most recent version (v2025-04-18) reveals substantial changes in ammonia emissions, with increases or decreases exceeding a factor of 10 in several regions; particularly reductions over the Tibetan Plateau and large parts of North America, North Africa, and North Asia (see Fig. C1).

Particulate ammonium and nitrate concentrations in the atmosphere are highly sensitive to ammonia emissions (e.g., Xenofontos et al., 2024). Figure C2 compares simulations using CEDS version v2021-04-21 with those using the updated version v2025-04-18, revealing that the more recent emission inventory leads to a substantial reduction in ammonium and nitrate concentrations in the ATAL region. This results in reduced agreement with observations, particularly in comparison to the ACCLIP campaign data.

https://doi.org/10.5194/egusphere-2026-3649
Preprint. Discussion started: 9 July 2026

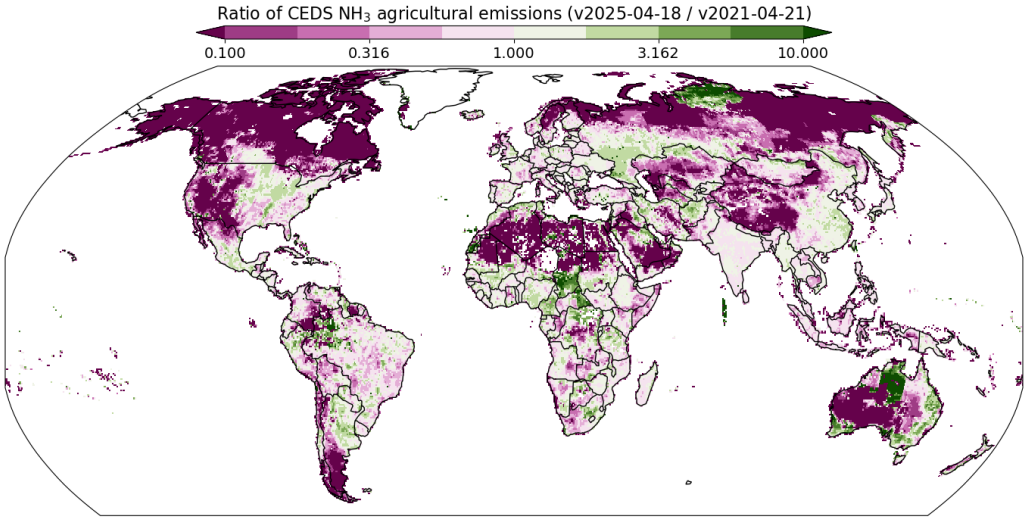

Figure C1. Changes in agricultural NH_3 emissions from CEDS v2021-04-21 to CEDS v2025-04-18 for the year 2017.

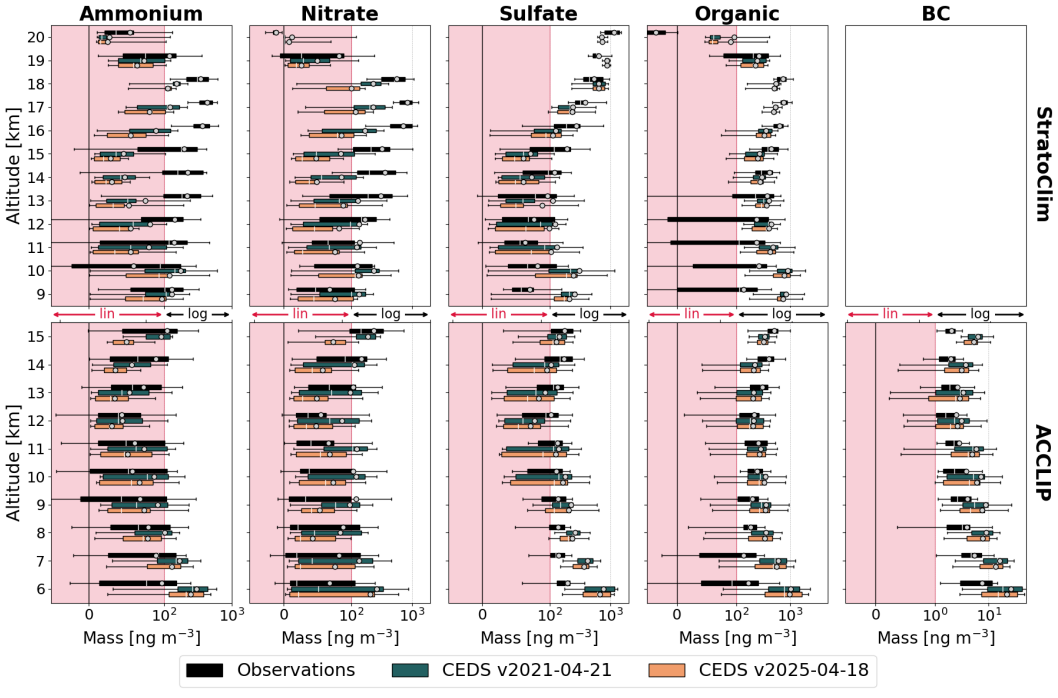

Figure C2. Comparison of simulations with the TS simulations using the emission datasets CEDS v2021-04-21 and CEDS v2025-04-18 with observations from the StratoClim and ACCLIP mission. Box-whisker plots follow the format of Fig. 4

https://doi.org/10.5194/egusphere-2026-3649
Preprint. Discussion started: 9 July 2026

Code and data availability. The Modular Earth Submodel System (MESSy, https://zenodo.org/communities/messy) is continuously further developed and applied by a consortium of institutions. The usage of MESSy and access to the source code is licenced to all affiliates of institutions which are members of the MESSy Consortium. Institutions can become a member of the MESSy Consortium by signing the MESSy Memorandum of Understanding. More information can be found on the MESSy Consortium Website (http://www.messy-interface.org). The code applied for the presented simulations is available via https://doi.org/10.5281/zenodo.20199551 (The MESSy consortium, 2025).

The GHOST dataset is publicly available via https://doi.org/10.5281/zenodo.15075961 (Bowdalo and Grodofzig, 2025). Supplementary EANET data (not included in the GHOST dataset due to data rights limitations) were obtained from https://monitoring.eanet.asia/document/public/index(EANET, 2026).

ATom observations are generally available from https://www.earthdata.nasa.gov/data/projects/atom/data-access-tools. The respective used datasets are available via https://doi.org/10.3334/ORNLDAAC/1716 (HR-AMS; Jimenez et al., 2019), https://doi.org/10.3334/ORNLDAAC/1672 (NOAA SP2; Schwarz and Katich, 2019), https://doi.org/10.3334/ORNLDAAC/1671 (AMP – Aerosol Microphysical Properties; Brock et al., 2019a), https://doi.org/10.3334/ORNLDAAC/1733 (PALMS biomass burning and sea salt mass; Froyd et al., 2021), https://doi.org/10.3334/ORNLDAAC/2006 (PALMS desert dust; Froyd et al., 2022a), https://doi.org/10.3334/ORNLDAAC/1734 (NO_yO_3 – NO; Ryerson et al., 2019), https://doi.org/10.3334/ORNLDAAC/1732 (Picarro – CO; McKain and Sweeney, 2021), https://doi.org/10.3334/ORNLDAAC/1930 (ATHOS – OH; Brune et al., 2021), https://doi.org/10.3334/ORNLDAAC/1927 (CIT-CIMS – SO_2 & HNO_3; Allen et al., 2021),https://doi.org/10.3334/ORNLDAAC/1750 (UCATS – O_3; Elkins et al., 2020).

C-ToF-AMS observations from the HALO campaigns are available on the HALO database https://halo-db.pa.op.dlr.de/ (HALO, 2026), BC measurements from the HALO campaigns are available on request.

ERICA-AMS measurements for StratoClim are published at https://doi.org/10.17617/3.8X (Appel, 2022), ACCLIP ERICA-AMS measurements are available at https://doi.org/10.26023/T7RT-01YD-A110 (Eppers et al., 2025a), and ACCLIP BC measurements are taken from https://doi.org/10.26023/NTV8-17K4-5V0G (Schwarz et al., 2022).

GloSSAC observations are publicly available at https://doi.org/10.5067/GLOSSAC-L3-V2.21 (Thomason, 2023). MODIS AOD was taken from https://doi.org/10.5067/MODIS/MOD08_D3.061 (Platnick et al., 2015), and AERONET AOD from https://aeronet.gsfc.nasa.gov/ (AERONET, 2026). OMPS-LP Level-2 v2.1.0 data is available at https://doi.org/10.5281/zenodo.20765257 (Zawada et al., 2026).

Scientific colour maps (https://doi.org/10.5281/zenodo.5501399; Crameri, 2021) are used in this study to prevent visual distortion of the data and exclusion of readers with colour vision deficiencies (Crameri et al., 2020).

Author contributions. M.K. and A.P. planned the research. M.K. developed the new model setup with the help of A.P., C.B., H.T., C.X., T.C., and S.G. . M.K. performed and evaluated the simulations, analysed the results, and wrote the manuscript. O.A., S.B., A.B., P.C.-J., Y.C., O.E., K.D.F., B.A.H, J.L.J., P.Jop., A.K., K.Ka., J.M.K., F.K., C.P., M.L.P., U.P., L.R., G.P.S., J.S., C.S., J.P.S., C.J.W., Y.Y., and D.Z. provided observational datasets. P.Jöc., K.Kl., A.M., S.R., A.P.T., and R.V. contributed via testing and discussion on the new setup. J.L., H.T., and A.P. supervised the work. All authors contributed to the editing of the manuscript.

Competing interests. At least three of the (co-)authors are members of the editorial board of Atmospheric Chemistry and Physics.

https://doi.org/10.5194/egusphere-2026-3649
Preprint. Discussion started: 9 July 2026

Acknowledgements. We acknowledge the contributions of Charles A. Brock for measurements of aerosol microphysical properties and Daniel M. Murphy for the PALMS measurements. We thank the research groups responsible for the surface $PM_{2.5}$ observations included in the GHOST dataset. We gratefully acknowledge the teams operating the MODIS instrument for providing AOD data. We also thank the AERONET teams for establishing and maintaining the ground-based measurement sites used in this study, and for their ongoing provision of high-quality AOD data. We thank M. Dolores Andrés-Hernández and John P. Burrows for their leadership in planning and coordinating the EMeRGe mission. The model simulations have been performed at the German Climate Computing Centre (DKRZ) through support from the Max Planck Society.

M.K., A.M., and S.R. acknowledge the financial support of the Max Planck Graduate Center with the Johannes Gutenberg University (Mainz). M.K., O.E., P.Jöc, P.Jop, F.K, J.S., and H.T. acknowledge funding support from the Deutsche Forschungsgemeinschaft (DFG, German Research Foundation) – TRR 301 – Project-ID 428312742. M.K. and S.G. acknowledge funding support of the European Commission Horizon Europe project FOCI (Grant Agreement No 101056783). T.C. acknowledges funding support from the European Union's Horizon 2020 research and innovation programme under grant agreement No. 856612 and the Cyprus Government. O.A. acknowledges the support by the NSFC–DFG 2020 project ATAL-track (BO 1829/12-1). J.S. acknowledges support from the DFG through the priority program HALO-SPP 1294 (project IDs 316589531 and 461448963). A.K. acknowledges support by the Austrian Science Fund FWF's Erwin Schrodinger Fellowship J-3613. P.C.-J. and J.L.J. acknowledge NASA Support, Grants NNX15AH33A, NNX15AJ23G and 80NSSC23K0828.

https://doi.org/10.5194/egusphere-2026-3649
Preprint. Discussion started: 9 July 2026

References

AERONET: AERosol RObotic NETwork - AOD Level 2.0, NASA Goddard Space Flight Center [data set], https://aeronet.gsfc.nasa.gov/new_web/download_all_v3_aod.html, last access: 19 June 2026, 2026.

Akagi, S. K., Yokelson, R. J., Wiedinmyer, C., Alvarado, M. J., Reid, J. S., Karl, T., Crounse, J. D., and Wennberg, P. O.: Emission factors for open and domestic biomass burning for use in atmospheric models, Atmospheric Chemistry and Physics, 11, 4039–4072, https://doi.org/10.5194/acp-11-4039-2011, 2011.

Allen, H., Crounse, J., Kim, M., Teng, A., Xu, L., and Wennberg, P.: ATom: In Situ Data from Caltech Chemical Ionization Mass Spectrometer (CIT-CIMS), V2, ORNL Distributed Active Archive Center [data set], https://doi.org/10.3334/ORNLDAAC/1927, 2021.

Andreae, M. O.: Emission of trace gases and aerosols from biomass burning – an updated assessment, Atmospheric Chemistry and Physics, 19, 8523–8546, https://doi.org/10.5194/acp-19-8523-2019, 2019.

Andreae, M. O., Acevedo, O. C., Araùjo, A., Artaxo, P., Barbosa, C. G. G., Barbosa, H. M. J., Brito, J., Carbone, S., Chi, X., Cintra, B. B. L., da Silva, N. F., Dias, N. L., Dias-Júnior, C. Q., Ditas, F., Ditz, R., Godoi, A. F. L., Godoi, R. H. M., Heimann, M., Hoffmann, T., Kesselmeier, J., Könemann, T., Krüger, M. L., Lavric, J. V., Manzi, A. O., Lopes, A. P., Martins, D. L., Mikhailov, E. F., Moran-Zuloaga, D., Nelson, B. W., Nölscher, A. C., Santos Nogueira, D., Piedade, M. T. F., Pöhlker, C., Pöschl, U., Quesada, C. A., Rizzo, L. V., Ro, C.-U., Ruckteschler, N., Sá, L. D. A., de Oliveira Sá, M., Sales, C. B., dos Santos, R. M. N., Saturno, J., Schöngart, J., Sörgel, M., de Souza, C. M., de Souza, R. A. F., Su, H., Targhetta, N., Tóta, J., Trebs, I., Trumbore, S., van Eijck, A., Walter, D., Wang, Z., Weber, B., Williams, J., Winderlich, J., Wittmann, F., Wolff, S., and Yáñez Serrano, A. M.: The Amazon Tall Tower Observatory (ATTO): overview of pilot measurements on ecosystem ecology, meteorology, trace gases, and aerosols, Atmospheric Chemistry and Physics, 15, 10 723–10 776, https://doi.org/10.5194/acp-15-10723-2015, 2015.

Andrés Hernández, M. D., Hilboll, A., Ziereis, H., Förster, E., Krüger, O. O., Kaiser, K., Schneider, J., Barnaba, F., Vrekoussis, M., Schmidt, J., Huntrieser, H., Blechschmidt, A.-M., George, M., Nenakhov, V., Harlass, T., Holanda, B. A., Wolf, J., Eirenschmalz, L., Krebsbach, M., Pöhlker, M. L., Kalisz Hedegaard, A. B., Mei, L., Pfeilsticker, K., Liu, Y., Koppmann, R., Schlager, H., Bohn, B., Schumann, U., Richter, A., Schreiner, B., Sauer, D., Baumann, R., Mertens, M., Jöckel, P., Kilian, M., Stratmann, G., Pöhlker, C., Campanelli, M., Pandolfi, M., Sicard, M., Gómez-Amo, J. L., Pujadas, M., Bigge, K., Kluge, F., Schwarz, A., Daskalakis, N., Walter, D., Zahn, A., Pöschl, U., Bönisch, H., Borrmann, S., Platt, U., and Burrows, J. P.: Overview: On the transport and transformation of pollutants in the outflow of major population centres – observational data from the EMeRGe European intensive operational period in summer 2017, Atmospheric Chemistry and Physics, 22, 5877–5924, https://doi.org/10.5194/acp-22-5877-2022, 2022.

Appel, O.: ERICA-MS-Data StratoClim2017, Edmond [data set], https://doi.org/10.17617/3.8X, 2022.

Appel, O., Köllner, F., Dragoneas, A., Hünig, A., Molleker, S., Schlager, H., Mahnke, C., Weigel, R., Port, M., Schulz, C., Drewnick, F., Vogel, B., Stroh, F., and Borrmann, S.: Chemical analysis of the Asian tropopause aerosol layer (ATAL) with emphasis on secondary aerosol particles using aircraft-based in situ aerosol mass spectrometry, Atmospheric Chemistry and Physics, 22, 13 607–13 630, https://doi.org/10.5194/acp-22-13607-2022, 2022.

Baccarini, A., Dommen, J., Lehtipalo, K., Henning, S., Modini, R. L., Gysel-Beer, M., Baltensperger, U., and Schmale, J.: Low-Volatility Vapors and New Particle Formation Over the Southern Ocean During the Antarctic Circumnavigation Expedition, Journal of Geophysical Research: Atmospheres, 126, e2021JD035 126, https://doi.org/10.1029/2021JD035126, 2021.

Berberich, J., Jacoby, S. A., Michailoudi, G., Schwarz, J. P., Viciani, S., D'Amato, F., Bianchini, G., Barucci, M., Campos, T., Ullman, K., Podolske, J. R., Gurganus, C., Smith, W. P., Ueyama, R., Honomichl, S. B., Pan, L. L., Woods, S., Wienzierl, B., Dollner, M., and Perring,

https://doi.org/10.5194/egusphere-2026-3649
Preprint. Discussion started: 9 July 2026

A. E.: Black Carbon Reflects Extremely Efficient Aerosol Wet Removal in Monsoonal Convective Transport, Journal of Geophysical Research: Atmospheres, 130, e2024JD042 692, https://doi.org/10.1029/2024JD042692, 2025.

Beusen, A., Bouwman, A., Heuberger, P., Van Drecht, G., and Van Der Hoek, K.: Bottom-up uncertainty estimates of global ammonia emissions from global agricultural production systems, Atmospheric Environment, 42, 6067–6077, https://doi.org/10.1016/j.atmosenv.2008.03.044, 2008.

Borrmann, S., Kunkel, D., Weigel, R., Minikin, A., Deshler, T., Wilson, J. C., Curtius, J., Volk, C. M., Homan, C. D., Ulanovsky, A., Ravegnani, F., Viciani, S., Shur, G. N., Belyaev, G. V., Law, K. S., and Cairo, F.: Aerosols in the tropical and subtropical UT/LS: in-situ measurements of submicron particle abundance and volatility, Atmospheric Chemistry and Physics, 10, 5573–5592, https://doi.org/10.5194/acp-10-5573-2010, 2010.

Bossolasco, A., Jegou, F., Sellitto, P., Berthet, G., Kloss, C., and Legras, B.: Global modeling studies of composition and decadal trends of the Asian Tropopause Aerosol Layer, Atmospheric Chemistry and Physics, 21, 2745–2764, https://doi.org/10.5194/acp-21-2745-2021, 2021.

Boucher, O.: Atmospheric Aerosols, pp. 9–24, Springer Netherlands, Dordrecht, ISBN 978-94-017-9649-1, https://doi.org/10.1007/978-94-017-9649-1_2, 2015.

Bourassa, A. E., Rieger, L. A., Lloyd, N. D., and Degenstein, D. A.: Odin-OSIRIS stratospheric aerosol data product and SAGE III intercomparison, Atmospheric Chemistry and Physics, 12, 605–614, https://doi.org/10.5194/acp-12-605-2012, 2012.

Bourassa, A. E., Zawada, D. J., Rieger, L. A., Warnock, T. W., Toohey, M., and Degenstein, D. A.: Tomographic Retrievals of Hunga Tonga-Hunga Ha'apai Volcanic Aerosol, Geophysical Research Letters, 50, e2022GL101 978, https://doi.org/https://doi.org/10.1029/2022GL101978, 2023.

Bowdalo, D. and Grodofzig, R.: GHOST: A globally harmonised dataset of surface atmospheric composition measurements, Zenodo [data set], https://doi.org/10.5281/zenodo.15075961, 2025.

Bowdalo, D., Basart, S., Guevara, M., Jorba, O., Pérez García-Pando, C., Jaimes Palomera, M., Rivera Hernandez, O., Puchalski, M., Gay, D., Klausen, J., Moreno, S., Netcheva, S., and Tarasova, O.: GHOST: a globally harmonised dataset of surface atmospheric composition measurements, Earth System Science Data, 16, 4417–4495, https://doi.org/10.5194/essd-16-4417-2024, 2024.

Brock, C., Kupc, A., Williamson, C., Froyd, K., Erdesz, F., Murphy, D., Schill, G., Gesler, D., McLaughlin, R., Richardson, M., Wagner, N., and Wilson, J.: ATom: L2 In Situ Measurements of Aerosol Microphysical Properties (AMP), ORNL Distributed Active Archive Center [data set], https://doi.org/10.3334/ORNLDAAC/1671, 2019a.

Brock, C. A., Williamson, C., Kupc, A., Froyd, K. D., Erdesz, F., Wagner, N., Richardson, M., Schwarz, J. P., Gao, R.-S., Katich, J. M., Campuzano-Jost, P., Nault, B. A., Schroder, J. C., Jimenez, J. L., Weinzierl, B., Dollner, M., Bui, T., and Murphy, D. M.: Aerosol size distributions during the Atmospheric Tomography Mission (ATom): methods, uncertainties, and data products, Atmospheric Measurement Techniques, 12, 3081–3099, https://doi.org/10.5194/amt-12-3081-2019, 2019b.

Brühl, C., Lelieveld, J., Crutzen, P. J., and Tost, H.: The role of carbonyl sulphide as a source of stratospheric sulphate aerosol and its impact on climate, Atmospheric Chemistry and Physics, 12, 1239–1253, https://doi.org/10.5194/acp-12-1239-2012, 2012.

Brühl, C., Schallock, J., Klingmüller, K., Robert, C., Bingen, C., Clarisse, L., Heckel, A., North, P., and Rieger, L.: Stratospheric aerosol radiative forcing simulated by the chemistry climate model EMAC using Aerosol CCI satellite data, Atmospheric Chemistry and Physics, 18, 12 845–12 857, https://doi.org/10.5194/acp-18-12845-2018, 2018.

https://doi.org/10.5194/egusphere-2026-3649
Preprint. Discussion started: 9 July 2026

Brühl, C., Kohl, M., and Lelieveld, J.: Radiative forcing and stratospheric ozone changes due to major forest fires and recent volcanic eruptions including Hunga Tonga, Atmospheric Chemistry and Physics, 25, 18 697–18 718, https://doi.org/10.5194/acp-25-18697-2025, 2025.

Brune, W., Miller, D., and Thames, A.: ATom: Measurements from Airborne Tropospheric Hydrogen Oxides Sensor (ATHOS), V2, ORNL Distributed Active Archive Center[data set], https://doi.org/10.3334/ORNLDAAC/1930, 2021.

Canagaratna, M., Jayne, J., Jimenez, J., Allan, J., Alfarra, M., Zhang, Q., Onasch, T., Drewnick, F., Coe, H., Middlebrook, A., Delia, A., Williams, L., Trimborn, A., Northway, M., DeCarlo, P., Kolb, C., Davidovits, P., and Worsnop, D.: Chemical and microphysical characterization of ambient aerosols with the aerodyne aerosol mass spectrometer, Mass Spectrometry Reviews, 26, 185–222, https://doi.org/10.1002/mas.20115, 2007.

Choi, J.-O. and Chung, C. E.: Sensitivity of aerosol direct radiative forcing to aerosol vertical profile, Tellus B: Chemical and Physical Meteorology, 66, 24 376, https://doi.org/10.3402/tellusb.v66.24376, 2014.

Crameri, F.: Scientific colour maps, Zenodo [code], https://doi.org/10.5281/zenodo.5501399, 2021.

Crameri, F., Shephard, G. E., and Heron, P. J.: The misuse of colour in science communication, Nature communications, 11, 1–10, https://doi.org/10.1038/s41467-020-19160-7, 2020.

Crutzen, P. J.: The possible importance of CSO for the sulphatelayer of the stratosphere, Geophysical Research Letters, 3, 73–76, 1976.

Curtius, J., Weigel, R., Vössing, H.-J., Wernli, H., Werner, A., Volk, C.-M., Konopka, P., Krebsbach, M., Schiller, C., Roiger, A., Schlager, H., Dreiling, V., and Borrmann, S.: Observations of meteoric material and implications for aerosol nucleation in the winter Arctic lower stratosphere derived from in situ particle measurements, Atmospheric Chemistry and Physics, 5, 3053–3069, https://doi.org/10.5194/acp-5-3053-2005, 2005.

Curtius, J., Heinritzi, M., Beck, L. J., Pöhlker, M. L., Tripathi, N., Krumm, B. E., Holzbeck, P., Nussbaumer, C. M., Hernández Pardo, L., Klimach, T., Barmpounis, K., Andersen, S. T., Bardakov, R., Bohn, B., Cecchini, M. A., Chaboureau, J.-P., Dauhut, T., Dienhart, D., Dörich, R., Edtbauer, A., Giez, A., Hartmann, A., Holanda, B. A., Joppe, P., Kaiser, K., Keber, T., Klebach, H., Krüger, O. O., Kürten, A., Mallaun, C., Marno, D., Martinez, M., Monteiro, C., Nelson, C., Ort, L., Raj, S. S., Richter, S., Ringsdorf, A., Rocha, F., Simon, M., Sreekumar, S., Tsokankunku, A., Unfer, G. R., Valenti, I. D., Wang, N., Zahn, A., Zauner-Wieczorek, M., Albrecht, R. I., Andreae, M. O., Artaxo, P., Crowley, J. N., Fischer, H., Harder, H., Herdies, D. L., Machado, L. A. T., Pöhlker, C., Pöschl, U., Possner, A., Pozzer, A., Schneider, J., Williams, J., and Lelieveld, J.: Isoprene nitrates drive new particle formation in Amazon's upper troposphere, Nature, 636, 124–130, https://doi.org/10.1038/s41586-024-08192-4, 2024.

Daniels, L. D., Gray, R. W., and Burton, P. J.: 2017 megafires in British Columbia: Urgent need to adapt and improve resilience to wildfire, In: Hood, Sharon M.; Drury, Stacy; Steelman, Toddi; Steffens, Ron,[eds.]. Proceedings of the Fire Continuum-Preparing for the future of wildland fire; 2018 May 21-24; Missoula, MT. Proceedings RMRS-P-78. Fort Collins, CO: US Department of Agriculture, Forest Service, Rocky Mountain Research Station. p. 51-62., 78, 51–62, 2020.

DeCarlo, P. F., Slowik, J. G., Worsnop, D. R., Davidovits, P., and Jimenez, J. L.: Particle Morphology and Density Characterization by Combined Mobility and Aerodynamic Diameter Measurements. Part 1: Theory, Aerosol Science and Technology, 38, 1185–1205, https://doi.org/10.1080/027868290903907, 2004.

DeCarlo, P. F., Kimmel, J. R., Trimborn, A., Northway, M. J., Jayne, J. T., Aiken, A. C., Gonin, M., Fuhrer, K., Horvath, T., Docherty, K. S., Worsnop, D. R., and Jimenez, J. L.: Field-Deployable, High-Resolution, Time-of-Flight Aerosol Mass Spectrometer, Analytical Chemistry, 78, 8281–8289, https://doi.org/10.1021/ac061249n, pMID: 17165817, 2006.

https://doi.org/10.5194/egusphere-2026-3649
Preprint. Discussion started: 9 July 2026

Deckert, R., Jöckel, P., Grewe, V., Gottschaldt, K.-D., and Hoor, P.: A quasi chemistry-transport model mode for EMAC, Geoscientific Model Development, 4, 195–206, https://doi.org/10.5194/gmd-4-195-2011, 2011.

Dentener, F., Kinne, S., Bond, T., Boucher, O., Cofala, J., Generoso, S., Ginoux, P., Gong, S., Hoelzemann, J. J., Ito, A., Marelli, L., Penner, J. E., Putaud, J.-P., Textor, C., Schulz, M., van der Werf, G. R., and Wilson, J.: Emissions of primary aerosol and precursor gases in the years 2000 and 1750 prescribed data-sets for AeroCom, Atmospheric Chemistry and Physics, 6, 4321–4344, https://doi.org/10.5194/acp-6-4321-2006, 2006.

Deshler, T., Hervig, M. E., Hofmann, D. J., Rosen, J. M., and Liley, J. B.: Thirty years of in situ stratospheric aerosol size distribution measurements from Laramie, Wyoming (41°N), using balloon-borne instruments, Journal of Geophysical Research: Atmospheres, 108, https://doi.org/10.1029/2002JD002514, 2003.

Dietmüller, S., Jöckel, P., Tost, H., Kunze, M., Gellhorn, C., Brinkop, S., Frömming, C., Ponater, M., Steil, B., Lauer, A., and Hendricks, J.: A new radiation infrastructure for the Modular Earth Submodel System (MESSy, based on version 2.51), Geoscientific Model Development, 9, 2209–2222, https://doi.org/10.5194/gmd-9-2209-2016, 2016.

Ditas, J., Ma, N., Zhang, Y., Assmann, D., Neumaier, M., Riede, H., Karu, E., Williams, J., Scharffe, D., Wang, Q., Saturno, J., Schwarz, J. P., Katich, J. M., McMeeking, G. R., Zahn, A., Hermann, M., Brenninkmeijer, C. A. M., Andreae, M. O., Pöschl, U., Su, H., and Cheng, Y.: Strong impact of wildfires on the abundance and aging of black carbon in the lowermost stratosphere, Proceedings of the National Academy of Sciences, 115, E11 595–E11 603, https://doi.org/10.1073/pnas.1806868115, 2018.

Doumbia, T., Granier, C., Elguindi, N., Bouarar, I., Darras, S., Brasseur, G., Gaubert, B., Liu, Y., Shi, X., Stavrakou, T., Tilmes, S., Lacey, F., Deroubaix, A., and Wang, T.: Changes in global air pollutant emissions during the COVID-19 pandemic: a dataset for atmospheric modeling, Earth System Science Data, 13, 4191–4206, https://doi.org/10.5194/essd-13-4191-2021, 2021.

Dragoneas, A., Molleker, S., Appel, O., Hünig, A., Böttger, T., Hermann, M., Drewnick, F., Schneider, J., Weigel, R., and Borrmann, S.: The realization of autonomous, aircraft-based, real-time aerosol mass spectrometry in the upper troposphere and lower stratosphere, Atmospheric Measurement Techniques, 15, 5719–5742, https://doi.org/10.5194/amt-15-5719-2022, 2022.

Drewnick, F., Hings, S. S., DeCarlo, P., Jayne, J. T., Gonin, M., Fuhrer, K., Weimer, S., Jimenez, J. L., Demerjian, K. L., Borrmann, S., and and, D. R. W.: A New Time-of-Flight Aerosol Mass Spectrometer (TOF-AMS)—Instrument Description and First Field Deployment, Aerosol Science and Technology, 39, 637–658, https://doi.org/10.1080/02786820500182040, 2005.

Dunne, E. M., Gordon, H., Kürten, A., Almeida, J., Duplissy, J., Williamson, C., Ortega, I. K., Pringle, K. J., Adamov, A., Baltensperger, U., Barmet, P., Benduhn, F., Bianchi, F., Breitenlechner, M., Clarke, A., Curtius, J., Dommen, J., Donahue, N. M., Ehrhart, S., Flagan, R. C., Franchin, A., Guida, R., Hakala, J., Hansel, A., Heinritzi, M., Jokinen, T., Kangasluoma, J., Kirkby, J., Kulmala, M., Kupc, A., Lawler, M. J., Lehtipalo, K., Makhmutov, V., Mann, G., Mathot, S., Merikanto, J., Miettinen, P., Nenes, A., Onnela, A., Rap, A., Reddington, C. L. S., Riccobono, F., Richards, N. A. D., Rissanen, M. P., Rondo, L., Sarnela, N., Schobesberger, S., Sengupta, K., Simon, M., Sipilä, M., Smith, J. N., Stozkhov, Y., Tomé, A., Tröstl, J., Wagner, P. E., Wimmer, D., Winkler, P. M., Worsnop, D. R., and Carslaw, K. S.: Global atmospheric particle formation from CERN CLOUD measurements, Science, 354, 1119–1124, https://doi.org/10.1126/science.aaf2649, 2016.

EANET: Data Report, Acid Deposition Monitoring Network in East Asia (EANET) [data set], https://monitoring.eanet.asia/document/public/index, last access: 19 June 2026, 2026.

Ebert, M., Weigel, R., Weinbruch, S., Schneider, L., Kandler, K., Lauterbach, S., Köllner, F., Plöger, F., Günther, G., Vogel, B., and Borrmann, S.: Characterization of refractory aerosol particles collected in the tropical upper troposphere–lower stratosphere (UTLS) within the Asian tropopause aerosol layer (ATAL), Atmospheric Chemistry and Physics, 24, 4771–4788, https://doi.org/10.5194/acp-24-4771-2024, 2024.

https://doi.org/10.5194/egusphere-2026-3649
Preprint. Discussion started: 9 July 2026

Ehrhart, S., Dunne, E. M., Manninen, H. E., Nieminen, T., Lelieveld, J., and Pozzer, A.: Two new submodels for the Modular Earth Submodel System (MESSy): New Aerosol Nucleation (NAN) and small ions (IONS) version 1.0, Geoscientific Model Development, 11, 4987–5001, https://doi.org/10.5194/gmd-11-4987-2018, 2018.

Elkins, J., Hintsa, E., and Moore, F.: ATom: Measurements from the UAS Chromatograph for Atmospheric Trace Species (UCATS), ORNL Distributed Active Archive Center [data set], https://doi.org/10.3334/ORNLDAAC/1750, 2020.

Eppers, O., Appel, O., Brauner, P., Ekinci, F., Köllner, F., and Borrmann, S.: ACCLIP: ERC Instrument for Chemical composition of Aerosols - Aerosol Mass Spectrometer (ERICA-AMS) Data., NSF NCAR Earth Observing Laboratory [data set], https://doi.org/10.26023/T7RT-01YD-A110, 2025a.

Eppers, O., Köllner, F., Appel, O., Brauner, P., Ekinci, F., Molleker, S., Dragoneas, A., Smith, W. P., Ueyama, R., Bucci, S., Legras, B., Williamson, C. J., Campos, T. L., Ullmann, K., Schill, G. P., Murphy, D. M., Pan, L. L., Cheng, Y., and Borrmann, S.: Regional contributions to the chemical composition of the Asian tropopause aerosol layer (ATAL), ESS Open Archive, 2025, https://doi.org/10.22541/essoar.175130383.35260852/v1, 2025b.

Fountoukis, C. and Nenes, A.: ISORROPIA II: a computationally efficient thermodynamic equilibrium model for K^+–Ca^{2+}–Mg^{2+}–$NH_4{}^+$–Na^+–$SO_4{}^-$–$NO_3{}^-$–Cl^-–H_2O aerosols, Atmospheric Chemistry and Physics, 7, 4639–4659, https://doi.org/10.5194/acp-7-4639-2007, 2007.

Froyd, K. D., Murphy, D. M., Brock, C. A., Campuzano-Jost, P., Dibb, J. E., Jimenez, J.-L., Kupc, A., Middlebrook, A. M., Schill, G. P., Thornhill, K. L., Williamson, C. J., Wilson, J. C., and Ziemba, L. D.: A new method to quantify mineral dust and other aerosol species from aircraft platforms using single-particle mass spectrometry, Atmospheric Measurement Techniques, 12, 6209–6239, https://doi.org/10.5194/amt-12-6209-2019, 2019.

Froyd, K. D., Murphy, D. M., Schill, G. P., and Brock, C. A.: ATom: Measurements from Particle Analysis By Laser Mass Spectrometry (PALMS), ORNL Distributed Active Archive Center [data set], https://doi.org/10.3334/ORNLDAAC/1733, 2021.

Froyd, K. D., Yu, P., Schill, G. P., Brock, C. A., Kupc, A., Williamson, C. J., Jensen, E., Ray, E. A., Rosenlof, K. H., Bian, H., Darmenov, A. S., Colarco, P. R., Diskin, G. S., Bui, T. P., and Murphy, D. M.: ATom: Dominant Role of Mineral Dust in Cirrus Cloud Formation (Version 1), ORNL Distributed Active Archive Center [data set], https://doi.org/10.3334/ORNLDAAC/1733, 2022a.

Froyd, K. D., Yu, P., Schill, G. P., Brock, C. A., Kupc, A., Williamson, C. J., Jensen, E. J., Ray, E., Rosenlof, K. H., Bian, H., et al.: Dominant role of mineral dust in cirrus cloud formation revealed by global-scale measurements, Nature Geoscience, 15, 177–183, https://doi.org/10.1038/s41561-022-00901-w, 2022b.

Gao, R. S., Schwarz, J. P., Kelly, K. K., Fahey, D. W., Watts, L. A., Thompson, T. L., Spackman, J. R., Slowik, J. G., Cross, E. S., Han, J.-H., Davidovits, P., Onasch, T. B., and and, D. R. W.: A Novel Method for Estimating Light-Scattering Properties of Soot Aerosols Using a Modified Single-Particle Soot Photometer, Aerosol Science and Technology, 41, 125–135, https://doi.org/10.1080/02786820601118398, 2007.

Gelaro, R., McCarty, W., Suárez, M. J., Todling, R., Molod, A., Takacs, L., Randles, C. A., Darmenov, A., Bosilovich, M. G., Reichle, R., Wargan, K., Coy, L., Cullather, R., Draper, C., Akella, S., Buchard, V., Conaty, A., da Silva, A. M., Gu, W., Kim, G.-K., Koster, R., Lucchesi, R., Merkova, D., Nielsen, J. E., Partyka, G., Pawson, S., Putman, W., Rienecker, M., Schubert, S. D., Sienkiewicz, M., and Zhao, B.: The Modern-Era Retrospective Analysis for Research and Applications, Version 2 (MERRA-2), Journal of Climate, 30, 5419 – 5454, https://doi.org/10.1175/JCLI-D-16-0758.1, 2017.

Gettelman, A., Hoor, P., Pan, L. L., Randel, W. J., Hegglin, M. I., and Birner, T.: THE EXTRATROPICAL UPPER TROPOSPHERE AND LOWER STRATOSPHERE, Reviews of Geophysics, 49, https://doi.org/10.1029/2011RG000355, 2011.

https://doi.org/10.5194/egusphere-2026-3649
Preprint. Discussion started: 9 July 2026

Giauque, W. F., Hornung, E. W., Kunzler, J. E., and Rubin, T. R.: The Thermodynamic Properties of Aqueous Sulfuric Acid Solutions and Hydrates from 15 to 300°K.1, Journal of the American Chemical Society, 82, 62–70, https://doi.org/10.1021/ja01486a014, 1960.

Giles, D. M., Sinyuk, A., Sorokin, M. G., Schafer, J. S., Smirnov, A., Slutsker, I., Eck, T. F., Holben, B. N., Lewis, J. R., Campbell, J. R., Welton, E. J., Korkin, S. V., and Lyapustin, A. I.: Advancements in the Aerosol Robotic Network (AERONET) Version 3 database – automated near-real-time quality control algorithm with improved cloud screening for Sun photometer aerosol optical depth (AOD) measurements, Atmospheric Measurement Techniques, 12, 169–209, https://doi.org/10.5194/amt-12-169-2019, 2019.

Giorgetta, M. A. and Bengtsson, L.: Potential role of the quasi-biennial oscillation in the stratosphere-troposphere exchange as found in water vapor in general circulation model experiments, Journal of Geophysical Research: Atmospheres, 104, 6003–6019, https://doi.org/10.1029/1998JD200112, 1999.

Gordon, H., Kirkby, J., Baltensperger, U., Bianchi, F., Breitenlechner, M., Curtius, J., Dias, A., Dommen, J., Donahue, N. M., Dunne, E. M., Duplissy, J., Ehrhart, S., Flagan, R. C., Frege, C., Fuchs, C., Hansel, A., Hoyle, C. R., Kulmala, M., Kürten, A., Lehtipalo, K., Makhmutov, V., Molteni, U., Rissanen, M. P., Stozkhov, Y., Tröstl, J., Tsagkogeorgas, G., Wagner, R., Williamson, C., Wimmer, D., Winkler, P. M., Yan, C., and Carslaw, K. S.: Causes and importance of new particle formation in the present-day and preindustrial atmospheres, Journal of Geophysical Research: Atmospheres, 122, 8739–8760, https://doi.org/10.1002/2017JD026844, 2017.

Granier, C., Darras, S., Denier van der Gon, H., Doubalova, J., Elguindi, N., Galle, B., Gauss, M., Guevara, M., Jalkanen, J.-P., Kuenen, J., Liousse, C., Quack, B., Simpson, D., and Sindelarova, K.: The Copernicus Atmosphere Monitoring Service global and regional emissions (April 2019 version), Copernicus Atmosphere Monitoring Service (CAMS) report, https://doi.org/10.24380/d0bn-kx16, 2019.

Guelle, W., Schulz, M., Balkanski, Y., and Dentener, F.: Influence of the source formulation on modeling the atmospheric global distribution of sea salt aerosol, Journal of Geophysical Research: Atmospheres, 106, 27 509–27 524, https://doi.org/10.1029/2001JD900249, 2001.

Guenther, A. B., Jiang, X., Heald, C. L., Sakulyanontvittaya, T., Duhl, T., Emmons, L. K., and Wang, X.: The Model of Emissions of Gases and Aerosols from Nature version 2.1 (MEGAN2.1): an extended and updated framework for modeling biogenic emissions, Geoscientific Model Development, 5, 1471–1492, https://doi.org/10.5194/gmd-5-1471-2012, 2012.

Guo, H., Campuzano-Jost, P., Nault, B. A., Day, D. A., Schroder, J. C., Kim, D., Dibb, J. E., Dollner, M., Weinzierl, B., and Jimenez, J. L.: The importance of size ranges in aerosol instrument intercomparisons: a case study for the Atmospheric Tomography Mission, Atmospheric Measurement Techniques, 14, 3631–3655, https://doi.org/10.5194/amt-14-3631-2021, 2021.

HALO: HALO database, German Aerospace Center [data set], https://doi.org/10.17616/R39Q0T, last access: 19 June 2026, 2026.

He, X.-C., Tham, Y. J., Dada, L., Wang, M., Finkenzeller, H., Stolzenburg, D., Iyer, S., Simon, M., Kürten, A., Shen, J., Rörup, B., Rissanen, M., Schobesberger, S., Baalbaki, R., Wang, D. S., Koenig, T. K., Jokinen, T., Sarnela, N., Beck, L. J., Almeida, J., Amanatidis, S., Amorim, A., Ataei, F., Baccarini, A., Bertozzi, B., Bianchi, F., Brilke, S., Caudillo, L., Chen, D., Chiu, R., Chu, B., Dias, A., Ding, A., Dommen, J., Duplissy, J., Haddad, I. E., Carracedo, L. G., Granzin, M., Hansel, A., Heinritzi, M., Hofbauer, V., Junninen, H., Kangasluoma, J., Kemppainen, D., Kim, C., Kong, W., Krechmer, J. E., Kvashin, A., Laitinen, T., Lamkaddam, H., Lee, C. P., Lehtipalo, K., Leiminger, M., Li, Z., Makhmutov, V., Manninen, H. E., Marie, G., Marten, R., Mathot, S., Mauldin, R. L., Mentler, B., Möhler, O., Müller, T., Nie, W., Onnela, A., Petäjä, T., Pfeifer, J., Philippov, M., Ranjithkumar, A., Saiz-Lopez, A., Salma, I., Scholz, W., Schuchmann, S., Schulze, B., Steiner, G., Stozhkov, Y., Tauber, C., Tomé, A., Thakur, R. C., Väisänen, O., Vazquez-Pufleau, M., Wagner, A. C., Wang, Y., Weber, S. K., Winkler, P. M., Wu, Y., Xiao, M., Yan, C., Ye, Q., Ylisirniö, A., Zauner-Wieczorek, M., Zha, Q., Zhou, P., Flagan, R. C., Curtius, J., Baltensperger, U., Kulmala, M., Kerminen, V.-M., Kurtén, T., Donahue, N. M., Volkamer, R., Kirkby, J., Worsnop, D. R., and Sipilä, M.: Role of iodine oxoacids in atmospheric aerosol nucleation, Science, 371, 589–595, https://doi.org/10.1126/science.abe0298, 2021.

https://doi.org/10.5194/egusphere-2026-3649
Preprint. Discussion started: 9 July 2026

He, X.-C., Abraham, N. L., Ding, H., Russo, M. R., Grosvenor, D. P., Ge, Y., Wang, X., Jones, A. C., Campuzano-Jost, P., Nault, B., Kupc, A., Blake, D., Jimenez, J. L., Williamson, C. J., Weber, J., Archibald, A. T., and Gordon, H.: Evaluation of UKESM aerosol size and composition using ATom measurements indicates missing marine aerosol formation mechanisms, Atmospheric Chemistry and Physics, 26, 3805–3851, https://doi.org/10.5194/acp-26-3805-2026, 2026.

Heald, C. L., Coe, H., Jimenez, J. L., Weber, R. J., Bahreini, R., Middlebrook, A. M., Russell, L. M., Jolleys, M., Fu, T.-M., Allan, J. D., Bower, K. N., Capes, G., Crosier, J., Morgan, W. T., Robinson, N. H., Williams, P. I., Cubison, M. J., DeCarlo, P. F., and Dunlea, E. J.: Exploring the vertical profile of atmospheric organic aerosol: comparing 17 aircraft field campaigns with a global model, Atmospheric Chemistry and Physics, 11, 12 673–12 696, https://doi.org/10.5194/acp-11-12673-2011, 2011.

Healy, R. M., Wang, J. M., Sofowote, U., Su, Y., Debosz, J., Noble, M., Munoz, A., Jeong, C.-H., Hilker, N., Evans, G. J., and Doerksen, G.: Black carbon in the Lower Fraser Valley, British Columbia: Impact of 2017 wildfires on local air quality and aerosol optical properties, Atmospheric Environment, 217, 116 976, https://doi.org/10.1016/j.atmosenv.2019.116976, 2019.

Hersbach, H., Bell, B., Berrisford, P., Hirahara, S., Horányi, A., Muñoz-Sabater, J., Nicolas, J., Peubey, C., Radu, R., Schepers, D., Simmons, A., Soci, C., Abdalla, S., Abellan, X., Balsamo, G., Bechtold, P., Biavati, G., Bidlot, J., Bonavita, M., De Chiara, G., Dahlgren, P., Dee, D., Diamantakis, M., Dragani, R., Flemming, J., Forbes, R., Fuentes, M., Geer, A., Haimberger, L., Healy, S., Hogan, R. J., Hólm, E., Janisková, M., Keeley, S., Laloyaux, P., Lopez, P., Lupu, C., Radnoti, G., de Rosnay, P., Rozum, I., Vamborg, F., Villaume, S., and Thépaut, J.-N.: The ERA5 global reanalysis, Quarterly Journal of the Royal Meteorological Society, 146, 1999–2049, https://doi.org/10.1002/qj.3803, 2020.

Hertzog, A. and Plougonven, R.: Strateole-2: High-resolution observations of the tropical tropopause layer with long-duration balloons, in: Egu general assembly conference abstracts, pp. EGU21–7109, https://doi.org/10.5194/egusphere-egu21-7109, 2021.

Holanda, B. A., Pöhlker, M. L., Walter, D., Saturno, J., Sörgel, M., Ditas, J., Ditas, F., Schulz, C., Franco, M. A., Wang, Q., Donth, T., Artaxo, P., Barbosa, H. M. J., Borrmann, S., Braga, R., Brito, J., Cheng, Y., Dollner, M., Kaiser, J. W., Klimach, T., Knote, C., Krüger, O. O., Fütterer, D., Lavrič, J. V., Ma, N., Machado, L. A. T., Ming, J., Morais, F. G., Paulsen, H., Sauer, D., Schlager, H., Schneider, J., Su, H., Weinzierl, B., Walser, A., Wendisch, M., Ziereis, H., Zöger, M., Pöschl, U., Andreae, M. O., and Pöhlker, C.: Influx of African biomass burning aerosol during the Amazonian dry season through layered transatlantic transport of black carbon-rich smoke, Atmospheric Chemistry and Physics, 20, 4757–4785, https://doi.org/10.5194/acp-20-4757-2020, 2020.

Holben, B., Eck, T., Slutsker, I., Tanré, D., Buis, J., Setzer, A., Vermote, E., Reagan, J., Kaufman, Y., Nakajima, T., Lavenu, F., Jankowiak, I., and Smirnov, A.: AERONET—A Federated Instrument Network and Data Archive for Aerosol Characterization, Remote Sensing of Environment, 66, 1–16, https://doi.org/10.1016/S0034-4257(98)00031-5, 1998.

Höpfner, M., Ungermann, J., Borrmann, S., Wagner, R., Spang, R., Riese, M., Stiller, G., Appel, O., Batenburg, A. M., Bucci, S., et al.: Ammonium nitrate particles formed in upper troposphere from ground ammonia sources during Asian monsoons, Nature Geoscience, 12, 608–612, https://doi.org/10.1038/s41561-019-0385-8, 2019.

Hsu, N., Tsay, S.-C., King, M., and Herman, J.: Aerosol properties over bright-reflecting source regions, IEEE Transactions on Geoscience and Remote Sensing, 42, 557–569, https://doi.org/10.1109/TGRS.2004.824067, 2004.

Hünig, A., Appel, O., Dragoneas, A., Molleker, S., Clemen, H.-C., Helleis, F., Klimach, T., Köllner, F., Böttger, T., Drewnick, F., Schneider, J., and Borrmann, S.: Design, characterization, and first field deployment of a novel aircraft-based aerosol mass spectrometer combining the laser ablation and flash vaporization techniques, Atmospheric Measurement Techniques, 15, 2889–2921, https://doi.org/10.5194/amt-15-2889-2022, 2022.

https://doi.org/10.5194/egusphere-2026-3649
Preprint. Discussion started: 9 July 2026

Inness, A., Ades, M., Agustí-Panareda, A., Barré, J., Benedictow, A., Blechschmidt, A.-M., Dominguez, J. J., Engelen, R., Eskes, H., Flemming, J., Huijnen, V., Jones, L., Kipling, Z., Massart, S., Parrington, M., Peuch, V.-H., Razinger, M., Remy, S., Schulz, M., and Suttie, M.: The CAMS reanalysis of atmospheric composition, Atmospheric Chemistry and Physics, 19, 3515–3556, https://doi.org/10.5194/acp-19-3515-2019, 2019.

Jeuken, A. B. M., Siegmund, P. C., Heijboer, L. C., Feichter, J., and Bengtsson, L.: On the potential of assimilating meteorological analyses in a global climate model for the purpose of model validation, Journal of Geophysical Research: Atmospheres, 101, 16 939–16 950, https://doi.org/10.1029/96JD01218, 1996.

Jimenez, J., Campuzano-Jost, P., Day, D., Nault, B., Price, D., and Schroder, J.: ATom: L2 Measurements from CU High-Resolution Aerosol Mass Spectrometer (HR-AMS), ORNL Distributed Active Archive Center [data set], https://doi.org/10.3334/ORNLDAAC/1716, 2019.

Jöckel, P., Tost, H., Pozzer, A., Brühl, C., Buchholz, J., Ganzeveld, L., Hoor, P., Kerkweg, A., Lawrence, M. G., Sander, R., Steil, B., Stiller, G., Tanarhte, M., Taraborrelli, D., van Aardenne, J., and Lelieveld, J.: The atmospheric chemistry general circulation model ECHAM5/MESSy1: consistent simulation of ozone from the surface to the mesosphere, Atmospheric Chemistry and Physics, 6, 5067–5104, https://doi.org/10.5194/acp-6-5067-2006, 2006.

Jöckel, P., Kerkweg, A., Pozzer, A., Sander, R., Tost, H., Riede, H., Baumgaertner, A., Gromov, S., and Kern, B.: Development cycle 2 of the Modular Earth Submodel System (MESSy2), Geoscientific Model Development, 3, 717–752, https://doi.org/10.5194/gmd-3-717-2010, 2010.

Joppe, P., Schneider, J., Kaiser, K., Fischer, H., Hoor, P., Kunkel, D., Lachnitt, H.-C., Marsing, A., Röder, L., Schlager, H., Tomsche, L., Voigt, C., Zahn, A., and Borrmann, S.: The influence of extratropical cross-tropopause mixing on the correlation between ozone and sulfate aerosol in the lowermost stratosphere, Atmospheric Chemistry and Physics, 24, 7499–7522, https://doi.org/10.5194/acp-24-7499-2024, 2024.

Junge, C. E., Chagnon, C. W., and Manson, J. E.: Stratospheric aerosols, Journal of Meteorology, 18, 81–108, 1961.

Katich, J. M., Samset, B. H., Bui, T. P., Dollner, M., Froyd, K. D., Campuzano-Jost, P., Nault, B. A., Schroder, J. C., Weinzierl, B., and Schwarz, J. P.: Strong Contrast in Remote Black Carbon Aerosol Loadings Between the Atlantic and Pacific Basins, Journal of Geophysical Research: Atmospheres, 123, 13,386–13,395, https://doi.org/10.1029/2018JD029206, 2018.

Katich, J. M., Apel, E. C., Bourgeois, I., Brock, C. A., Bui, T. P., Campuzano-Jost, P., Commane, R., Daube, B., Dollner, M., Fromm, M., Froyd, K. D., Hills, A. J., Hornbrook, R. S., Jimenez, J. L., Kupc, A., Lamb, K. D., McKain, K., Moore, F., Murphy, D. M., Nault, B. A., Peischl, J., Perring, A. E., Peterson, D. A., Ray, E. A., Rosenlof, K. H., Ryerson, T., Schill, G. P., Schroder, J. C., Weinzierl, B., Thompson, C., Williamson, C. J., Wofsy, S. C., Yu, P., and Schwarz, J. P.: Pyrocumulonimbus affect average stratospheric aerosol composition, Science, 379, 815–820, https://doi.org/10.1126/science.add3101, 2023.

Kerkweg, A., Sander, R., Tost, H., and Jöckel, P.: Technical note: Implementation of prescribed (OFFLEM), calculated (ONLEM), and pseudo-emissions (TNUDGE) of chemical species in the Modular Earth Submodel System (MESSy), Atmospheric Chemistry and Physics, 6, 3603–3609, https://doi.org/10.5194/acp-6-3603-2006, 2006.

Kirkby, J., Duplissy, J., Sengupta, K., Frege, C., Gordon, H., Williamson, C., Heinritzi, M., Simon, M., Yan, C., Almeida, J., et al.: Ion-induced nucleation of pure biogenic particles, Nature, 533, 521–526, https://doi.org/10.1038/nature17953, 2016.

Klingmüller, K., Metzger, S., Abdelkader, M., Karydis, V. A., Stenchikov, G. L., Pozzer, A., and Lelieveld, J.: Revised mineral dust emissions in the atmospheric chemistry–climate model EMAC (MESSy 2.52 DU_Astitha1 KKDU2017 patch), Geoscientific Model Development, 11, 989–1008, https://doi.org/10.5194/gmd-11-989-2018, 2018.

https://doi.org/10.5194/egusphere-2026-3649
Preprint. Discussion started: 9 July 2026

Klobas, J. E., Wilmouth, D. M., Weisenstein, D. K., Anderson, J. G., and Salawitch, R. J.: Ozone depletion following future volcanic eruptions, Geophysical Research Letters, 44, 7490–7499, https://doi.org/10.1002/2017GL073972, 2017.

Kloss, C., Sellitto, P., Legras, B., Vernier, J.-P., Jégou, F., Venkat Ratnam, M., Suneel Kumar, B., Lakshmi Madhavan, B., and Berthet, G.: Impact of the 2018 Ambae Eruption on the Global Stratospheric Aerosol Layer and Climate, Journal of Geophysical Research: Atmospheres, 125, e2020JD032 410, https://doi.org/10.1029/2020JD032410, 2020.

Kohl, M., Lelieveld, J., Chowdhury, S., Ehrhart, S., Sharma, D., Cheng, Y., Tripathi, S. N., Sebastian, M., Pandithurai, G., Wang, H., and Pozzer, A.: Numerical simulation and evaluation of global ultrafine particle concentrations at the Earth's surface, Atmospheric Chemistry and Physics, 23, 13 191–13 215, https://doi.org/10.5194/acp-23-13191-2023, 2023.

Kohl, M., Brühl, C., Schallock, J., Tost, H., Jöckel, P., Jost, A., Beirle, S., Höpfner, M., and Pozzer, A.: New submodel for emissions from Explosive Volcanic ERuptions (EVER v1.1) within the Modular Earth Submodel System (MESSy, version 2.55.1), Geoscientific Model Development, 18, 3985–4007, https://doi.org/10.5194/gmd-18-3985-2025, 2025.

Kovilakam, M., Thomason, L. W., Ernest, N., Rieger, L., Bourassa, A., and Millán, L.: The Global Space-based Stratospheric Aerosol Climatology (version 2.0): 1979–2018, Earth System Science Data, 12, 2607–2634, https://doi.org/10.5194/essd-12-2607-2020, 2020.

Kovilakam, M., Thomason, L., and Knepp, T.: SAGE III/ISS aerosol/cloud categorization and its impact on GloSSAC, Atmospheric Measurement Techniques, 16, 2709–2731, https://doi.org/10.5194/amt-16-2709-2023, 2023.

Kremser, S., Thomason, L. W., von Hobe, M., Hermann, M., Deshler, T., Timmreck, C., Toohey, M., Stenke, A., Schwarz, J. P., Weigel, R., Fueglistaler, S., Prata, F. J., Vernier, J.-P., Schlager, H., Barnes, J. E., Antuña-Marrero, J.-C., Fairlie, D., Palm, M., Mahieu, E., Notholt, J., Rex, M., Bingen, C., Vanhellemont, F., Bourassa, A., Plane, J. M. C., Klocke, D., Carn, S. A., Clarisse, L., Trickl, T., Neely, R., James, A. D., Rieger, L., Wilson, J. C., and Meland, B.: Stratospheric aerosol—Observations, processes, and impact on climate, Reviews of Geophysics, 54, 278–335, https://doi.org/10.1002/2015RG000511, 2016.

Krüger, O. O., Holanda, B. A., Chowdhury, S., Pozzer, A., Walter, D., Pöhlker, C., Andrés Hernández, M. D., Burrows, J. P., Voigt, C., Lelieveld, J., Quaas, J., Pöschl, U., and Pöhlker, M. L.: Black carbon aerosol reductions during COVID-19 confinement quantified by aircraft measurements over Europe, Atmospheric Chemistry and Physics, 22, 8683–8699, https://doi.org/10.5194/acp-22-8683-2022, 2022.

Kupc, A., Williamson, C., Wagner, N. L., Richardson, M., and Brock, C. A.: Modification, calibration, and performance of the Ultra-High Sensitivity Aerosol Spectrometer for particle size distribution and volatility measurements during the Atmospheric Tomography Mission (ATom) airborne campaign, Atmospheric Measurement Techniques, 11, 369–383, https://doi.org/10.5194/amt-11-369-2018, 2018.

Lelieveld, J., Evans, J. S., Fnais, M., Giannadaki, D., and Pozzer, A.: The contribution of outdoor air pollution sources to premature mortality on a global scale, Nature, 525, 367–371, https://doi.org/10.1038/nature15371, 2015.

Lohmann, U. and Feichter, J.: Global indirect aerosol effects: a review, Atmospheric Chemistry and Physics, 5, 715–737, https://doi.org/10.5194/acp-5-715-2005, 2005.

Lund, M. T., Samset, B. H., Skeie, R. B., Watson-Parris, D., Katich, J. M., Schwarz, J. P., and Weinzierl, B.: Short Black Carbon lifetime inferred from a global set of aircraft observations, Npj Climate and Atmospheric Science, 1, 31, https://doi.org/10.1038/s41612-018-0040-x, 2018.

Lyu, M., Ahern, A. T., Schill, G. P., Lawler, M. J., Murphy, D. M., Taylor, S. J., Fodel, A., Abou-Ghanem, M., Gurganus, C., Zhu, Y., Tilmes, S., Ray, E., Thornberry, T. D., Gao, R.-S., Hintsa, E. J., Moore, F., Dutton, G., Nance, D., Hall, B., Rollins, A. W., Waxman, E. M., Zuraski, K., Diskin, G. S., Choi, Y., Pierce, R. B., Weinzierl, B., Kuderna, F., Dollner, M., Jensen, E., and Brock, C. A.: An unrecognized mode of small particles in the lower stratosphere, Science, 392, eadw8939, https://doi.org/10.1126/science.adw8939, 2026.

https://doi.org/10.5194/egusphere-2026-3649
Preprint. Discussion started: 9 July 2026

Ma, C., Su, H., Lelieveld, J., Randel, W., Yu, P., Andreae, M. O., and Cheng, Y.: Smoke-charged vortex doubles hemispheric aerosol in the middle stratosphere and buffers ozone depletion, Science Advances, 10, eadn3657, https://doi.org/10.1126/sciadv.adn3657, 2024.

Ma, J., Brühl, C., He, Q., Steil, B., Karydis, V. A., Klingmüller, K., Tost, H., Chen, B., Jin, Y., Liu, N., Xu, X., Yan, P., Zhou, X., Abdelrahman, K., Pozzer, A., and Lelieveld, J.: Modeling the aerosol chemical composition of the tropopause over the Tibetan Plateau during the Asian summer monsoon, Atmospheric Chemistry and Physics, 19, 11 587–11 612, https://doi.org/10.5194/acp-19-11587-2019, 2019.

Maclean, A. M., Li, Y., Crescenzo, G. V., Smith, N. R., Karydis, V. A., Tsimpidi, A. P., Butenhoff, C. L., Faiola, C. L., Lelieveld, J., Nizkorodov, S. A., Shiraiwa, M., and Bertram, A. K.: Global Distribution of the Phase State and Mixing Times within Secondary Organic Aerosol Particles in the Troposphere Based on Room-Temperature Viscosity Measurements, ACS Earth and Space Chemistry, 5, 3458–3473, https://doi.org/10.1021/acsearthspacechem.1c00296, 2021.

Maheshwarkar, P., Cuesta, J., Formenti, P., and Lemmouchi, F.: Three-dimensional distribution of aerosols of multiple types at daily scale using TROPOMI spaceborne observations, Science of The Total Environment, 955, 177 037, https://doi.org/10.1016/j.scitotenv.2024.177037, 2024.

Mahnke, C., Weigel, R., Cairo, F., Vernier, J.-P., Afchine, A., Krämer, M., Mitev, V., Matthey, R., Viciani, S., D'Amato, F., Ploeger, F., Deshler, T., and Borrmann, S.: The Asian tropopause aerosol layer within the 2017 monsoon anticyclone: microphysical properties derived from aircraft-borne in situ measurements, Atmospheric Chemistry and Physics, 21, 15 259–15 282, https://doi.org/10.5194/acp-21-15259-2021, 2021.

Martinsson, B. G., Friberg, J., Sandvik, O. S., Hermann, M., van Velthoven, P. F., and Zahn, A.: Formation and composition of the UTLS aerosol, npj Climate and Atmospheric Science, 2, 40, https://doi.org/10.1038/s41612-019-0097-1, 2019.

McDuffie, E. E., Smith, S. J., O'Rourke, P., Tibrewal, K., Venkataraman, C., Marais, E. A., Zheng, B., Crippa, M., Brauer, M., and Martin, R. V.: A global anthropogenic emission inventory of atmospheric pollutants from sector- and fuel-specific sources (1970–2017): an application of the Community Emissions Data System (CEDS), Earth System Science Data, 12, 3413–3442, https://doi.org/10.5194/essd-12-3413-2020, 2020.

McKain, K. and Sweeney, C.: ATom: CO2, CH4, and CO Measurements from Picarro, 2016-2018, ORNL Distributed Active Archive Center [data set], https://doi.org/10.3334/ORNLDAAC/1732, 2021.

Mishra, A. K., Koren, I., and Rudich, Y.: Effect of aerosol vertical distribution on aerosol-radiation interaction: A theoretical prospect, Heliyon, 1, https://doi.org/10.1016/j.heliyon.2015.e00036, 2015.

Murphy, D. M., Thomson, D. S., and Mahoney, M. J.: In Situ Measurements of Organics, Meteoritic Material, Mercury, and Other Elements in Aerosols at 5 to 19 Kilometers, Science, 282, 1664–1669, https://doi.org/10.1126/science.282.5394.1664, 1998.

Murphy, D. M., Cziczo, D. J., Froyd, K. D., Hudson, P. K., Matthew, B. M., Middlebrook, A. M., Peltier, R. E., Sullivan, A., Thomson, D. S., and Weber, R. J.: Single-particle mass spectrometry of tropospheric aerosol particles, Journal of Geophysical Research: Atmospheres, 111, https://doi.org/10.1029/2006JD007340, 2006.

Murphy, D. M., Cziczo, D. J., Hudson, P. K., and Thomson, D. S.: Carbonaceous material in aerosol particles in the lower stratosphere and tropopause region, Journal of Geophysical Research: Atmospheres, 112, https://doi.org/10.1029/2006JD007297, 2007.

Murphy, D. M., Froyd, K. D., Bourgeois, I., Brock, C. A., Kupc, A., Peischl, J., Schill, G. P., Thompson, C. R., Williamson, C. J., and Yu, P.: Radiative and chemical implications of the size and composition of aerosol particles in the existing or modified global stratosphere, Atmospheric Chemistry and Physics, 21, 8915–8932, https://doi.org/10.5194/acp-21-8915-2021, 2021.

https://doi.org/10.5194/egusphere-2026-3649
Preprint. Discussion started: 9 July 2026

Murphy, D. M., Abou-Ghanem, M., Cziczo, D. J., Froyd, K. D., Jacquot, J., Lawler, M. J., Maloney, C., Plane, J. M. C., Ross, M. N., Schill, G. P., and Shen, X.: Metals from spacecraft reentry in stratospheric aerosol particles, Proceedings of the National Academy of Sciences, 120, e2313374 120, https://doi.org/10.1073/pnas.2313374120, 2023.

Murray, C. J., Aravkin, A. Y., Zheng, P., Abbafati, C., Abbas, K. M., Abbasi-Kangevari, M., Abd-Allah, F., Abdelalim, A., Abdollahi, M., Abdollahpour, I., et al.: Global burden of 87 risk factors in 204 countries and territories, 1990–2019: a systematic analysis for the Global Burden of Disease Study 2019, The lancet, 396, 1223–1249, https://doi.org/10.1016/S0140-6736(20)30752-2, 2020.

Nault, B. A., Jo, D. S., McDonald, B. C., Campuzano-Jost, P., Day, D. A., Hu, W., Schroder, J. C., Allan, J., Blake, D. R., Canagaratna, M. R., Coe, H., Coggon, M. M., DeCarlo, P. F., Diskin, G. S., Dunmore, R., Flocke, F., Fried, A., Gilman, J. B., Gkatzelis, G., Hamilton, J. F., Hanisco, T. F., Hayes, P. L., Henze, D. K., Hodzic, A., Hopkins, J., Hu, M., Huey, L. G., Jobson, B. T., Kuster, W. C., Lewis, A., Li, M., Liao, J., Nawaz, M. O., Pollack, I. B., Peischl, J., Rappenglück, B., Reeves, C. E., Richter, D., Roberts, J. M., Ryerson, T. B., Shao, M., Sommers, J. M., Walega, J., Warneke, C., Weibring, P., Wolfe, G. M., Young, D. E., Yuan, B., Zhang, Q., de Gouw, J. A., and Jimenez, J. L.: Secondary organic aerosols from anthropogenic volatile organic compounds contribute substantially to air pollution mortality, Atmospheric Chemistry and Physics, 21, 11 201–11 224, https://doi.org/10.5194/acp-21-11201-2021, 2021.

Nützel, M., Stecher, L., Jöckel, P., Winterstein, F., Dameris, M., Ponater, M., Graf, P., and Kunze, M.: Updating the radiation infrastructure in MESSy (based on MESSy version 2.55), Geoscientific Model Development, 17, 5821–5849, https://doi.org/10.5194/gmd-17-5821-2024, 2024.

Platnick, S., Hubanks, P., Meyer, K., and King, M. D.: MODIS Atmosphere L3 Daily Product, NASA MODIS Adaptive Processing System, Goddard Space Flight Center, USA [data set], https://doi.org/10.5067/MODIS/MOD08_D3.061, 2015.

Pöhlker, M. L., Ditas, F., Saturno, J., Klimach, T., Hrabě de Angelis, I., Araùjo, A. C., Brito, J., Carbone, S., Cheng, Y., Chi, X., Ditz, R., Gunthe, S. S., Holanda, B. A., Kandler, K., Kesselmeier, J., Könemann, T., Krüger, O. O., Lavrič, J. V., Martin, S. T., Mikhailov, E., Moran-Zuloaga, D., Rizzo, L. V., Rose, D., Su, H., Thalman, R., Walter, D., Wang, J., Wolff, S., Barbosa, H. M. J., Artaxo, P., Andreae, M. O., Pöschl, U., and Pöhlker, C.: Long-term observations of cloud condensation nuclei over the Amazon rain forest – Part 2: Variability and characteristics of biomass burning, long-range transport, and pristine rain forest aerosols, Atmospheric Chemistry and Physics, 18, 10 289–10 331, https://doi.org/10.5194/acp-18-10289-2018, 2018.

Pöschl, U., von Kuhlmann, R., Poisson, N., and Crutzen, P. J.: Development and intercomparison of condensed isoprene oxidation mechanisms for global atmospheric modeling, Journal of Atmospheric Chemistry, 37, 29–52, https://doi.org/10.1023/A:1006391009798, 2000.

Pozzer, A., de Meij, A., Pringle, K. J., Tost, H., Doering, U. M., van Aardenne, J., and Lelieveld, J.: Distributions and regional budgets of aerosols and their precursors simulated with the EMAC chemistry-climate model, Atmospheric Chemistry and Physics, 12, 961–987, https://doi.org/10.5194/acp-12-961-2012, 2012.

Pozzer, A., Reifenberg, S. F., Kumar, V., Franco, B., Kohl, M., Taraborrelli, D., Gromov, S., Ehrhart, S., Jöckel, P., Sander, R., Fall, V., Rosanka, S., Karydis, V., Akritidis, D., Emmerichs, T., Crippa, M., Guizzardi, D., Kaiser, J. W., Clarisse, L., Kiendler-Scharr, A., Tost, H., and Tsimpidi, A.: Simulation of organics in the atmosphere: evaluation of EMACv2.54 with the Mainz Organic Mechanism (MOM) coupled to the ORACLE (v1.0) submodel, Geoscientific Model Development, 15, 2673–2710, https://doi.org/10.5194/gmd-15-2673-2022, 2022.

Pringle, K. J., Tost, H., Metzger, S., Steil, B., Giannadaki, D., Nenes, A., Fountoukis, C., Stier, P., Vignati, E., and Lelieveld, J.: Description and evaluation of GMXe: a new aerosol submodel for global simulations (v1), Geosci. Model Dev., 3, 391–412, https://doi.org/10.5194/gmd-3-391-2010, 2010.

https://doi.org/10.5194/egusphere-2026-3649
Preprint. Discussion started: 9 July 2026

Putaud, J.-P., Raes, F., Van Dingenen, R., Brüggemann, E., Facchini, M.-C., Decesari, S., Fuzzi, S., Gehrig, R., Hüglin, C., Laj, P., Lorbeer, G., Maenhaut, W., Mihalopoulos, N., Müller, K., Querol, X., Rodriguez, S., Schneider, J., Spindler, G., ten Brink, H., Tørseth, K., and Wiedensohler, A.: A European aerosol phenomenology—2: chemical characteristics of particulate matter at kerbside, urban, rural and background sites in Europe, Atmospheric Environment, 38, 2579–2595, https://doi.org/10.1016/j.atmosenv.2004.01.041, 2004.

Pöschl, U.: Atmospheric Aerosols: Composition, Transformation, Climate and Health Effects, Angewandte Chemie International Edition, 44, 7520–7540, https://doi.org/10.1002/anie.200501122, 2005.

Randles, C. A., da Silva, A. M., Buchard, V., Colarco, P. R., Darmenov, A., Govindaraju, R., Smirnov, A., Holben, B., Ferrare, R., Hair, J., Shinozuka, Y., and Flynn, C. J.: The MERRA-2 Aerosol Reanalysis, 1980 Onward. Part I: System Description and Data Assimilation Evaluation, Journal of Climate, 30, 6823 – 6850, https://doi.org/10.1175/JCLI-D-16-0609.1, 2017.

Reddington, C. L., Carslaw, K. S., Stier, P., Schutgens, N., Coe, H., Liu, D., Allan, J., Browse, J., Pringle, K. J., Lee, L. A., Yoshioka, M., Johnson, J. S., Regayre, L. A., Spracklen, D. V., Mann, G. W., Clarke, A., Hermann, M., Henning, S., Wex, H., Kristensen, T. B., Leaitch, W. R., Pöschl, U., Rose, D., Andreae, M. O., Schmale, J., Kondo, Y., Oshima, N., Schwarz, J. P., Nenes, A., Anderson, B., Roberts, G. C., Snider, J. R., Leck, C., Quinn, P. K., Chi, X., Ding, A., Jimenez, J. L., and Zhang, Q.: The Global Aerosol Synthesis and Science Project (GASSP): Measurements and Modeling to Reduce Uncertainty, Bulletin of the American Meteorological Society, 98, 1857 – 1877, https://doi.org/10.1175/BAMS-D-15-00317.1, 2017.

Reifenberg, S. F., Martin, A., Kohl, M., Bacer, S., Hamryszczak, Z., Tadic, I., Röder, L., Crowley, D. J., Fischer, H., Kaiser, K., Schneider, J., Dörich, R., Crowley, J. N., Tomsche, L., Marsing, A., Voigt, C., Zahn, A., Pöhlker, C., Holanda, B. A., Krüger, O., Pöschl, U., Pöhlker, M., Jöckel, P., Dorf, M., Schumann, U., Williams, J., Bohn, B., Curtius, J., Harder, H., Schlager, H., Lelieveld, J., and Pozzer, A.: Numerical simulation of the impact of COVID-19 lockdown on tropospheric composition and aerosol radiative forcing in Europe, Atmospheric Chemistry and Physics, 22, 10 901–10 917, https://doi.org/10.5194/acp-22-10901-2022, 2022.

Rieger, L. A., Zawada, D. J., Bourassa, A. E., and Degenstein, D. A.: A Multiwavelength Retrieval Approach for Improved OSIRIS Aerosol Extinction Retrievals, Journal of Geophysical Research: Atmospheres, 124, 7286–7307, https://doi.org/10.1029/2018JD029897, 2019.

Rieger, L. A., Randel, W. J., Bourassa, A. E., and Solomon, S.: Stratospheric Temperature and Ozone Anomalies Associated With the 2020 Australian New Year Fires, Geophysical Research Letters, 48, e2021GL095 898, https://doi.org/https://doi.org/10.1029/2021GL095898, 2021.

Roeckner, E., Bäuml, G., Bonaventura, L., Brokopf, R., Esch, M., Giorgetta, M., Hagemann, S., Kirchner, I., Kornblueh, L., Manzini, E., et al.: The atmospheric general circulation model ECHAM 5. PART I: Model description, Tech. rep., Max-Planck-Institut für Meteorologie, https://doi.org/10.17617/2.995269, 2003.

Rosanka, S., Franco, B., Clarisse, L., Coheur, P.-F., Pozzer, A., Wahner, A., and Taraborrelli, D.: The impact of organic pollutants from Indonesian peatland fires on the tropospheric and lower stratospheric composition, Atmospheric Chemistry and Physics, 21, 11 257–11 288, https://doi.org/10.5194/acp-21-11257-2021, 2021.

Ryerson, T., Thompson, C., Peischl, J., and Bourgeois, I.: ATom: L2 In Situ Measurements from NOAA Nitrogen Oxides and Ozone (NOyO3) Instrument, ORNL Distributed Active Archive Center [data set], https://doi.org/10.3334/ORNLDAAC/1734, 2019.

Sander, R., Baumgaertner, A., Cabrera-Perez, D., Frank, F., Gromov, S., Grooß, J.-U., Harder, H., Huijnen, V., Jöckel, P., Karydis, V. A., Niemeyer, K. E., Pozzer, A., Riede, H., Schultz, M. G., Taraborrelli, D., and Tauer, S.: The community atmospheric chemistry box model CAABA/MECCA-4.0, Geoscientific Model Development, 12, 1365–1385, https://doi.org/10.5194/gmd-12-1365-2019, 2019.

https://doi.org/10.5194/egusphere-2026-3649
Preprint. Discussion started: 9 July 2026

Schallock, J., Brühl, C., Bingen, C., Höpfner, M., Rieger, L., and Lelieveld, J.: Reconstructing volcanic radiative forcing since 1990, using a comprehensive emission inventory and spatially resolved sulfur injections from satellite data in a chemistry-climate model, Atmospheric Chemistry and Physics, 23, 1169–1207, https://doi.org/10.5194/acp-23-1169-2023, 2023.

Schill, G. P., Froyd, K. D., Bian, H., Kupc, A., Williamson, C., Brock, C. A., Ray, E., Hornbrook, R. S., Hills, A. J., Apel, E. C., Chin, M., Colarco, P. R., and Murphy, D. M.: Widespread biomass burning smoke throughout the remote troposphere, Nature Geoscience, 13, 422–427, https://doi.org/10.1038/s41561-020-0586-1, 2020.

Schmidt, A., Mills, M. J., Ghan, S., Gregory, J. M., Allan, R. P., Andrews, T., Bardeen, C. G., Conley, A., Forster, P. M., Gettelman, A., Portmann, R. W., Solomon, S., and Toon, O. B.: Volcanic Radiative Forcing From 1979 to 2015, Journal of Geophysical Research: Atmospheres, 123, 12 491–12 508, https://doi.org/10.1029/2018JD028776, 2018.

Schneider, J., Weigel, R., Klimach, T., Dragoneas, A., Appel, O., Hünig, A., Molleker, S., Köllner, F., Clemen, H.-C., Eppers, O., Hoppe, P., Hoor, P., Mahnke, C., Krämer, M., Rolf, C., Grooß, J.-U., Zahn, A., Obersteiner, F., Ravegnani, F., Ulanovsky, A., Schlager, H., Scheibe, M., Diskin, G. S., DiGangi, J. P., Nowak, J. B., Zöger, M., and Borrmann, S.: Aircraft-based observation of meteoric material in lower-stratospheric aerosol particles between 15 and 68° N, Atmospheric Chemistry and Physics, 21, 989–1013, https://doi.org/10.5194/acp-21-989-2021, 2021.

Schneider, J., Schulz, C., Rubach, F., Ludwig, A., Wilsch, J., Joppe, P., Gurk, C., Molleker, S., Poulain, L., Obersteiner, F., Gehrlein, T., Bönisch, H., Zahn, A., Hoor, P., Emig, N., Bozem, H., Borrmann, S., and Hermann, M.: CARIBIC-AMS: a fully automated aerosol mass spectrometer for operation on routine passenger flights (IAGOS-CARIBIC) – instrument description and first flight application, Atmospheric Measurement Techniques, 18, 5103–5128, https://doi.org/10.5194/amt-18-5103-2025, 2025.

Schueneman, M. K., Nault, B. A., Campuzano-Jost, P., Jo, D. S., Day, D. A., Schroder, J. C., Palm, B. B., Hodzic, A., Dibb, J. E., and Jimenez, J. L.: Aerosol pH indicator and organosulfate detectability from aerosol mass spectrometry measurements, Atmospheric Measurement Techniques, 14, 2237–2260, https://doi.org/10.5194/amt-14-2237-2021, 2021.

Schulz, C., Schneider, J., Amorim Holanda, B., Appel, O., Costa, A., de Sá, S. S., Dreiling, V., Fütterer, D., Jurkat-Witschas, T., Klimach, T., Knote, C., Krämer, M., Martin, S. T., Mertes, S., Pöhlker, M. L., Sauer, D., Voigt, C., Walser, A., Weinzierl, B., Ziereis, H., Zöger, M., Andreae, M. O., Artaxo, P., Machado, L. A. T., Pöschl, U., Wendisch, M., and Borrmann, S.: Aircraft-based observations of isoprene-epoxydiol-derived secondary organic aerosol (IEPOX-SOA) in the tropical upper troposphere over the Amazon region, Atmospheric Chemistry and Physics, 18, 14 979–15 001, https://doi.org/10.5194/acp-18-14979-2018, 2018.

Schulz, L. and Glassmeier, K.-H.: On the anthropogenic and natural injection of matter into Earth's atmosphere, Advances in Space Research, 67, 1002–1025, https://doi.org/10.1016/j.asr.2020.10.036, 2021.

Schutgens, N., Tsyro, S., Gryspeerdt, E., Goto, D., Weigum, N., Schulz, M., and Stier, P.: On the spatio-temporal representativeness of observations, Atmospheric Chemistry and Physics, 17, 9761–9780, https://doi.org/10.5194/acp-17-9761-2017, 2017.

Schutgens, N. A. J., Gryspeerdt, E., Weigum, N., Tsyro, S., Goto, D., Schulz, M., and Stier, P.: Will a perfect model agree with perfect observations? The impact of spatial sampling, Atmospheric Chemistry and Physics, 16, 6335–6353, https://doi.org/10.5194/acp-16-6335-2016, 2016.

Schwarz, J. and Katich, J.: ATom: L2 In Situ Measurements from Single Particle Soot Photometer (SP2), ORNL Distributed Active Archive Center [data set], https://doi.org/10.3334/ORNLDAAC/1672, 2019.

Schwarz, J. P., Spackman, J. R., Gao, R. S., Perring, A. E., Cross, E., Onasch, T. B., Ahern, A., Wrobel, W., Davidovits, P., Olfert, J., Dubey, M. K., Mazzoleni, C., and and, D. W. F.: The Detection Efficiency of the Single Particle Soot Photometer, Aerosol Science and Technology, 44, 612–628, https://doi.org/10.1080/02786826.2010.481298, 2010.

https://doi.org/10.5194/egusphere-2026-3649
Preprint. Discussion started: 9 July 2026

Schwarz, J. P., Michailoudi, G., and Perring, A. E.: ACCLIP: NOAA Single-Particle Soot Photometer (SP2) Data, NSF NCAR Earth Observing Laboratory [data set], https://doi.org/10.26023/NTV8-17K4-5V0G, 2022.

Shen, J., Russell, D. M., DeVivo, J., Kunkler, F., Baalbaki, R., Mentler, B., Scholz, W., Yu, W., Caudillo-Plath, L., Sommer, E., et al.: New particle formation from isoprene under upper-tropospheric conditions, Nature, 636, 115–123, https://doi.org/10.1038/s41586-024-08196-0, 2024a.

Shen, S., Li, C., van Donkelaar, A., Jacobs, N., Wang, C., and Martin, R. V.: Enhancing Global Estimation of Fine Particulate Matter Concentrations by Including Geophysical a Priori Information in Deep Learning, ACS ES&T Air, 1, 332–345, https://doi.org/10.1021/acsestair.3c00054, 2024b.

Shen, X., Jacquot, J., Li, Y., Sharpe, S., Dykema, J., Schill, G., Bowman, K., Homeyer, C., Fraund, M., Moffet, R., et al.: Stratospheric aerosol perturbation by tropospheric biomass burning and deep convection, Nature Geoscience, pp. 1–8, https://doi.org/10.1038/s41561-025-01821-1, 2025.

Shiraiwa, M., Ammann, M., Koop, T., and Pöschl, U.: Gas uptake and chemical aging of semisolid organic aerosol particles, Proceedings of the National Academy of Sciences, 108, 11 003–11 008, https://doi.org/10.1073/pnas.1103045108, 2011.

Shiraiwa, M., Li, Y., Tsimpidi, A. P., Karydis, V. A., Berkemeier, T., Pandis, S. N., Lelieveld, J., Koop, T., and Pöschl, U.: Global distribution of particle phase state in atmospheric secondary organic aerosols, Nature communications, 8, 15 002, https://doi.org/10.1038/ncomms15002, 2017.

Szopa, S., Naik, V., Adhikary, B., Artaxo, P., Berntsen, T., Collins, W., Fuzzi, S., Gallardo, L., Kiendler-Scharr, A., Klimont, Z., Liao, H., Unger, N., and Zanis, P.: Short-Lived Climate Forcers, p. 817–922, Cambridge University Press, Cambridge, United Kingdom and New York, NY, USA, https://doi.org/10.1017/9781009157896.008, 2021.

Tabazadeh, A., Toon, O. B., Clegg, S. L., and Hamill, P.: A new parameterization of H2SO4/H2O aerosol composition: Atmospheric implications, Geophysical Research Letters, 24, 1931–1934, https://doi.org/10.1029/97GL01879, 1997.

The MESSy Consortium: The Modular Earth Submodel System, Zenodo [code], https://doi.org/10.5281/zenodo.20199551, 2025.

Thomason, L.: Global Space-based Stratospheric Aerosol Climatology Version 2.21, NASA Langley Atmospheric Science Data Center Distributed Active Archive Center [data set], https://doi.org/10.5067/GLOSSAC-L3-V2.21, 2023.

Thomason, L. W., Ernest, N., Millán, L., Rieger, L., Bourassa, A., Vernier, J.-P., Manney, G., Luo, B., Arfeuille, F., and Peter, T.: A global space-based stratospheric aerosol climatology: 1979–2016, Earth System Science Data, 10, 469–492, https://doi.org/10.5194/essd-10-469-2018, 2018.

Thompson, C. R., Wofsy, S. C., Prather, M. J., Newman, P. A., Hanisco, T. F., Ryerson, T. B., Fahey, D. W., Apel, E. C., Brock, C. A., Brune, W. H., Froyd, K., Katich, J. M., Nicely, J. M., Peischl, J., Ray, E., Veres, P. R., Wang, S., Allen, H. M., Asher, E., Bian, H., Blake, D., Bourgeois, I., Budney, J., Bui, T. P., Butler, A., Campuzano-Jost, P., Chang, C., Chin, M., Commane, R., Correa, G., Crounse, J. D., Daube, B., Dibb, J. E., DiGangi, J. P., Diskin, G. S., Dollner, M., Elkins, J. W., Fiore, A. M., Flynn, C. M., Guo, H., Hall, S. R., Hannun, R. A., Hills, A., Hintsa, E. J., Hodzic, A., Hornbrook, R. S., Huey, L. G., Jimenez, J. L., Keeling, R. F., Kim, M. J., Kupc, A., Lacey, F., Lait, L. R., Lamarque, J.-F., Liu, J., McKain, K., Meinardi, S., Miller, D. O., Montzka, S. A., Moore, F. L., Morgan, E. J., Murphy, D. M., Murray, L. T., Nault, B. A., Neuman, J. A., Nguyen, L., Gonzalez, Y., Rollins, A., Rosenlof, K., Sargent, M., Schill, G., Schwarz, J. P., Clair, J. M. S., Steenrod, S. D., Stephens, B. B., Strahan, S. E., Strode, S. A., Sweeney, C., Thames, A. B., Ullmann, K., Wagner, N., Weber, R., Weinzierl, B., Wennberg, P. O., Williamson, C. J., Wolfe, G. M., and Zeng, L.: The NASA Atmospheric Tomography (ATom) Mission: Imaging the Chemistry of the Global Atmosphere, Bulletin of the American Meteorological Society, 103, E761 – E790, https://doi.org/10.1175/BAMS-D-20-0315.1, 2022.

https://doi.org/10.5194/egusphere-2026-3649
Preprint. Discussion started: 9 July 2026

Thomson, D. S., Schein, M. E., and Murphy, D. M.: Particle Analysis by Laser Mass Spectrometry WB-57F Instrument Overview, Aerosol Science and Technology, 33, 153–169, https://doi.org/10.1080/027868200410903, 2000.

Tost, H., Jöckel, P., Kerkweg, A., Sander, R., and Lelieveld, J.: Technical note: A new comprehensive SCAVenging submodel for global atmospheric chemistry modelling, Atmospheric Chemistry and Physics, 6, 565–574, https://doi.org/10.5194/acp-6-565-2006, 2006.

Tsimpidi, A. P., Karydis, V. A., Pozzer, A., Pandis, S. N., and Lelieveld, J.: ORACLE (v1.0): module to simulate the organic aerosol composition and evolution in the atmosphere, Geoscientific Model Development, 7, 3153–3172, https://doi.org/10.5194/gmd-7-3153-2014, 2014.

Tsimpidi, A. P., Karydis, V. A., Pandis, S. N., and Lelieveld, J.: Global-scale combustion sources of organic aerosols: sensitivity to formation and removal mechanisms, Atmospheric Chemistry and Physics, 17, 7345–7364, https://doi.org/10.5194/acp-17-7345-2017, 2017.

Tsimpidi, A. P., Scholz, S. M. C., Milousis, A., Mihalopoulos, N., and Karydis, V. A.: Aerosol composition trends during 2000–2020: in-depth insights from model predictions and multiple worldwide near-surface observation datasets, Atmospheric Chemistry and Physics, 25, 10 183–10 213, https://doi.org/10.5194/acp-25-10183-2025, 2025.

van Donkelaar, A., Martin, R. V., Brauer, M., Hsu, N. C., Kahn, R. A., Levy, R. C., Lyapustin, A., Sayer, A. M., and Winker, D. M.: Global Estimates of Fine Particulate Matter using a Combined Geophysical-Statistical Method with Information from Satellites, Models, and Monitors, Environmental Science & Technology, 50, 3762–3772, https://doi.org/10.1021/acs.est.5b05833, pMID: 26953851, 2016.

Vernier, J. P., Pommereau, J. P., Garnier, A., Pelon, J., Larsen, N., Nielsen, J., Christensen, T., Cairo, F., Thomason, L. W., Leblanc, T., and McDermid, I. S.: Tropical stratospheric aerosol layer from CALIPSO lidar observations, Journal of Geophysical Research: Atmospheres, 114, https://doi.org/10.1029/2009JD011946, 2009.

Vernier, J.-P., Thomason, L. W., and Kar, J.: CALIPSO detection of an Asian tropopause aerosol layer, Geophysical Research Letters, 38, https://doi.org/10.1029/2010GL046614, 2011.

Voigt, C., Lelieveld, J., Schlager, H., Schneider, J., Curtius, J., Meerkötter, R., Sauer, D., Bugliaro, L., Bohn, B., Crowley, J. N., Erbertseder, T., Groß, S., Hahn, V., Li, Q., Mertens, M., Pöhlker, M. L., Pozzer, A., Schumann, U., Tomsche, L., Williams, J., Zahn, A., Andreae, M., Borrmann, S., Bräuer, T., Dörich, R., Dörnbrack, A., Edtbauer, A., Ernle, L., Fischer, H., Giez, A., Granzin, M., Grewe, V., Harder, H., Heinritzi, M., Holanda, B. A., Jöckel, P., Kaiser, K., Krüger, O. O., Lucke, J., Marsing, A., Martin, A., Matthes, S., Pöhlker, C., Pöschl, U., Reifenberg, S., Ringsdorf, A., Scheibe, M., Tadic, I., Zauner-Wieczorek, M., Henke, R., and Rapp, M.: Cleaner Skies during the COVID-19 Lockdown, Bulletin of the American Meteorological Society, 103, E1796 – E1827, https://doi.org/10.1175/BAMS-D-21-0012.1, 2022.

Wang, M., Xiao, M., Bertozzi, B., Marie, G., Rörup, B., Schulze, B., Bardakov, R., He, X.-C., Shen, J., Scholz, W., Marten, R., Dada, L., Baalbaki, R., Lopez, B., Lamkaddam, H., Manninen, H. E., Amorim, A., Ataei, F., Bogert, P., Brasseur, Z., Caudillo, L., De Menezes, L.-P., Duplissy, J., Ekman, A. M. L., Finkenzeller, H., Carracedo, L. G., Granzin, M., Guida, R., Heinritzi, M., Hofbauer, V., Höhler, K., Korhonen, K., Krechmer, J. E., Kürten, A., Lehtipalo, K., Mahfouz, N. G. A., Makhmutov, V., Massabò, D., Mathot, S., Mauldin, R. L., Mentler, B., Müller, T., Onnela, A., Petäjä, T., Philippov, M., Piedehierro, A. A., Pozzer, A., Ranjithkumar, A., Schervish, M., Schobesberger, S., Simon, M., Stozhkov, Y., Tomé, A., Umo, N. S., Vogel, F., Wagner, R., Wang, D. S., Weber, S. K., Welti, A., Wu, Y., Zauner-Wieczorek, M., Sipilä, M., Winkler, P. M., Hansel, A., Baltensperger, U., Kulmala, M., Flagan, R. C., Curtius, J., Riipinen, I., Gordon, H., Lelieveld, J., El-Haddad, I., Volkamer, R., Worsnop, D. R., Christoudias, T., Kirkby, J., Möhler, O., and Donahue, N. M.: Synergistic HNO3–H2SO4–NH3 upper tropospheric particle formation, Nature, 605, 483–489, https://doi.org/10.1038/s41586-022-04605-4, 2022.

https://doi.org/10.5194/egusphere-2026-3649
Preprint. Discussion started: 9 July 2026

Wang, S., Brock, C., Kondragunta, S., Laszlo, I., and McDonald, B.: Evaluating Aerosol Optical Depth Retrieved From VIIRS Using Global Scale, Multi-Seasonal Airborne Observations, Journal of Geophysical Research: Atmospheres, 129, e2023JD040 700, https://doi.org/10.1029/2023JD040700, 2024.

Watson-Parris, D., Schutgens, N., Reddington, C., Pringle, K. J., Liu, D., Allan, J. D., Coe, H., Carslaw, K. S., and Stier, P.: In situ constraints on the vertical distribution of global aerosol, Atmospheric Chemistry and Physics, 19, 11 765–11 790, https://doi.org/10.5194/acp-19-11765-2019, 2019.

Weigel, R., Mahnke, C., Baumgartner, M., Dragoneas, A., Vogel, B., Ploeger, F., Viciani, S., D'Amato, F., Bucci, S., Legras, B., Luo, B., and Borrmann, S.: In situ observation of new particle formation (NPF) in the tropical tropopause layer of the 2017 Asian monsoon anticyclone – Part 1: Summary of StratoClim results, Atmospheric Chemistry and Physics, 21, 11 689–11 722, https://doi.org/10.5194/acp-21-11689-2021, 2021.

Williamson, C. J., Kupc, A., Axisa, D., Bilsback, K. R., Bui, T., Campuzano-Jost, P., Dollner, M., Froyd, K. D., Hodshire, A. L., Jimenez, J. L., Kodros, J. K., Luo, G., Murphy, D. M., Nault, B. A., Ray, E. A., Weinzierl, B., Wilson, J. C., Yu, F., Yu, P., Pierce, J. R., and Brock, C. A.: A large source of cloud condensation nuclei from new particle formation in the tropics, Nature, 574, 399–403, https://doi.org/10.1038/s41586-019-1638-9, 2019.

Winker, D. M., Vaughan, M. A., Omar, A., Hu, Y., Powell, K. A., Liu, Z., Hunt, W. H., and Young, S. A.: Overview of the CALIPSO Mission and CALIOP Data Processing Algorithms, Journal of Atmospheric and Oceanic Technology, 26, 2310 – 2323, https://doi.org/10.1175/2009JTECHA1281.1, 2009.

Winker, D. M., Tackett, J. L., Getzewich, B. J., Liu, Z., Vaughan, M. A., and Rogers, R. R.: The global 3-D distribution of tropospheric aerosols as characterized by CALIOP, Atmospheric Chemistry and Physics, 13, 3345–3361, https://doi.org/10.5194/acp-13-3345-2013, 2013.

Xenofontos, C., Kohl, M., Ruhl, S., Almeida, J., Beckmann, H. M., Caudillo-Plath, L., Ehrhart, S., Höhler, K., Kaniyodical Sebastian, M., Kong, W., et al.: The impact of ammonia on particle formation in the Asian Tropopause Aerosol Layer, npj Climate and Atmospheric Science, 7, 215, https://doi.org/10.1038/s41612-024-00758-3, 2024.

Xenofontos, C., Kohl, M., Ruhl, S., Almeida, J., Caudillo-Plath, L., Cruz-Simbron, R., Dada, L., Duplissy, J., Ehrhart, S., Finkenzeller, H., Höhler, K., Kong, W., Kunkler, F., Lietzke, C. J., Mentler, B., Morawiec, A., Onnela, A., Rato, P., Rörup, B., Russell, D. M., Schervish, M., Scholz, W., Sebastian, M. K., Simon, M., Sommer, E., Tong, Y., Umo, N. S., Unfer, G. R., Vettikkat, L., Yang, B., Yu, W., Zgheib, I., Zheng, Z., Curtius, J., Donahue, N. M., Flagan, R. C., Gordon, H., Haddad, I. E., Hansel, A., Harder, H., He, X.-C., Kirkby, J., Kulmala, M., Lehtipalo, K., Möhler, O., Petäjä, T., Pöhlker, M. L., Schobesberger, S., Stolzenburg, D., Wang, M., Winkler, P. M., Worsnop, D. R., Höpfner, M., Volkamer, R., Pozzer, A., Lelieveld, J., and Christoudias, T.: Global impact of anthropogenic NH_3 emissions on upper tropospheric aerosol formation, Proceedings of the National Academy of Sciences, 122, e2506658 122, https://doi.org/10.1073/pnas.2506658122, 2025.

Yu, P., Murphy, D. M., Portmann, R. W., Toon, O. B., Froyd, K. D., Rollins, A. W., Gao, R.-S., and Rosenlof, K. H.: Radiative forcing from anthropogenic sulfur and organic emissions reaching the stratosphere, Geophysical Research Letters, 43, 9361–9367, https://doi.org/10.1002/2016GL070153, 2016.

Zawada, D., Rieger, L., Bourassa, A., Degenstein, D., and Warnock, T.: OMPS-NPP L2 LP University of Saskatchewan, Zenodo [data set], https://doi.org/10.5281/zenodo.20765257, 2026.

Zhang, Q., Jimenez, J. L., Canagaratna, M. R., Allan, J. D., Coe, H., Ulbrich, I., Alfarra, M. R., Takami, A., Middlebrook, A. M., Sun, Y. L., Dzepina, K., Dunlea, E., Docherty, K., DeCarlo, P. F., Salcedo, D., Onasch, T., Jayne, J. T., Miyoshi, T., Shimono, A., Hatakeyama, S., Takegawa, N., Kondo, Y., Schneider, J., Drewnick, F., Borrmann, S., Weimer, S., Demerjian, K., Williams, P., Bower, K.,

https://doi.org/10.5194/egusphere-2026-3649
Preprint. Discussion started: 9 July 2026

Bahreini, R., Cottrell, L., Griffin, R. J., Rautiainen, J., Sun, J. Y., Zhang, Y. M., and Worsnop, D. R.: Ubiquity and dominance of oxygenated species in organic aerosols in anthropogenically-influenced Northern Hemisphere midlatitudes, Geophysical Research Letters, 34, https://doi.org/10.1029/2007GL029979, 2007.

Zhang, R., Xie, H.-B., Ma, F., Yin, R., Chen, J., and He, X.-C.: Quaternary Nucleation of Iodine and Sulfur Oxoacids in the Marine Atmosphere: Unexpected Role of Methanesulfonic Acid, Journal of Geophysical Research: Atmospheres, 130, e2024JD042 220, https://doi.org/10.1029/2024JD042220, 2025.

Zhao, B., Shrivastava, M., Donahue, N. M., Gordon, H., Schervish, M., Shilling, J. E., Zaveri, R. A., Wang, J., Andreae, M. O., Zhao, C., Gaudet, B., Liu, Y., Fan, J., and Fast, J. D.: High concentration of ultrafine particles in the Amazon free troposphere produced by organic new particle formation, Proceedings of the National Academy of Sciences, 117, 25 344–25 351, https://doi.org/10.1073/pnas.2006716117, 2020.

Zhu, H., Martin, R. V., van Donkelaar, A., Hammer, M. S., Li, C., Meng, J., Oxford, C. R., Liu, X., Li, Y., Zhang, D., Singh, I., and Lyapustin, A.: Importance of aerosol composition and aerosol vertical profiles in global spatial variation in the relationship between $PM_{2.5}$ and aerosol optical depth, Atmospheric Chemistry and Physics, 24, 11 565–11 584, https://doi.org/10.5194/acp-24-11565-2024, 2024.